UNIVERSIDADE DE LISBOA
FACULDADE DE CIÊNCIAS
DEPARTAMENTO DE QUÍMICA E BIOQUÍMICA

Factors Affecting the ZIKV Life Cycle

Catarina Prazeres Sabino

Mestrado em Bioquímica
Especialização em Bioquímica Médica

Dissertação orientada por:
Prof. Dr. Eberhard Hildt, Prof. Dr. Francisco Pinto

2017

ACKNOWLEDGEMENTS/AGRADECIMENTOS

First of all, I would like to express my gratitude to Prof. Dr. Eberhard Hildt for accepting me in his group and for providing me the incredible opportunity to do my master thesis research at the Paul-Ehrlich-Institut. I want to truly thank him for all the guidance, knowledge and support required for the accomplishment of this work.

Also, I would like to thank my co-supervisor Prof. Dr. Francisco Pinto for all the support and availability.

A special thanks goes to “The Hildt Guys”, in particular to Dr. Daniela Ploen, to Dr. Sami Akhras and to Dr. Fabian Elgner, for all the help at the lab, for their patience, and for answering all my “thousands” questions. Thank you for sharing your knowledge and experience with me. To the rest of the lab’s group, thank you for making me feel welcome in the group, for the friendly environment, and for all the great moments shared. To Sami, thank you for all the talks during coffee breaks and for your wise advices. To Sophia, my ZIKV-autophagy partner, for all the laughs while working in the lab and for sharing “my pain” in this complicated world of ZIKV. To Michael, I really do not have words to describe all the help that you gave me. I know that I could not have done this without you. Thank you for listening my long discussions about the results and pretending that you understood something.

In addition, I would like to thank Dr. Regina Eberle for the preparation of the ultrathin sections.

I also want to show my appreciation to Gert, Dagmar and Jasminka for all their excellent work that contributes and improves ours.

Por fim, quero agradecer à minha família por todo o apoio durante esta longa jornada da minha vida e por todas as conversas de Skype que me fizeram sentir como se nunca tivesse saído de casa. Um especial obrigado aos meus pais por me proporcionarem esta experiência incrível!

ABSTRACT

The Zika virus (ZIKV) infection has spread widely, mainly in Africa, South and Central America, and South Pacific. This mosquito-borne virus had its first appearance on a rhesus monkey in the Zika forest of Uganda, in 1947. Like other flaviviruses, the ZIKV has a single-stranded positive RNA genome that encodes a polyprotein, which is processed by viral and host proteases. In the context with the epidemic in the South America, a clear correlation between the infection of pregnant women and the development of microcephaly in fetuses was observed. Thus, understanding the life cycle of the virus and discovering ways to reduce or even eradicate the infection of ZIKV has become urgent.

Autophagy, as an essential process for the cellular homeostasis and survival, is responsible for the lysosomal degradation of damaged or unwanted cytoplasmic proteins and organelles. The relationship between virus and autophagy is not yet fully understood. Several reports suggest that flaviviruses lead to an increase of autophagic activity to promote different stages of the viral life cycle. The same holds true for ZIKV, as it was shown in infected fibroblasts. However, the relevance of this pathway for the numerous steps of the ZIKV life cycle is poorly studied. To investigate the relevance of autophagy, ZIKV-infected cells were treated with various chemical compounds. In this study, Bafilomycin A1, a V-ATPase inhibitor, was capable to diminish viral infection effectively. Moreover, the intracellular cholesterol transport inhibitor, U18666A, was shown to reduce the spreading of infection. 3-Methyladenine, an early autophagy inhibitor, contributed to a decrease of viral replication, whereas Rapamycin, an autophagy inducer, promoted it.

This work provided new insights into the relationship between autophagy and ZIKV infection. Clearly, the acidification of endosomal-lysosomal compartments is extremely important for the entry process and for the establishment of infection. As for the importance of intracellular cholesterol trafficking, further experiments need to be performed to clarify which stages of the ZIKV life cycle are affected. These data suggest that the main influence of autophagy lies in the augmentation of viral replication.

Keywords: ZIKV; life cycle; acidification of endosomal-lysosomal compartments; trafficking of intracellular cholesterol; autophagy

RESUMO

O vírus Zika (ZIKV) é um arbovírus, isto é, é um vírus transmitido por artrópodes, sendo o seu principal vetor de transmissão o mosquito do género *Aedes*. ZIKV teve a sua origem na Floresta Zika, na República de Uganda, tendo sido isolado, em 1947, do sangue de um macaco *rhesus*. Em 1954, foram relatados, na Nigéria, os primeiros casos de humanos infetados com o vírus e, nos 57 anos seguintes, apenas 13 casos foram reportados. O primeiro grande surto surgiu, em 2007, no estado de Yap (Estados federados da Micronésia), atingindo a Polinésia Francesa e o Brasil no ano de 2013 e 2015, respetivamente. O facto do vírus também ser transmitido sexualmente e por transfusões sanguíneas pode promover a sua rápida dissiminação, conduzindo a uma potencial pandemia. Atualmente, a presença do ZIKV já foi documentada na maior parte dos países europeus e nos Estados Unidos da América, mas a sua maior incidência tem lugar em África, América central e do sul, bem como no Pacífico.

Somente cerca de 20% das pessoas infetadas com o vírus apresenta manifestações clínicas, sendo que os principais sintomas são febre ligeira, erupções cutâneas, dores de cabeça, dores nas articulações e conjuntivite. Porém, complicações neurológicas como síndrome de Guillain-Barré (GBS) e, em recém-nascidos, microcefalia têm sido associadas ao ZIKV. A sua rápida expansão e o aumento de casos de microcefalia levaram a Organização Mundial de Saúde (do inglês: *World Heath Organization*), em fevereiro de 2016, a declarar a infeção pelo ZIKV um estado de emergência pública.

Semelhante a outros flavivírus, o ZIKV é constituído por uma nucleocápside viral composta pela proteína C associada a um genoma de RNA de cadeia simples e polaridade positiva. Esta cápside encontra-se rodeada por uma bicamada lipídica, na qual se encontram ancoradas as proteínas E e M, formando o envelope. O ciclo de vida destes flavivírus começa pela internalização das partículas virais na célula hospedeira, através de endocitose-mediada por recetores. O meio acídico dos endossomas favorece a ocorrência de alterações conformacionais e, consequentemente, na libertação do genoma viral para o citoplasma, onde é traduzido numa poliproteína. Esta poliproteína é, então, processada por enzimas virais e celulares em proteínas estruturais e não estruturais. Enquanto que as proteínas estruturais integram novas partículas virais, as não estruturais participam na replicação viral e na clivagem proteolítica da poliproteína. O ZIKV induz reorganizações do retículo endoplasmático (RE), de modo a formar os locais de replicação. Perto destes locais, as novas partículas virais são montadas e conduzidas para a via secretora, onde, na rede *trans*-Golgi (do inglês: *trans-Golgi network*), sofrem maturação e, portanto, tornam-se infeciosas. Depois das partículas virais serem maturadas, estas saem da célula por exocitose.

Macroautofagia, mais conhecida por autofagia, é um processo catabólico conservado em células eucarióticas. Este processo celular é responsável pela degradação de proteínas citoplasmáticas e organelos envelhecidos ou em excesso. Deste modo, este sistema é extremamente importante para a manutenção da homeostasia e sobrevivência das células. Sendo um processo altamente regulado, tem capacidade de combater infeções virais através da sua degradação direta nos lisossomas ou estimulando respostas imunes. A relação entre vírus e autofagia ainda não está compreendida na sua totalidade. Curiosamente, vários estudos provaram que os flavivírus aumentam a atividade desta via para seu próprio benefício, promovendo diferentes passos do seu ciclo de vida. Recentemente, partículas do ZIKV foram encontradas em vesículas semelhantes a autofagossomas, associados ao RE. No entanto, a importância desta via para os diversos passos do ciclo de vida do ZIKV está ainda pouco estudada.

Desta forma, pretendeu-se investigar a relevância de certos fatores, tais como, a acidificação de compartimentos endossomais-lisossomais, o tráfego de colesterol intracelular e a autofagia, para o ciclo de vida deste vírus. Neste estudo, células epiteliais provenientes de adenocarcinoma de pulmão humano

(A549) foram infetadas com duas estirpes do ZIKV isoladas na Polinésia Francesa e na República de Uganda.

De modo a compreender como é que a acidificação do lúmen dos endossomas e lisossomas afeta o ciclo de vida do vírus, células infetadas com as estirpes do ZIKV foram tratadas com Bafilomicina A1 (BFLA). Nesta parte do trabalho, tratamento pré-infeção (do inglês: *pre-infection*) e pós-infeção (do inglês: *post-infection*) foram usados com o intuito de perceber como é que este composto interfere com a entrada do vírus nas células hospedeiras e com o desenrolar da infeção, respetivamente. No tratamento pré-infeção, as células foram em primeiro lugar tratadas e, duas horas mais tarde, infetadas com o vírus. Por outro lado, o tratamento pós-infeção, tal como o nome indica, consiste no tratamento das células duas horas após terem sido infetadas. BFLA é um inibidor da bomba de protões V-ATPase, impedindo a acidificação de organelos como, por exemplo, os endossomas e os lisossomas. O tratamento pré-infeção impediu a entrada de ambas as estirpes do ZIKV, enquanto que, o tratamento pós-infeção conduziu à diminuição da infeção viral ao longo do tempo. Assim sendo, é possível inferir que a BFLA dificulta a endocitose-mediada por recetores e, quando a infeção já está estabelecida, a acidificação do lúmen dos endossomas e lisossomas é fulcral, tanto no início como no fim do ciclo de vida do ZIKV.

Na segunda parte deste trabalho, tentou-se perceber a importância do tráfego de colesterol intracelular para a infeção do vírus. Para tal, células infetadas foram tratadas pré- e pós-infeção com U18666A (U18). U18 bloqueia o tráfego de colesterol intracelular como consequência da sua acumulação em endossomas tardios (do inglês: *late endosomes*) e lisossomas. Ambas as estirpes revelaram um decréscimo da infeção viral consoante o tempo e bastante semelhante entre os dois tipos de tratamentos aplicados. Contudo, os resultados não permitiram retirar conclusões acerca do passo do ciclo de vida afetado por este inibidor.

Por fim, de modo a compreender a influência direta da autofagia para o ciclo de vida do ZIKV, Rapamicina (RAPA) e 3-Metiladenina (3-MA) foram utilizados para tratar células infetadas. Neste caso, apenas tratamento pós-infeção foi necessário, uma vez que estes moduladores não interferem com processos relacionados com a entrada viral. A RAPA é um ativador da autofagia, enquanto que a 3-MA previne a sua iniciação. O seu efeito parece refletir-se, maioritariamente, no aumento do nível da replicação. Tal como sugerido por Liang *et al.*, 2016, o ZIKV aparenta necessitar da via autofágica da célula hospedeira para criar estruturas membranares para os locais de replicação.

Em suma, este trabalho permitiu aprofundar a relação entre a autofagia e o ZIKV, podendo contribuir para posteriores estudos a realizar, não só com o ZIKV, mas também com outros flavivírus. Como se veio a demonstrar, a acidificação de compartimentos endosomais-lisosomais é de extrema importância para a entrada viral e para o estabelecimento da infeção. Ficou, igualmente, demonstrado que o tráfego de colesterol intracelular é requerido para poder haver uma eficiente infeção. Porém, estudos adicionais devem ser realizados para clarificar qual ou quais os passos do ciclo de vida é que são afetados. Os resultados obtidos sugerem que a atividade autofágica seja aumentada em células infetadas com o intuito de promover a replicação do ZIKV. Devido à falta de uma vacina ou de compostos específicos com atividade antiviral contra o ZIKV, aliados ao aumento de casos de GBS e microcefalia, esforços devem ser feitos na medida de melhor compreender o ciclo de vida deste flavivírus, bem como, a sua patogenicidade.

Palavras-chave: ZIKV; ciclo de vida; acidificação de compartimentos endossomais-lisossomais; tráfego de colesterol intracelular; autofagia

INDEX

INDEX OF TABLE AND FIGURES

ABBREVIATIONS

%	Percentage
3-MA	3-Methyladenine
A549	Adenocarcinoma human alveolar basal epithelial cells
A	Adenine
aa	Amino acids
Abs 260 nm, Abs 280 nm	Absorbance at 260 and 280 nm
Akt	Protein kinase B
AMP	Adenosine monophosphate
AMPK	AMP-activated protein kinase
APS	Ammonium persulfate
Atg	Autophagy-related gene
AXL	AXL receptor tyrosine kinase
BFLA	Bafilomycin A1
BSA	Bovine serum albumin
BSL-3	Biosafety level 3
C	Capsid
C	Cytosine
cDNA	Complementary DNA
CLSM	Confocal laser scanning microscopy
CH	Switzerland
CQ	Chloroquine
Cy3	Cyanine3
Cy5	Cyanine5
DABCO	1,4-diazabicyclo[2.2.2]octane
DAPI	4,6-diamidino-2-phenylindole
DC-SIGN	Dendritic cell-specific ICAM-grabbing non-integrin
DE	Germany
DENV	Dengue virus
DFPC1	Double FYVE-containing protein 1
DEPC-H_2O	Diethylpyrocarbonate water
DMEM	Dulbecco’s Modified Eagle Medium
DMSO	Dimethyl sufoxide

DNA	Deoxyribonucleic acid
DNase	Deoxyribonuclease
dNTPs	Deoxynucleosides triphosphate
E	Envelope
ECL	Enhanced chemiluminescence
EDTA	Ethylenediaminetetraacetic acid
ELISA	Enzyme-linked immunosorbent assay
ER	Endoplasmic reticulum
et al.	*et alia* (and others)
FBS	Fetal bovine serum
FDA	Food and Drug Administration
fNSCs	Human fetal neural steam cells
FR	France
fw	Forward
G	Guanine
GBS	Guillain-Barré syndrome
Gly	Glycine
GM130	*cis*-Golgi matrix protein 130
HCV	Hepatitis C virus
hpi	Hours post-infection
HRP	Horseradish peroxidase
hRPL27	Human ribosomal protein 27
IF	Indirect immunofluorescence
IgG	Immunoglobulin G
IgM	Immunoglobulin M
JEG-3	Human trophoblasts
JEV	Japanese encephalitis virus
kb	Kilobase
kDa	Kilodalton
KO	Knock out
LAMP2	Lysosome-associated membrane glycoprotein 2
LC3-I	Cytosolic form of LC3
LC3-II	Lipidated form of LC3
LDH	Lactate dehydrogenase

LDs	Lipid droplets
M	Membrane
M	Mitochondria
MAP1LC3 or LC3	Microtubule-associated protein 1 light chain 3
MLBs	Multilamellar bodies
MOI	Multiplicity of infection
mRNA	Messenger RNA
mTOR	Mammalian target of rapamycin
MVBs	Multivesicular bodies
n	Number of replicates
N	Nucleus
NCR	Non-coding region
no.	number
NPC1	Niemann-Pick disease type C1 protein
ns	Non-significant
NS	Non-sctrutural protein
NSAID	Nonsteroidal anti-inflammatory drugs
ºC	Celsius degrees
ORF	Open reading frame
PBS	Phosphate buffered saline
PBST	PBS supplemented with Triton X-100
PCR	Polymerase chain reaction
PDI	Protein disulfide-isomerase
PE	Phosphatidylethanolamine
pfu	Plaque-forming units
PHEIC	Public health emergency of international concern
PI3K	Phosphatidylinositol-3-kinase
PI3KC3	Class III phosphatidylinositol-3-kinase
PI3P	Phosphatidylinositol-3-phosphate
PMSF	Phenylmethylsulfonyl fluoride
prM	Precursor of membrane
PVDF	Polyvinylidene fluoride
Rapa	Rapamycin
RE	Retículo endoplasmático

rev	Reverse
RFs	Replication factories
RIPA	Radioimmunoprecipitation assay
RNA	Ribonucleic acid
RNase	Ribonuclease
Rpm	Revolutions per minute
RT	Reverse transcriptase
RT-PCR	Reverse transcriptase polymerase chain reaction
RT-qPCR	Quantitative RT-PCR
SDS	Sodium dodecyl sulfate
SDS-PAGE	Sodium dodecyl sulfate polyacrylamide gel electrophoresis
SEM	Standard error of the mean
sfRNA	Subgenomic flavivirus RNA
SPOV	Spondweni virus
SQSTM1	Sequestosome 1
ssRNA	Single stranded RNA
TBEV	Tick-borne encephalitis virus
TBST	Tris buffered saline supplemented with Tween 20
TEM	Transmission electron microscopy
TEMED	Tetramethylethylenediamine
Tim-1	T-cell immunoglobulin and mucin domain protein 1
TGN	*trans*-Golgi network
TGN46	*trans*-Golgi netwrok protein 46
Tyro3	Tyrosine-protein kinase receptor Tyro3
U	Uridine
U18	U18666A
UK	United Kingdom
ULK1/2	Unc-like kinase 1 and 2
USA	United States of America
v/v	Volume per volume
V-ATPase	Vacuolar type H^+-ATPase
Vero	African green monkey kidney cells
VMP1	Vacuolar membrane protein 1
VPs	Vesicle packets

Vsp34	Vacuolar protein sorting 34
w/v	Weight per volume
WB	Western blot
WHO	World health organization
WIPI	WD-repeat domain phosphoinositide interacting protein
WNV	West Nile virus
XRN1	5’-3’ Exoribonuclease 1
YFV	Yellow Fever virus
ZIKV	Zika virus

1. INTRODUCTION

1.1 Zika virus

1.1.1 Classification and structure

The Zika virus (ZIKV) is an emerging arbovirus (arthropod-borne virus) which belongs to the genus *Flavivirus* in the *Flaviviridae* family. This genus is comprised of 53 viruses that are divided within clusters based on virus transmission.[1] As a mosquito-borne virus, ZIKV shares similarities with Spondweni virus (SPOV), representing the only members of their clade (clade X).[2,3] Other flaviviruses, closely related to ZIKV, are yellow fever virus (YFV), dengue virus (DENV), West Nile virus (WNV), Japanese encephalitis virus (JEV), and tick-borne encephalitis virus (TBEV).[4,5]

Like other flaviviruses, the ZIKV genome is a positive sense single-stranded RNA and it has a size of approximately 11 kilobases (kb). It encodes 3419 and 3410 amino acids (aa) for the African and French Polynesia strains, respectively.[6,7] Additionally, two non-coding regions (5' and 3'NCR) flank a single long open reading frame (ORF). The 3'NCR holds conserved sequences, including the dinucleotide CU at the end of the transcript, which are replacing the Poly(A) tract that is usual present in cellular mRNA.[8] Secondary structures are also present and, by the host XRN1 exoribonuclease, form a subgenomic flavivirus RNA (sfRNA) important for viral replication.[9] The other extremity (5') contains the promoter and a type I cap, followed by the conserved dinucleotide sequence AG. Besides that, another secondary RNA structure is encoded in this NCR.[8] The ORF encodes a viral polyprotein which is cleaved to give three structural proteins (capsid [C], precursor of membrane/membrane [prM/M] and envelope [E]) and seven non-structural proteins (NS1, NS2A, NS2B, NS3, NS4A, NS4B and NS5).[6,7,10] This cleavage is carried out by cellular host and viral proteases. The cellular host signalase is responsible for cleaving M/E, E/NS1 and the C-terminal hydrophobic region of NS4A (denominated as 2k peptide)/NS4B. As for the NS1/NS2 junction, the cleavage is accomplished by an unknown cellular signalase. Moreover, to create mature infectious viral particles, the proteolytic cleavage of prM into the pr peptide and M protein in the *trans*-Golgi network (TGN) by furin-like protease is necessary. [6,11,12] Meanwhile, it is presumed that the viral serine protease (NS3) splits the sites between virion capsid protein (C_v) and the C-terminal hydrophobic domain of capsid protein (C_i) [C_v/C_i], NS2A/NS2B, NS2B/NS3, NS3/NS4A, NS4A/2k peptide, and NS4B/NS5 **(Fig 1.1)**.[6]

The expected function of these proteins concurs with those of other flaviviruses. The structural proteins are involved in the assembly of new virions (viral particles). The C protein is associated with the viral genome, forming the capsid, while the E glycoprotein is involved in receptor binding, attachment and virus fusion during the internalization of the virion. As for the prM, it stabilizes the E protein, preventing premature fusion of the virions before its release from the cell. When the particle is reaching the cell membrane, this pr fragment is no longer required and thus, the cleavage of prM into M occurs.[13,14] In relation to non-structural proteins, NS1 is required for virus replication and acts as an immunomodulator; NS2A is also implicated in immunomodulatory and replication processes, as well as in viral assembly; NS2B serves as a cofactor of the protease NS3; NS3 is a serine protease that cleaves part of the viral polyprotein and has an additional helicase, nucleoside triphosphatase, and RNA triphosphatase activity essential for replication; NS4A induces autophagy and membrane rearrangements necessary for the replication site and, together with NS4B, inhibits the interferon signalling pathway in infected cells; NS5 is the viral RNA-dependent RNA polymerase that is

responsible for the replication of the viral genome. It possesses a methyltransferase domain, indispensable for capping the 5'end of the viral RNA.[15,16]

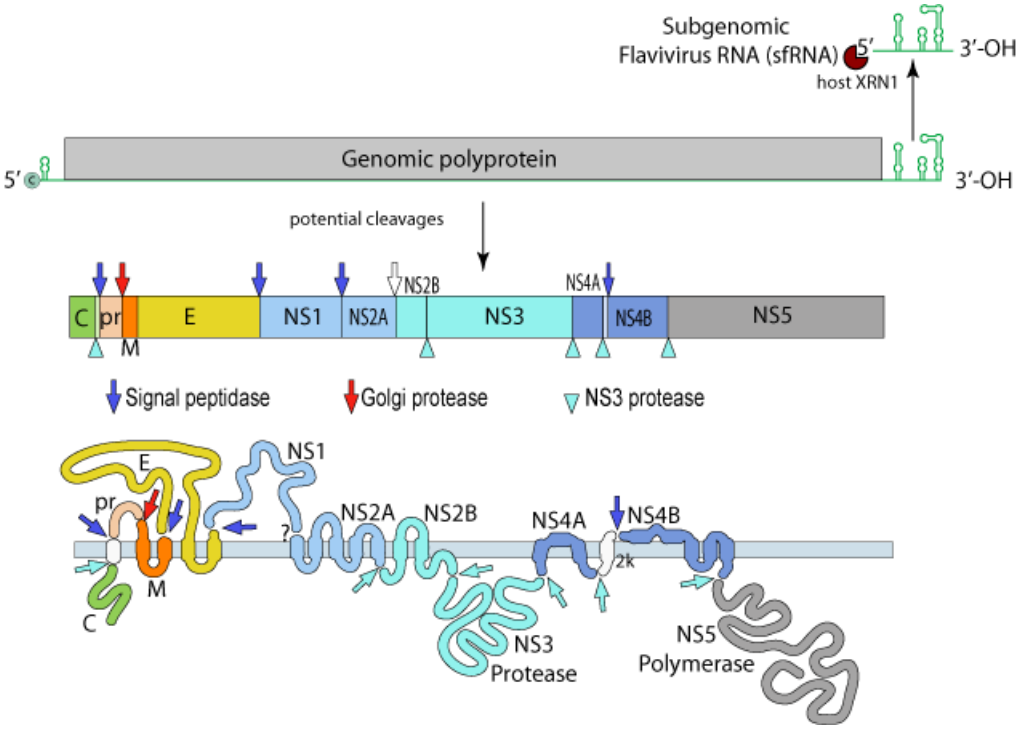

Figure 1.1 – Schematic representation of ZIKV genome. The viral genome is composed by a single ORF flanked by two NCR. The 3'NCR owns secondary structures, which form a sfRNA after cleavage by the host XRN1. The ORF encodes a polyprotein which is cleaved into three non-structural proteins (C, prM/M, and E) and seven structural proteins (NS1, NS2A, NS2B, NS3, NS4A, NS4B, NS5). Both linear (top) and predicted membrane topology (bottom) of the polyprotein are represented. The polyprotein is processed by host signal peptidase (signalase), Golgi protease and viral NS3 protease. All sites cleaved are marked with the respective enzyme name. Retrieved from ViralZone.[17]

ZIKV particles consist of a nucleocapsid, which is formed by the C protein in association with the viral genome, surrounded by a lipid bilayer derived from the host cell. This lipid envelope is coated with E and M proteins 90 E:M dimeric heterodimers, with a total of 180 copies of each, displaying an icosahedral arrangement. (**Fig 1.2)**.[18,19] The particles have a total diameter of approximately 40 nm with a central core of 28-30 nm.[20–22]

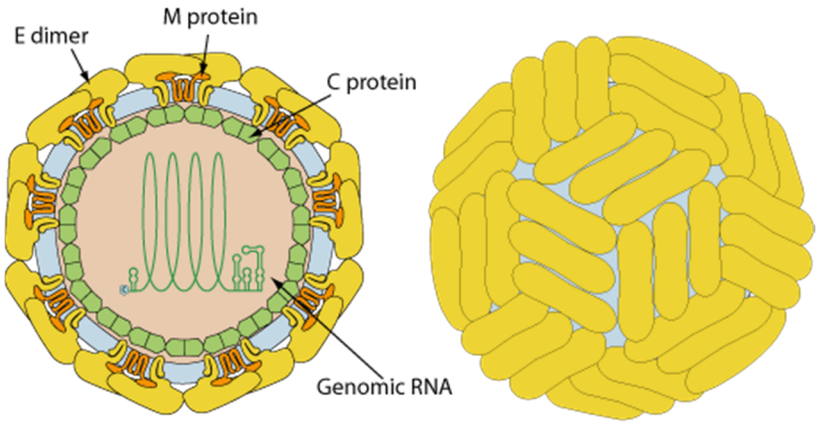

Figure 1.2 – Schematic representation of ZIKV virion structure. The genomic RNA is associated with the C protein, both surrounded by a E:M coated-lipid bilayer. The surface dimers are displayed in an icosahedral arrangement. Retrieved from ViralZone.[17]

1.1.2 Epidemiology and pathogenesis

In the course of a study on yellow fever, multiple arboviruses, including ZIKV, were isolated in 1947 at the Yellow Fever Research Institute, in Entebbe, Uganda.[23] In April 1947, ZIKV was isolated from blood of a rhesus monkey (no. 766) that had been caged in the Zika Forest of Uganda **(Fig 1.3)**. This isolated virus gave birth to the African ZIKV MR766 strain.[24] In January 1948, researchers started to consider that ZIKV might be mosquito-borne when the virus was isolated from *Aedes africanus* mosquitoes.[24] The first human illness report of ZIKV was in three African people, in Nigeria (1954), suggesting the virus as a human pathogen. The patients reported cough, fever, headache and pain behind the eyes and in the joints.[25] In 1969, ZIKV was isolated for the first time outside Africa, in Malaysia, from the *Aedes aegypti* mosquito **(Fig 1.3)**.[26]

In the next 57 years after the first ZIKV human isolation, only 13 cases of illness were reported until a sudden outbreak in 2007, in the State of Yap (Federated States of Micronesia) **(Fig 1.3)**.[27–31] Of 59 probable cases, 49 were confirmed as infected and promptly, 5005 out of 6892 total residents had been infected with ZIKV. During the 3 months of the outbreak, rash, fever, arthritis or arthralgia, and conjunctivitis were the most commonly observed clinical signs.[31]

Afterwards, between October 2013 and April 2014, French Polynesia suffered the largest outbreak ever documented until that time, with an estimation of 32 000 persons suspected to had been infected with ZIKV. Maculopapular rash, asthenia, fever, arthralgia, conjunctival hyperaemia were the most commonly reported symptoms.[32–34] Although ZIKV disease was as mild as the one described in Yap, some cases of neurologic and autoimmune complications were associated with this infection. In fact, 42 cases of Guillain-Barré syndrome (GBS) were stated.[34,35] GBS is an acute immune-mediated neuropathy that causes nerve damage, muscle weakness and paralysis, among others. The effects of this disorder are mostly temporary, but they can be permanent and, in some cases, life threating.[36–38] From French Polynesia, ZIKV spread in the Pacific, where outbreaks were reported in most of the islands, including New Caledonia (2014)[39], Easter Island (2014)[40], Cook Islands (2014)[41], Vanuatu (2015)[41] and Solomon Islands (2015)[41] **(Fig 1.3)**.

By March 2015, ZIKV arrived to Latin American and, in May 2015, the presence of the virus was confirmed in Brazil, in the city of Natal.[42,43] Patients complained of arthralgia, edema of extremities, mild fever, maculopapular rashes frequently pruritic, headaches, retro-orbital pain, no purulent conjunctivitis, vertigo, myalgia, and digestive disorder.[42] As of October 2015, autochthonous transmission of ZIKV have been confirmed in 14 Brazilian states with an estimation of 440 000 to 1 300 000 cases by the Ministry of Health of Brazil.[44,45] The spreading of the virus proceeded to Colombia with the first report in October 2015 [44] and by March 2016, it had reached at least 33 countries in South and Central America, the Caribbean, and Mexico **(Fig 1.3)**.[45–48]

Several cases of ZIKV have been reported where travellers carried the virus into non-endemic countries, promoting a faster dissemination of the virus and leading to a potential pandemic threat. In Europe, cases of ZIKV were detected in Portugal, Spain, France, Italy, Germany, Netherlands, Switzerland, Belgium, England, Ireland, Finland, Denmark, Austria, and Sweden. As for the United States, many states reported cases, but the main risk of secondary transmission is in Texas and Florida, due to the prevalence of *Aedes* mosquitos. Hawaii, Canada, Chile, Japan, China, Australia, and New Zealand also reported cases of ZIKV infection.[49,50]

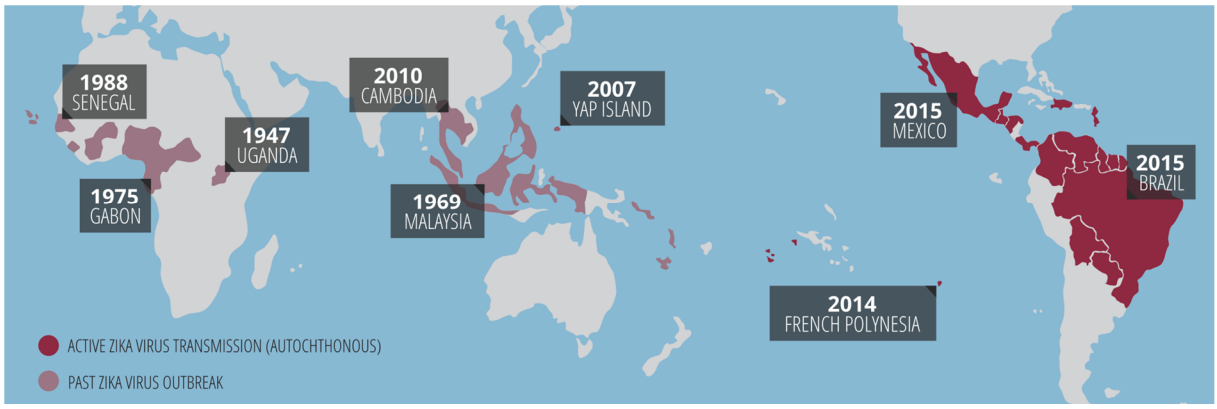

Figure 1.3 – ZIKV chronological dissemination map from Africa to Asia, and subsequently, to America. In 1947, ZIKV was first isolated from blood of a rhesus monkey in Uganda. The first isolation of ZIKV outside Africa took place in 1969, in Malaysia (Asia). Meanwhile, the virus continued to spread on the African continent with outbreaks in Gabon (1975) and Senegal (1988). In 2007, approximately 75% of the population in the state of Yap (Federated States of Micronesia) were infected with ZIKV. In 2010, it had reached Cambodia and in 2014, the largest outbreak documented until then occurred in French Polynesia. In the next year, the virus was detected on the American continent, affecting Brazil and Mexico, among other countries. Retrieved from goinvo website.[51]

Unexpectedly, besides GBS reports, the epidemic in Brazil revealed another neurological complication. More precisely, cases of microcephaly in newborns were linked to ZIKV infection and, until 30th January 2016, 4783 suspected cases had been reported, including some fetal deaths and miscarriages.[52] These neurological manifestations were non-existent on the African continent. Furthermore, a retrospective study of the outbreak in French Polynesia uncovered cases of microcephaly which were not connected to ZIKV before this epidemic in Brazil.[53] Microcephaly is a neurological condition in which the head circumference is smaller than expected for age, sex or ethnicity **(Fig 1.4)**.[54] This disorder can be evident at birth or postnatally, associated with a underdeveloped brain, and consequently, motor and cognitive dysfunction.[55] The rapid spread of ZIKV on the American continent and the possible association with microcephaly and GBS led the World Health Organization (WHO) to declare ZIKV infection a public health emergency of international concern (PHEIC) on 1st February 2016.[56]

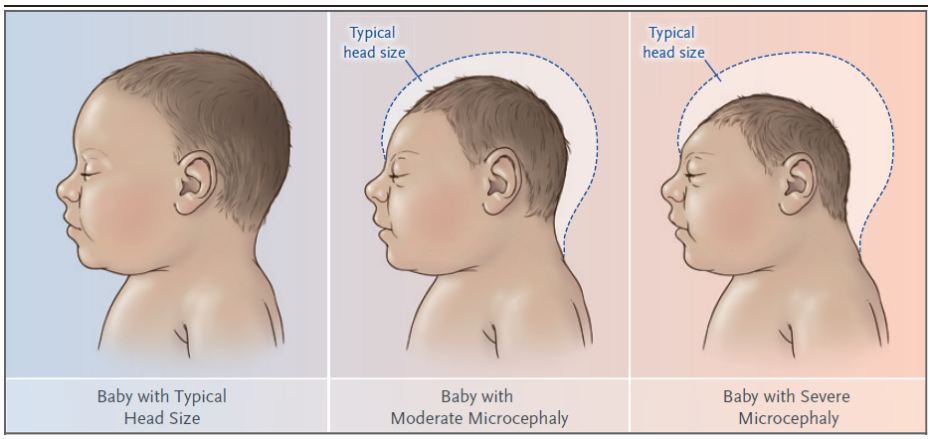

Figure 1.4 – Representative illustration of newborns with microcephaly. ZIKV infection is associated with microcephaly in newborns, resulted from maternal fetal transmission. This neurological complication can be moderate or severe and is characterised by a smaller head size. Retrieved from Petersen *et al.*, 2016.[48]

Up to now, multiple ZIKV strains have been identified and phylogenetic studies suggest the classification of the strains into two distinct lineages – African and Asian lineages.[57,58] The African lineage has its origin in Uganda with the strain MR766, whereas the Asian lineage evolved from the isolate in Malaysia. Only ≤11.7% of nucleotide divergence separates the two lineages.[58] This fact

indicates that the Asian lineage resulted from the African one, and consequently, the migration of the virus from one continent to another introduced minor modifications. The Asian lineage expanded to the Pacific and, according to phylogenetic analysis, the ZIKV strains, which were responsible for the outbreaks in the Americas, hold 99.7% of nucleotides and 99.9% of amino acid identity with the strain from the outbreak in French Polynesia.[59]

Only about 20% of ZIKV-infected people develop symptoms.[60] The most common ones include low fever grade, skin rashes, conjunctivitis, arthralgia, myalgia, fatigue, and headaches.[60,61] The incubation period of ZIKV is estimated to be 3-12 days and the symptoms have a duration of 2-7 days.[60,61] Despite these mild symptoms, evidence of neurological complications, including GBS and, microcephaly in newborns are associated to ZIKV infection.

1.1.3 Transmission, diagnosis and therapy

ZIKV is an arbovirus mainly transmitted by mosquito bites. The first isolations of ZIKV from *Aedes africanus* and *Aedes aegypti* mosquitoes, in Africa (1948) and in Asia (1969), respectively, suggested mosquitos from *Aedes* genus as the principal vector of transmission.[24,26] *Aedes aegypti* and *Aedes albobictus* are considered the most important vectors in the transmission of ZIKV, due to their wider geographical distributions, in detriment of other *Aedes* mosquitoes.[62] Besides the bite of an infected mosquito, cases of non-vector transmission have been reported. Risk of infection through perinatal transmission (transplacental, breastfeeding, saliva, and exchange of other body fluids)[63], sexual contact[64,65], blood transfusion[66,67], animal bites[68], and laboratory exposure[30,69] can occur.

In the absence of ZIKV epidemics, diagnosis can rely on clinical signs. However, most of the outbreaks overlap with other infections that show similar symptoms, and up to 80% of infected people are asymptomatic.[60,70] Therefore, ZIKV diagnosis depends on laboratory tests. Reverse Transcriptase Polymerase Chain Reaction (RT-PCR) is the most sensitive and specific assay performed for diagnosis.[71] The recognition of ZIKV RNA rests on the viral load during the acute phase of disease, but the viremia is relative short (mainly from days 0 to 4 after clinical manifestation). Only in rare cases, viral RNA could be measured up to 11 days.[72] Other specimen types besides serum can be considered for virus confirmation. In fact, ZIKV RNA has been detected in saliva[73], urine[74], and semen[65], presenting significant longer duration than the viremic period. [65,73,74] When molecular tests are negative from day 5 after the onset of symptoms, serological analysis should be performed to detect ZIKV IgM antibodies. In contrast, serological tests are not recommended during viremia because antibodies may be undetectable.[75] Even though, detection of virus IgM by ELISA is an effective method, most of the times cross-reactivity with other arboviruses causes false-positives, limiting specificity.[72] That being said, all positive results should be confirmed by a plaque-reduction neutralization assay.[72,75]

Currently, there is no vaccine or specific antiviral drug available for ZIKV infection. Since no therapy for infection exists, treatment focuses only on relieving symptoms. Thus, during the acute phase, acetaminophen for fever and pain, antihistaminic for pruritic rash, and ingestion of fluids for dehydration are recommended. Acetylsalicylic acid and nonsteroidal anti-inflammatory drugs (NSAID) should be avoided to prevent risk of haemorrhagic complications.[76] The lack of a vaccine until the present day is comprehensive due to its production and testing, which takes years and requires highly monetary funding. In addition to that, until recently, only sporadically mild disease was associated to ZIKV. Hence, almost no research was done in this field. Nonetheless, either inactivated or live attenuated virus vaccines are licensed for four flaviviruses and the same principle and research has been utilised for ZIKV.[77] Subunit, DNA, and viral vector vaccine platforms, containing or expressing ZIKV structural proteins, are also highly attractive as an alternative approach.[77] In the course of this research, the ZIKV

vaccine trials are now ongoing, with an experimental DNA vaccine already in Phase 2 .[78–80] In relation to an antiviral drug, a screen of approved drugs, designed for other diseases, can be performed to discover a compound with antiviral activity against ZIKV.[77] As an example, Chloroquine, an antimalarial drug, was shown to inhibit ZIKV.[81] Another possibility is the development of new inhibitors.[77]

1.1.4 Life cycle

The ZIKV life cycle follows the same mechanism as other flaviviruses. The cycle begins with the internalisation of an infectious viral particle into the host cell membrane. At the cell surface, multiple receptors and attachment factors interact with the viral envelope protein. AXL, DC-SIGN, Tyro3 and Tim-1 were recently described to take part in this process.[22] Then, the virion is internalised by clathrin-mediated endocytosis, providing it access to the acidic compartment of the endosome.[13] This acidification facilitates conformational changes and the disassembling of the virus particle, leading to the uncoating of the ssRNA.[82] In the host cell cytoplasm, the ssRNA is recognised as a mRNA and translated into a polyprotein, which is subsequently formed and cleaved to yield structural and non-structural proteins.[6,7,10] The structural proteins are going to assemble into new viral particles, while the non-structural proteins play a role on viral replication and protein cleavage **(Fig 1.5)**.[13]

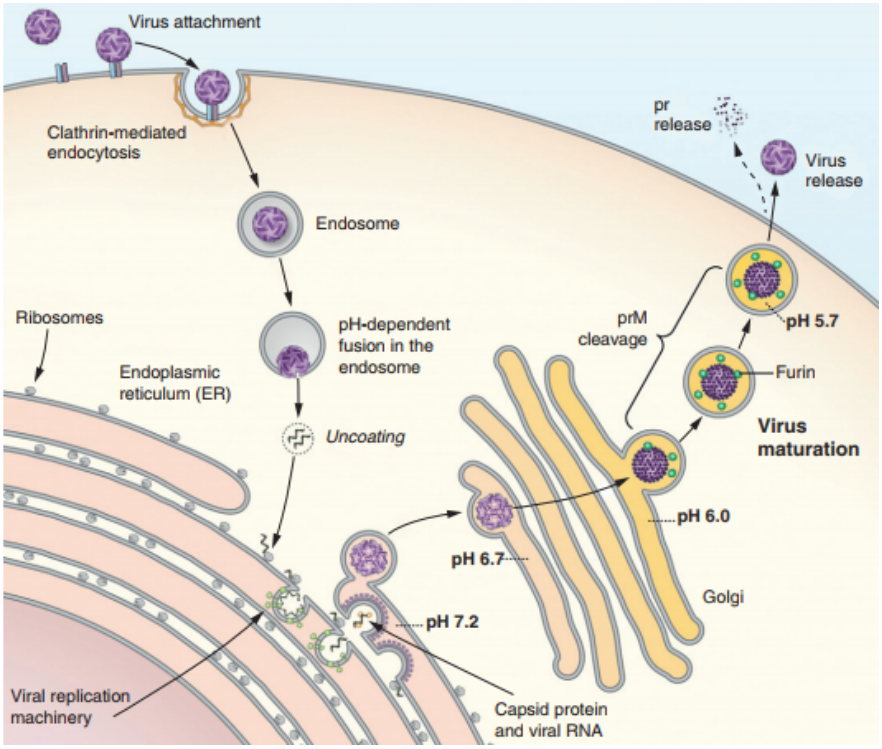

Figure 1.5 – ZIKV life cycle. The viral life cycle is initiated by the attachment of the virion to the cell surface and consecutive internalisation by clathrin-mediated endocytosis. In the endosome, the low pH of the lumen promotes conformational changes and, consequently, the release of the viral genomic RNA into the cytoplasm. Hither, the viral genome is translated into structural and non-structural proteins. The virus induces ER-rearrangements to form RFs, where ZIKV replication occurs. Close to these sites, the immature viral particles are assembled and conducted to the secretory pathway. The virions undergo maturation, where the low pH of the TGN induces a conformation change, allowing the cleavage of the prM by a furin-like protease. After maturation, the virions become infectious and leave the cell by exocytosis. Retrieved from Pierson and Diamond, 2013.[83]

The ZIKV replication occurs on virus-induced membranous replication factories (RFs) derived from the endoplasmic reticulum (ER), more specifically in vesicle packets (VPs).[22,84,85] Here, a negative-sense stranded RNA is copied from the viral RNA template, producing a double-stranded RNA (dsRNA). Afterwards, this dsRNA is transcribed asymmetrically, favouring the positive sense RNA.[86] The newly synthetised strand is packaged and immature viral particles are assembled near the replication vesicles.[87,88] These particles are conducted to the secretory pathway, where they become mature viral particles.[11,12] This virus maturation consists of a conformational change induced by the low pH present in the TGN, reorganising the virion surface.[89] The structural modification allows the cleavage of the prM by a furin-like protease.[11,12] Lastly, the infectious viral particles leave the cells by exocytosis and the pr fragment is dissociated from the virion due to the neutral pH of the extracellular environment **(Fig 1.5)**.[89]

1.2 Autophagy

Autophagy, also known as the process of cellular "self-eating", is a catabolic pathway that is highly conserved among eukaryotes. This system is extremely important for the maintenance of the cellular homeostasis and survival, since it degrades damaged or unwanted cytoplasmic proteins and organelles.[90] There are three types of autophagy described so far, namely, microautophagy, chaperone-mediated autophagy and macroautophagy.[91] The latter is going to be addressed here and referred to hereafter as autophagy. Autophagy can be triggered by stress factors such as nutrient starvation, accumulation of damaged cytoplasmic components, pathogen infection, ER stress, among others.[92,93] Thereby, it is tightly regulated to provide intracellular nutrients and energy if needed, ensuring the function of indispensable cellular processes.[94]

The first step of the autophagy pathway corresponds to the formation of the phagophore, also termed as isolation membrane, which is believed to derive mainly from the ER.[95,96] However, other additional autophagosomal membrane sources have been implicated, for example, plasma membrane,[97] Golgi complex,[98] and mitochondria.[99] This phagophore elongates to wrap and fully surround intracellular cargo or a portion of the cytoplasm, forming a double-membraned autophagosome. Afterwards, autophagosomes can go through an optional step that consists in the fusion with late endosomes, also named, multivesicular bodies (MVBs), from the endocytic pathway, to generate amphisomes.[100,101] Subsequently, autophagosomes and amphisomes fuse with lysosomes to give birth to autolysosomes.[101] This fusion allows the autophagosome to obtain an acidic lumen and hydrolases, which are responsible for the degradation of the autophagosome's inner membrane and the autophagic cargo.[102] The degradation products are exported back into the cytoplasm, by lysosomal permeases and transporters, where they can be reused for biosynthesis or to produce energy **(Fig 1.6)**.[102,103]

More than 30 autophagy-related genes (Atgs) are involved in the formation of the autophagosome, strictly regulating this process.[104] One of the key regulators of the initiation of autophagy is a nutrient sensing serine/threonine kinase, the mammalian target of rapamycin (mTOR).[105] Under nutrient-rich conditions, mTOR phosphorylates the Unc-like kinase 1 and 2 (ULK1/2) complex, suppressing autophagy.[106] On the other hand, during starvation, AMP-activated protein kinase (AMPK) represses the kinase activity of mTOR, which leads to the activation of the ULK1/2 complex, thereby inducing autophagy.[107]

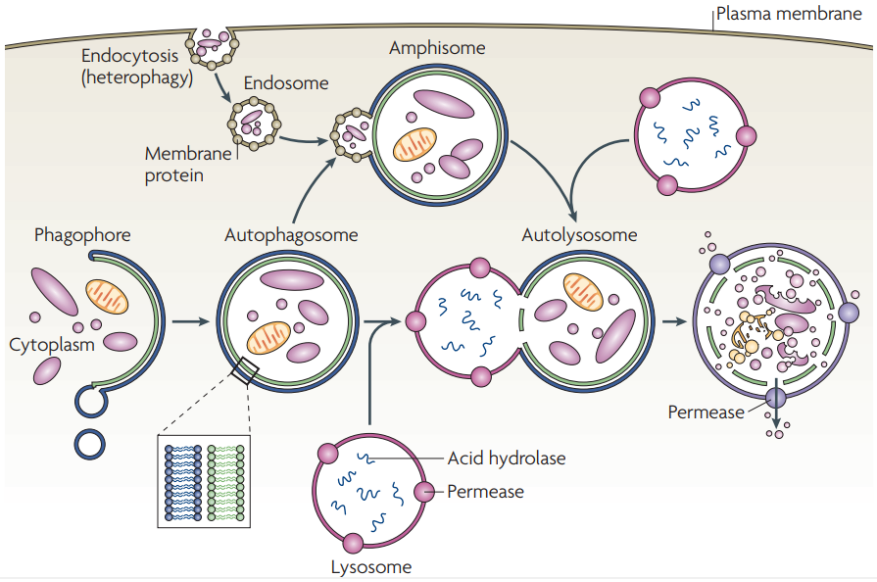

Figure 1.6 – Representative illustration of the autophagy pathway. Autophagy initiates with the formation of the phagophore, which elongates and fully enwraps the cargo, creating a double-membraned autophagosome. Then, the autophagosome can undergo an optional step and fuse with late endosomes/MVBs from the endocytic pathway, to generate amphisomes. The autophagosomes and amphisomes merge with lysosomes to form autolysosomes. This fusion allows the autophagosome to receive acidic hydrolases responsible for the degradation of the cargo and the inner membrane of the autolysosome. The degradation products leave the autolysosome by permeases, which were inherited by the lysosomes, for recycling. Retrieved from Klionsky, 2007.[108]

Upon autophagy activation, the ULK1/2 complex interacts with the vacuole membrane protein 1 (VMP1), activating the class III phosphatidylinositol-3-kinase (PI3KC3) complex which is composed by the vacuolar protein sorting 34 (Vsp34), p150, Beclin-1, and Atg14.[106,109] After being targeted the site of autophagosome initiation, the PI3KC3 complex synthetises a specific pool of phosphatidylinositol-3-phosphate (PI3P) that enriches this membrane region.[110] Hence, effectors harbouring PI3P-binding molecules, like double-FYVE-containing protein 1 (DFPC1) and WD-repeat domain phosphoinositide interacting (WIPI) protein family members, are translocated to this site.[111,112] These proteins promote the formation of an ER-associated membrane with an Ω-like shape ("omegasome").[111,113] Subsequently, the phagophore derived from the omegasome, elongates and encloses to form the autophagosome. This process is mediated by actions of two ubiquitin-like conjugation complexes Atg5-Atg12-Atg16L1 and Atg4-Atg3-LC3.[114] Initially, the Atg12-Atg5 conjugate is produced by Atg7 activation (E1-like enzyme), followed by Atg10 transfer (E2-like enzyme). Finally, this conjugate associates with Atg16L1 to create the Atg12-Atg5-Atg16L1 complex (E3-like enzyme).[109,114] The second ubiquitin-like system is the MAP1LC3 (microtubule-associated protein 1 light-chain 3) or short LC3. The C-terminal of LC3 is cleaved by the cysteine protease Atg4, exposing a glycine residue.[115,116] Then, the cytosolic LC3-I form is conjugated with the head group amine of phosphatidylethanolamine (PE), resulting in the lipidated LC3-II form.[117] This conjugation is mediated by the Atg7 (E1-like enzyme), the Atg3 (E2-like enzyme) and the Atg12-Atg5-Atg16L1 complex (E3-like enzyme).[117,118] The lipidated LC3-II form integrates into both the outer and inner membranes of autophagosomes.[115] The LC3-II present in the inner membrane is degraded together with the autophagic cargo, while the LC3-II located in the outer membrane is delipidated.[115,119] For this reason, LC3-II constitutes a common marker of autophagy. Furthermore, the protein p62, also termed sequestosome 1 (SQSTM1), recruits ubiquitinated cargos for degradation in the autophagic process, through directly binding to LC3-II during the autophagosome formation **(Fig 1.7)**.[120] Intracellular levels of p62 reflect the autophagic activity because its degradation is dependent on this process.[121] Thus, p62

is usually used as an autophagy marker, since an accumulation of p62 corresponds to autophagy inhibition.

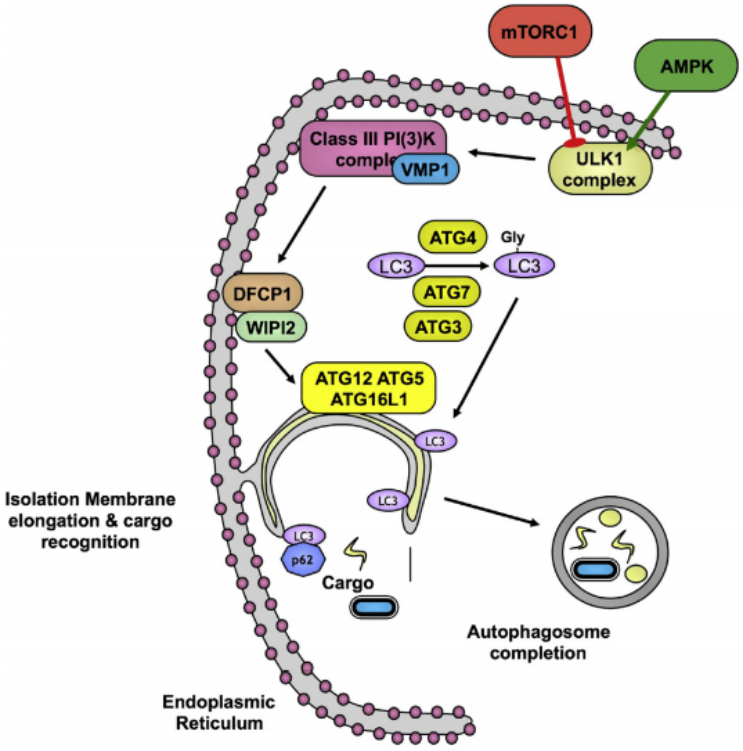

Figure 1.7 – Representative scheme of autophagosome formation. During starvation, AMPK supresses the kinase activity of mTOR, activating the ULK1/2 complex and thus, inducing autophagy. Upon activation of this complex, the VMP1 initiates the PI3KC3 complex to produce PIP3 to enrich the site chosen for the autophagosome formation. Later, the effectors DFCP1 and WIPI2 are recruited to this region and bind to the PIP3, promoting the phagophore formation. This phagophore elongates with the complex Atg12-Atg5-Atg16L1, whereas Atg4 cleaves LC3, exposing a Gly residue. Afterwards, Atg7, Atg3 and Atg12-Atg5-Atg16L1 mediate the conjugation of LC3 with PE, resulting in a lipidated form of LC3. This lipidated form will integrate into both inner and outer membrane of the autophagosome. The adaptor protein p62 recruits the cargo for degradation and binds to the LC3 on the inner membrane, followed by enclosing of the autophagosome. Retrieved and adapted from Harnett *et al.*, 2017.[106]

1.2.1 Autophagy modulators

Given the association of autophagy in many diseases, several chemical compounds have been developed or repurposed as therapeutic agents, to either enhance or suppress this process, according to its role on the progression of the disease.[122–124] From the innumerous autophagy modulators, 3-Methyladenine (3-MA), Bafilomycin A1 (BFLA), Ammonium Chloride (NH_4Cl), Chloroquine (CQ), U18666A (U18), and Rapamycin (Rapa) are going to be approached.

3-MA was first implied as an autophagy inhibitor, as a result of a screening of purines and related substances.[125] It is a class III PI3K inhibitor, repressing the production of PIP3, which is essential for the initiation of autophagy.[126,127]

BFLA is a plecomacrolide antibiotic, which contains a 16-membered lactone ring, produced by *Streptomyces griseus*.[128] This compound was demonstrated to be a potent and highly selective inhibitor of the vacuolar H^+-ATPase (V-ATPase) at nanomolar concentrations.[129] The V-ATPases, which are present in lysosomes and endosomes, are responsible for the acidification of the organelles' lumen.[130] By suppressing these proton pumps, the activation of lysosomal hydrolases is prevented, and consequently, the cargo degradation is impaired.[131] Therefore, BFLA is a late autophagy inhibitor.

NH_4Cl is dissociated until it reaches the membrane-permeable form, NH_3, which diffuses across lipid membranes and easily penetrates acidic compartments of the cell. Due to the low pH of these compartments, it gets protonated and impeded to diffuse back to the cytosol, hither accumulating.[132] As a lysosomotropic agent, it acts by raising the internal pH of lysosomes.[133] That being said, NH_4Cl inactivates lysosomal hydrolases and thus, inhibits autophagic cargo degradation.

CQ is also a lysosomotropic weak base that inhibits autophagy using the same principle as NH_4Cl. With this mechanism of action, it became a well-known FDA-approved drug to treat malaria.[134] CQ is also used to treat rheumatoid arthritis and other autoimmune diseases.[135]

U18 is an amphipathic steroid that prevents the intracellular trafficking of cholesterol, leading to its accumulation in late endosomes/MVBs and lysosomes.[136] As a result, their function in autophagy pathway is impaired. Cholesterol accumulation interferes with the function of the NPC1 protein, mimicking the lysosomal storage disease, Niemann-Pick type C disease.[136]

Rapa or Sirolimus, is a macrocyclic lactone produced by *Streptomyces hygroscopicus*.[137] This chemical is an immunosuppressive FDA-approved drug with antitumor and antifungal properties.[138] Rapa induces autophagy by downregulating the mTOR pathway.[138]

1.2.2 ZIKV and autophagy

As a highly regulated complex cellular system, autophagy can respond to viral infections in different ways. It can directly target pathogens for lysosomal degradation or can stimulate innate and adaptive immune responses.[90] Besides the antiviral protective mechanisms, the autophagic machinery can be exploited by viruses for their own benefit, promoting different stages of their life cycle[139].

Several studies have demonstrated the induction of autophagy by flaviviruses, including ZIKV. The first link between ZIKV and autophagy surged when viral particles were found in autophagosome-like structures associated with the ER in infected skin fibroblasts.[22] In the same study, the involvement of autophagy in ZIKV infection was further confirmed by treatment with Torin-1 (autophagy inducer), and 3-MA (autophagy inhibitor). Rapidly, other research on pharmacological modulation of autophagy were conducted on human fetal neural stem cells (fNSCs) and human trophoblasts (JEG-3), revealing changes in viral RNA copy and infectious viral particle numbers.[140,141] Recently, NS4A and NS4B were associated with the induction of autophagy by repressing the Akt-mTOR signalling pathway in human fNSCs.[140] On top of that, ZIKV infection results in ER membrane rearrangements, promoting the formation of VPs, which are believed to be the virus replication site.[22,84,85] Genetic knockout (KO) or knockdown of autophagy genes suppressed ZIKV replication, proposing that autophagy yields membrane structures for these RFs.[140] Another proviral function of autophagy is related with the ATG16L1, which was demonstrated to reduce the role of placenta as a protective barrier, allowing maternal-fetal transmission of ZIKV.[141]

2. OBJECTIVES

The main goal of this thesis was to investigate the impact of different factors, such as acidification of endosomal-lysosomal compartments, intracellular cholesterol trafficking and autophagy on the ZIKV life cycle.

Autophagy is a conserved cellular process that targets damaged or unwanted cytosolic proteins and organelles to lysosomal degradation, enabling cell survival and maintenance of cellular homeostasis. During virus infection, this pathway can be hijacked to promote different stages of the viral life cycle. Recently, the induction of autophagy was demonstrated on ZIKV-infected fibroblasts. To verify this effect on another line of ZIKV-permissive cells, A549 cells were infected with two strains of ZIKV. To define which steps of the autophagy pathway were essential for the ZIKV life cycle, modulation with Bafilomycin A1, U18666A, 3-Methyladenine, and Rapamycin was carried out. Bafilomycin A1 and U18666A have an indirect effect on autophagy by blocking the V-ATPases and causing accumulation of cholesterol in MVBs and lysosomes, respectively. Moreover, infected cells were treated with these modulators before or after infection to inspect the effects of treatment on the virus entry and on the spreading of the infection, respectively.

Thus, investigation of the relationship between autophagy and ZIKV infection can provide further insights in understanding the virus pathogenesis and to identify new therapeutic targets, and consequently, to develop compounds with antiviral activity against ZIKV.

3. MATERIALS AND METHODS

3.1 Materials

3.1.1 Mammalian cells

Table 3.1 – Mammalian cell lines used in the cell culture. Designation of the cell lines with correspondent description and source.

Cell line	Description	Source
A549	Adenocarcinoma human alveolar basal epithelial cells	Giard, D.J. (1962)[142]
Vero	African green monkey kidney cells	Yasumura, Y. & Kawakita, Y. (1962)[143]

3.1.2 Oligonucleotides for the light cycler

Table 3.2 – Oligonucleotides utilised for amplification of genomes in the light cycler. Designation of the oligonucleotides with the respective 5'→3' sequence. Oligonucleotides were synthetized by Biomers.net (Ulm, DE).

Oligonucleotide	Sequence (5'→3')
Human ribosomal protein L27 (hRPL27_fw)	aaa gct gtc atc gtg aag aac
Human ribosomal protein L27 (hRPL27_rev)	gct gct act ttg cgg ggg tag
Zika virus (ZIKV_fw)	aga tcc cgg ctg aaa cac tg
Zika virus (ZIKV_rev)	ttg caa ggt cca tct gtc cc

fw = forward; rev = reverse

3.1.3 Fluorescent dyes

Table 3.3 – Fluorescent dyes utilised in IF. Designation of the fluorescent dyes with the respective dilutions and manufacturer.

Fluorescent dye	Dilutions	Manufacturer
DAPI (0.1 mg/mL in PBS)	1:200	Carl Roth, Karlsruhe, DE
Filipin complex	1:100	Sigma-Aldrich, St.Louis, USA

3.1.4 Molecular weight markers

Table 3.4 – Protein marker used in WB. Designation of the protein marker with the correspondent manufacturer.

Protein marker	Manufacturer
PageRuler™ Prestained Protein Ladder	Thermo Fischer Scientific, Waltham, USA

3.1.5 Antibodies

Table 3.5 – Primary and secondary antibodies used in western blot (WB) and indirect immunofluorescence (IF). Designation of the antibodies with the correspondent species, clonality, dilutions, and manufacturer.

Antibody	Species/Clonality	Dilution (WB/IF)	Manufacturer
Primary antibodies			
Anti-ZIKV NS1	Mouse/Monoclonal	1:1000/-	BioFront Technologies, Tallahassee, USA
Anti-4G2	Mouse/Monoclonal	-/1:300	Merck Millipore, Darmstadt, DE
Anti-LC3	Rabbit/Polyclonal	1:1000/-	BIOZOL Diagnostica Vertrieb GmbH, Echnig, DE
Anti-p62	Guinea pig/Polyclonal	1:1000/1:200	Progen Biotechnik GmbH, Heidelberg, DE
Anti-LAMP2	Mouse/Monoclonal	1:800/-	BD Biosciences, Franklin Lakes, USA
Anti-Lamin (H-102)	Rabbit/Polyclonal	-/1:500	Santa Cruz Biotechnology, Dallas, USA
Anti-β-Actin	Mouse/Monoclonal	1:10.000/-	Sigma-Aldrich, St.Louis, USA
Secondary antibodies			
Anti-mouse IgG-HRP	Donkey/Polyclonal	1:2000/-	GE Healthcare, Little Chalfont, UK
Anti-rabbit IgG-HRP	Donkey/Polyclonal	1:2000/-	GE Healthcare, Little Chalfont, UK
Anti-mouse IRDye800CW	Donkey/Polyclonal	1:10.000/-	LI-COR Biosciences, Lincoln, USA
Anti-mouse IRDye680RD	Donkey/Polyclonal	1:10.000/-	LI-COR Biosciences, Lincoln, USA
Anti-mouse IgG-Alexa 488	Donkey/Polyclonal	-/1:1000	Thermo Fischer Scientific, Waltham, USA
Anti-guinea pig IgG-Cy3	Donkey/Polyclonal	-/1:400	Jackson ImmunoResearch, West Grove, USA
Anti-rabbit IgG-Cy5	Donkey/Polyclonal	-/1:400	Thermo Fischer Scientific, Waltham, USA

HRP = horseradish peroxidase; Cy3 = cyanine3; Cy5 = cyanine5

3.1.6 Inhibitors

Table 3.6 – Inhibitors used in this project. Designation of the inhibitors with the correspondent target and manufacturer.

Inhibitor	Target	Manufacturer
3-Methyladenine	PI3-kinase	Selleckchem, Houston, USA
Aprotinin	Serine proteases	AppliChem, Darmstadt, DE
Bafilomycin A1	Vacuolar-type H^+-ATPase	Sigma-Aldrich, St.Louis, USA
Leupeptin	Serine and cysteine proteases	AppliChem, Darmstadt, DE
Pepstatin	Acidic and aspartic proteases	AppliChem, Darmstadt, DE
PMSF	Serine proteases	Carl Roth, Karlsruhe, DE
Rapamycin	mTOR	Selleckchem, Houston, USA

3.1.7 Reagents for cell culture

Table 3.7 – Reagents utilised in cell culture. Designation of the reagents with the respective manufacturer.

Reagent	Manufacturer
DMEM medium (4.5 g/L glucose)	Biowest, Nuaillé, FR
PBS without Ca^{2+} and Mg^{2+}	Paul-Ehrlich-Institut, Langen, DE
Fetal bovine serum (FBS superior)	Biochrom GmbH, Berlin, DE
L-glutamine	Biochrom GmbH, Berlin, DE
Penicillin/streptomycin	Paul-Ehrlich-Institut, Langen, DE
Tripsin/EDTA (0.05% Trypsin)	Paul-Ehrlich-Institut, Langen, DE

3.1.8 Kits

Table 3.8 – Kits used in this project. Designation of the kits with the correspondent manufacturer.

Kit	Manufacturer
QIAamp® viral RNA Mini Kit	Qiagen, Hilden, DE
LightCycler® Multiplex RNA Virus Master	Roche, Basel, CH
LDH Cytotoxicity Detection Kit	Takara Bio USA, Inc., Mountain View, USA

3.1.9 Enzymes

Table 3.9 – Enzymes utilised for cDNA synthesis. Designation of the enzymes with the respective manufacturer.

Enzyme	Manufacturer
RevertAid H Minus Reverse Transcriptase	Thermo Fischer Scientific, Waltham, USA
RQ1 RNase-free DNase	Promega, Fitchburg, USA

3.1.10 Buffers and solutions

Table 3.10 – Buffers and solutions required in this project. Designation of the buffers and solutions with the respective composition. All buffers and solutions were prepared with DEPC-H_20, obtained from a Milli-Q Ultrapure water system (Paul-Ehrlich-Institut, Langen, DE). Exceptions are indicated.

Buffer	Composition
Anode buffer I	20% Ethanol (v/v) 300 mM Tris
Anode buffer II	20% Ethanol (v/v) 25 mM Tris
Cathode buffer	20% Ethanol (v/v) 40 mM 6-aminohexanoic acid
RIPA buffer	50 mM Tris-HCl pH 7.2 150 mM NaCl 0.1% SDS (w/v) 1% Sodium desoxycholate (w/v) 1% Triton X-100
SDS running buffer (10x)	0.25 M Tris-Base 2 M Glycine 1% SDS (w/v) pH 8.3
SDS loading buffer (4x)	4% SDS (w/v) 125 mM Tris-HCl pH 6.8 10% Glycerol (v/v) 10% β-Mercaptoethanol (v/v) 0.02% Bromophenol blue (w/v)
Separation gel buffer	1.5 M Tris 0.4% SDS (w/v) pH 8.8
Stacking gel buffer	0.5 M Tris 0.4% SDS (w/v) pH 6.7

Solution	Composition
10% APS	APS diluted 1:100
1x Roti-Block	10x Roti-Block diluted 1:10
4% Formaldehyde	Formaldehyde diluted in PBS
Crystal violet	0.1% crystal violet in 20% ethanol
Mowiol	10% Mowiol (w/v) 25% Glycerol (w/v) 2.5% DABCO 100 mM Tris-HCl pH 8.5
PBST	PBS without Ca^{2+} and Mg^{2+} 0,5 % Triton X-100 (v/v)

3.1.11 Chemicals

Table 3.11 – Chemicals required in this project. Designation of the chemical with the correspondent manufacturer.

Chemical	Manufacturer
3-MA	Selleckchem, Houston, USA
5x Reaction buffer for RT	Thermo Fischer Scientific, Waltham, USA
6-Aminohexanoic acid	Paul-Ehrlich-Institut, Langen, DE
10 mM dNTPs	Thermo Fischer Scientific, Waltham, USA
Acetone	Carl Roth, Karlsruhe, DE
Ammonium chloride	Merck Millipore, Darmstadt, DE
APS	Carl Roth, Karlsruhe, DE
BFLA	Sigma-Aldrich, St.Louis, USA
β-mercaptoethanol	Sigma-Aldrich, St.Louis, USA
BSA fraction V	AppliChem, Darmstadt, DE
Bradford reagent	Sigma-Aldrich, St.Louis, USA
Bromophenol blue	Merck Millipore, Darmstadt, DE
Butanol	Merck Millipore, Darmstadt, DE
Chloroform	Carl Roth, Karlsruhe, DE
CQ	Sigma-Aldrich, St.Louis, USA
Crystal violet	Sigma-Aldrich, St.Louis, USA
DABCO	Merck Millipore, Darmstadt, DE

DEPC-H_2O	Paul-Ehrlich-Institut, Langen, DE
DMSO	Genaxxon, Biberach, DE
EDTA	Paul-Ehrlich-Institut, Langen, DE
Ethanol (pure)	Carl Roth, Karlsruhe, DE
Formaldehyde (37,5%)	Carl Roth, Karlsruhe, DE
Glutaraldehyde	Carl Roth, Karlsruhe, DE
Glycerol	GERBU Biotechnik GmbH, Heidelberg, DE
Hydrochloric acid	Carl Roth, Karlsruhe, DE
Isopropanol	Carl Roth, Karlsruhe, DE
Luminata Forte Western HRP Substract	Merck Millipore, Darmstadt, DE
Maxima Probe SYBR Green qPCR Master Mix	Thermo Fischer Scientific, Waltham, USA
Methanol	Carl Roth, Karlsruhe, DE
Mowiol	Sigma-Aldrich, St.Louis, USA
PBS	Paul-Ehrlich-Institut, Langen, DE
peqGOLD TriFast	peqLab, Erlangen, DE
Phenol	AppliChem, Darmstadt, DE
PrestoBlue® cell viability reagent	Thermo Fischer Scientific, Waltham, USA
Random hexamer primer	Thermo Fischer Scientific, Waltham, USA
RAPA	Selleckchem, Houston, USA
Roti 40 Acrylamide/Bisacrylamide	Carl Roth, Karlsruhe, DE
Roti-Block (10x)	Carl Roth, Karlsruhe, DE
RQ1 DNase 10x reaction buffer	Promega, Fitchburg, USA
RQ1 DNase stop solution	Promega, Fitchburg, USA
SDS	Paul-Ehrlich-Institut, Langen, DE
SeaPlaque® Agarose	FMC BioProducts, Rockland, USA
Skim milk powder	Carl Roth, Karlsruhe, DE
Sodium chloride (NaCl)	Carl Roth, Karlsruhe, DE
Sodium hydroxide (NaOH)	Carl Roth, Karlsruhe, DE
Sodiumdesoxycholat	Carl Roth, Karlsruhe, DE
SuperSignal West Pico Luminol/Enhancer	Thermo Fischer Scientific, Waltham, USA
SuperSignal West Pico Stable Peroxide Solution	Thermo Fischer Scientific, Waltham, USA
TBST	Paul-Ehrlich-Institut, Langen, DE
TEMED	AppliChem, Darmstadt, DE
Tris	Carl Roth, Karlsruhe, DE

Tris-HCl	Paul-Ehrlich-Institut, Langen, DE
Triton X-100	Sigma-Aldrich, St.Louis, USA
U18	Sigma-Aldrich, St.Louis, USA

3.1.12 Expendables materials

Table 3.12 – Expendable materials utilised in this project. Designation of the material with the respective manufacturer.

Material	**Manufacturer**
Cell culture flasks (T175)	Greiner Bio-One GmbH, Frickenhausen, DE
Cell culture plates (6, 12, 96 wells)	Greiner Bio-One GmbH, Frickenhausen, DE
Cell scrapers	A. Hartenstein GmbH, Würzburg, DE
Coverslips (18 mm)	Thermo Fischer Scientific, Waltham, USA
Disposable syringes	B.Braun, Melsungen, DE
Falcon tubes (15 mL, 50 mL)	Greiner Bio-One GmbH, Frickenhausen, DE
Fixer type F 1-2	C & L GmbH, Planegg, DE
FrameStar® 96 PCR Plate for LC480	GeneON, Ludwigshafen, DE
Developer type E 1-3	C & L GmbH, Planegg, DE
Graduated pipettes (2 mL, 5 mL, 10 mL, 25 mL)	Greiner Bio-One GmbH, Frickenhausen, DE
Hybond-P, PVDF Membrane	Carl Roth, Karlsruhe, DE
Hyperfilm ECL Chemiluminescence	GE Healthcare, Freiburg, DE
LightCycler capillaries (polycarbonate)	Genaxxon, Biberach, DE
Microscope slides	Carl Roth, Karlsruhe, DE
Parafilm	Bemis, Bonn, DE
Petri Dishes	Sarstedt AG & Co, Nümbrecht, DE
Phase Lock Gel Heavy (2 mL)	5PRIME Hilden, DE
Pipette Tips (10 µL, 100 µL, 300 µL, 1000 µL)	Sarstedt AG & Co, Nümbrecht, DE
Pipette Tips with filter (10 µL, 100 µL, 300 µL, 1000 µL)	Biotix, California, USA
Reaction tubes (1.5 mL, 2 mL)	Sarstedt AG & Co, Nümbrecht, DE
Sterile filters (0.22 µm)	Carl Roth, Karlsruhe, DE
Whatman paper 3 mm	VWR International GmbH, Darmstadt, DE

3.1.13 Devices

Table 3.13 – Devices required in this project. Designation of the device with the correspondent manufacturer.

Device	Manufacturer
AGFA Curix60 Film Developer	AGFA, Köln, DE
Axiovert 40C	Zeiss, Oberkochen, DE
CO_2-Incubator BBD 6220	Thermo Fischer Scientific, Waltham, USA
Confocal laser scanning microscope LSM 510	Zeiss, Oberkochen, DE
EM 109	Zeiss, Oberkochen, DE
Eppendorf centrifuge 5415D	Eppendorf, Hamburg, DE
Hemocytometer	Carl Roth, Karlsruhe, DE
Heraeus Fresco 17 Centrifuge	Thermo Fischer Scientific, Waltham, USA
Heraeus Multifuge 1S-R	Thermo Fischer Scientific, Waltham, USA
Hoefer electrophoresis power supply EPS301	GE Healthcare, Freiburg, DE
Hypercassette™	GE Healthcare, Freiburg, DE
Infinite M1000	Tecan, Männedorf, CH
LightCycler 480	Roche, Basel, CH
LightCycler R1.5 instrument	Roche, Basel, CH
Microcentrifuge	Carl Roth, Karlsruhe, DE
Mighty small multiple gel caster SE200 Series	GE Healthcare, Freiburg, DE
Nanophotometer P300	Implen, München, DE
Odyssey infrared imaging system	LI-COR Biosciences, Lincoln, USA
Pipettes	Eppendorf, Hamburg, DE
Promax 1020 shaker	Heidolph, Kelheim, DE
RCT Classic Magnetic stirrer	IKA, Staufen, DE
S20 – SevenEasy™ pH	Mettler Toledo, Ohio, USA
Sartorius balance TP 6000 200S	Sartorius, Göttingen, DE
Sartorius universal analytical balance	Sartorius, Göttingen, DE
Sonopuls HD 220	Bandelin, Berlin, DE
Standard power pack P25	Biometra, Göttingen, DE
SterilGard®III Advance	The Baker Company, Maine, USA
Stuart roller mixer SRT9	Bibby Scientific, Stone, UK
TE77 ECL-Semi-Dry Transfer Unit	GE Healthcare, Freiburg, DE
Thermomixer compact	Eppendorf, Hamburg, DE

Vortex-Genie 2	Scientific Industries, New York, USA
Water bath TW12	Julabo, Seelbach, DE

3.1.14 Software

Table 3.14 – Software used in this project. Designation of the software with the respective manufacturer.

Software	**Manufacturer**
Graph Pad Prism 7	GraphPad Software, La Jolla, USA
i-control 1.8	Tecan, Männedorf, CH
Image Studio	LI-COR Biosciences, Lincoln, USA
Image Studio Lite	LI-COR Biosciences, Lincoln, USA
LightCycler Software Version 3.5	Roche, Basel, CH
MS Office	Microsoft, Redmond, USA
ZEN 2012 black edition	Zeiss, Oberkochen, DE
ZEN 2012 blue edition	Zeiss, Oberkochen, DE

3.2 Methods

3.2.1 Cell biology

3.2.1.1 Eukaryotic cell culture

In this study, A549 and Vero cells were used. Cells were cultivated in 175 cm^2 flasks with Dulbecco's Modified Eagle's Medium (DMEM) supplemented with 10% FBS superior, 1% penicillin/streptomycin and 1% L-glutamine, further referred to as DMEM complete. Both cell lines were grown in an incubator at 37ºC with a content of 5% CO_2 and 90% of relative humidity. Passaging of adherent cells was performed 3 times a week at 60%-90% confluence by trypsinisation. The cells were carefully washed with 10 mL of PBS and detached from cell culture flasks by incubation with 2.5 mL of trypsin/EDTA solution for 5 min at 37°C. Protease activity of trypsin was stopped by adding 7.5 mL of DMEM complete and cells were resuspended and seeded in fresh medium at different dilutions (1:2-1:10) to obtain optimal growth. To perform experiments, resuspended cells were seeded in 6-, 12- or 96-well plates at a density of $3x10^5$, $1.5x10^5$ and $1x10^4$ cells per well or $3.5x10^6$ cells in Petri dishes. All cell culture procedures were performed in laminar-flow hoods using aseptic techniques, sterile equipment and solutions.

3.2.1.2 Infection of A549 cells

All experiments and maintenance of infectious cells were performed under biosafety level 3 (BSL-3) conditions. A549 cells were infected with French Polynesia (PF13/251013-18) and Uganda (MR766) strains of Zika virus (ZIKV). Prior infection, cells were seeded in 12-well plates for 5 h, allowing the cells to adhere to the surface of the well. To infect seeded cells consistently with the same amount of virus, supernatants from previously infected cells were harvested and titrated by plaque forming assay (see Chapter 3.2.1.5). After determination of the virus titers, the supernatants were stored in aliquots at -80ºC. A multiplicity of infection (MOI) of 0.1 was chosen to infect A549 cells in this study. MOI represents the ratio of infectious viral particles per cell. Thus, a MOI of 0.1 indicates that there is one infectious viral particle present per 10 cells. The input of the virus was stopped 16 h post-infection (hpi) by removing the medium from the wells and washing cells once with PBS.

3.2.1.3 Autophagy modulation

A549 cells were treated with autophagy modulators for different periods of time and concentrations, as summarised in Table 3.15. The modulators were added 2 h before infection (pre-infection treatment) or 2 h after infection (post-infection treatment), according to the goal of the experiment. All substances were supplied with DMEM complete to the cells. The treatment was renewed every day to assure the maximum effect of the compounds in cells.

Table 3.15 – Autophagy modulators used in cell culture. Designation of the autophagy modulator with the correspondent final concentration in each well and the type of treatment applied.

Modulator	Final concentration	Type of treatment
Bafilomycin A1 (BFLA)	10 nM	Pre- and post-infection
U18666A (U18)	2 µg/mL	Pre- and post-infection
Rapamycin (RAPA)	100 nM	Post-infection
3-Methlyadenine (3-MA)	5 mM	Post-infection

3.2.1.4 Cell viability and cytotoxicity assays

To investigate the cell viability after treatment with autophagy modulators and to determine the cytotoxicity of these compounds, PrestoBlue and lactate dehydrogenase (LDH) assays were performed, respectively. For this purpose, A549 cells were treated with different concentrations of autophagy modulators for 24, 48, and 72 h.

The PrestoBlue assay is a calorimetric method that measures the metabolic active cells by using the PrestoBlue reagent. This reagent is metabolically reduced by viable cells from resazurin to resofurin, a fluorescent compound.[144] A549 cells were seeded in 96-well plates for 5 h to allow its adherence to the surface of the wells. Subsequently, cells were treated with the substances and the treatment was renewed every day. To determine the cell viability at the desired time points, the medium was removed, followed by the addition of 100 µL of the PrestoBlue reagent diluted 1:10 in DMEM complete to each well. After an incubation time of 1 h at 37ºC, the fluorescence of the reagent (excitation wavelength: 560 nm, 10 nm bandwidth; emission wavelength: 590 nm, 10 nm bandwidth) was measured in the Infinite M1000 (Tecan reader).

The LDH assay is a calorimetric method as well, which estimates the number of dead cells by quantitatively measuring the LDH released into the cell culture medium from damaged cells.[145] Therefore, it is commonly used as a biomarker for cytotoxicity and cytolysis. To measure the cytotoxicity of the autophagy modulators, A549 cells were seeded in 96-well plates for 5 h and treated with the compounds. At the appropriate time points, 100 µL of the supernatant was harvested and tested for LDH activity. 100 µL of the reaction mix included in the kit was added, upon which tetrazolium (yellow) is converted by diaphorase to formazan (red).[145] This conversion is only possible if LDH is present in the supernatant and provides necessary reduction equivalents. Thus, an increase in LDH activity stems from dead or membrane-damaged cells, which correlates directly with the amount of formazan formed. Plates were protected from light and incubated for 30 min at room temperature. Following this, the absorbance of formazan was measured at 490 nm in the Infinite M1000 (Tecan reader). The cytotoxicity was calculated by setting cells treated with 2% Triton X-100 to 100% (positive control) and untreated cells to 0% (negative control). In this assay, the DMEM was supplemented with 1% FBS superior instead of 10%, since it contains LDH, increasing the fluorescence measured.

In both assays, 2% of Triton X-100 was included as positive control, as it is a well-known non-ionic detergent that induces cellular apoptosis when used during long periods of time or in high concentrations.[146] On the other hand, DMEM complete was used as negative control.

3.2.1.5 Virus titration

To determine the virus concentration inside and outside cells, intra- and extracellular plaque forming assay was performed. For the intracellular plaque forming assay, infected A549 cells were harvested using 100 µL of trypsin per well. After 3 min incubation at 37ºC, the cell suspension was transferred into 1.5 mL reaction tubes and 600 µL DMEM complete was added. Subsequently, the suspension was frozen and thawed three times at -80ºC and 37ºC respectively, to achieve cell lysis. After cell lysis, the suspension was centrifuged at 4ºC, maximum speed for 15 min.

For both, intra- and extracellular plaque assay, 10-fold dilutions (non-diluted to 10^{-5}) of supernatant were utilised to infect seeded Vero cells in 6-well plates. Then, the plates were placed into the incubator at 37ºC for 2 h, allowing attachment of the infectious viral particles to the cell surface. Subsequently, the medium, including unbound infectious viral particles, was removed. To prevent a wide spread of newly synthesised viral particles, an agarose overlay was prepared. A solution of 4% SeaPlaque® agarose was boiled in a microwave and cooled to 65ºC in a water bath. Following this, the agarose was diluted 1:10 in DMEM complete (37ºC), well mixed and 2 mL were poured carefully over the cells in each well. Finally, after 15 min at room temperature, the solidification of the agarose overlay was achieved and the plates were placed into the incubator at 37ºC. After 4 days of incubation, to allow formation of sufficiently visible plaques, the overlay was carefully removed and a staining applied. First, cells were fixed for 15 min in 4% formaldehyde. The cells were washed once with PBS and stained with 400 µL crystal violet solution for 15 min. Subsequently, the plates were washed once with water and plaques counted.

3.2.1.6 Cell harvest and lysis

A549 cells were harvested after 24, 48, and 72 hpi. Medium was removed and cells were washed once with PBS. Subsequently, the plates were frozen in -80ºC for storage or fixed for indirect immunofluorescence (see Chapter 3.2.4.1) and placed at 4ºC in PBS. Different methods of cell lysis were performed according to the goal of the experiment. To assess to the intracellular RNA, 200 µL of TriFast was added to each well and cells collected into 1.5 mL reactions tubes. To create protein cell lysates, 100 µL of RIPA buffer, supplemented with protease inhibitors (see Chapter 3.1.3), was added to each well and incubated for 5 minutes. Subsequently, the cells were removed with a cell scraper and transferred into a 1.5 mL reaction tube. Finally, the samples were sonicated for 10 s at 20% power, centrifuged for 10 min at 4ºC and maximum speed, and stored at -20ºC. Protein concentration was estimated by Bradford assay (see Chapter 3.2.3.1).

3.2.2 Molecular biology

3.2.2.1 Isolation of the total intracellular RNA

After cells being lysed and homogenized with the TriFast reagent (see Chapter 3.2.1.6), the intracellular RNA was isolated by a phenol/chloroform extraction. After homogenization, a centrifugation of 10 min at 4ºC and 13.300 rpm was performed and the supernatant was transferred into a new reaction tube. With this step, insoluble material such as polysaccharides, extracellular membranes and high molecular weight DNA was removed.[147] To assure complete dissociation of nucleoprotein complexes, an incubation of 5 min at room temperature was necessary. Subsequently, 240 µL of chloroform were added to the reaction tube, followed by a mixing step of 15 s using a vortex. This step was followed by an incubation for 5 min at room temperature. Then, the whole sample was transferred to a Phase Lock Gel

tube and the phase separation was accomplished by a centrifugation at 13.300 rpm and 4ºC for 1 min. This tube contains a gel, which during centrifugation migrates and creates a barrier between the organic and aqueous phases, eliminating interphase-protein contamination. The aqueous phase, which contains the RNA, was transferred to a new reaction tube. The precipitation of RNA was carried out by adding 600 µL of isopropanol and subsequent centrifugation for 30 min at 13.300 rpm and 4ºC. Afterwards, the supernatant was removed and the RNA pellet was washed with 75% ethanol, followed by centrifugation for 30 min at 13.300 rpm and 4ºC. Lastly, the RNA was solubilised with 15-50 µL of DEPC-H_20, after the excess of isopropanol was removed.

3.2.2.2 Determination of RNA concentration

The concentration of RNA was accomplished by a nanophotometer at a wavelength of 260 nm. First, a blank with DEPC-H_20 was set. For the measurement of the RNA concentration, 1 µL of the sample was applied on the cuvette with a lid factor of 10 or 50. Each sample was measured in triplicates. To determine the purity of the RNA and detect possible DNA or phenol contaminations, the Abs260 nm/Abs280 nm ratio was calculated as well.

3.2.2.3 cDNA synthesis

To eliminate potential DNA contaminations derived from the RNA isolation procedure (see Chapter 3.2.2.1), a DNase digestion step was included. For this purpose, 4 µg of total RNA were incubated with DNase I (RQ1 RNase-free DNase) at 37ºC for 1 h with the corresponding buffer, as described in Table 3.16.

Table 3.16 – Components required for DNase digestion. Designation of the component with the respective volume applied per sample.

Component	Volume (µL)
RNA	x µL (equivalent to 4 µg)
RQ1 RNase-free DNase	1 µL
RQ1 DNase 10x Reaction Buffer	1.1 µL
DEPC-H_2O	Fill up to 11 µL

Inactivation of DNase I was achieved by adding 1 µL of RQ1 DNase Stop Solution to the reaction tube, followed by an incubation for 10 min at 65ºC. The transcription was started by incubating 1 µL of random hexamer primer at 65ºC for 15 min, allowing the primer annealing. First strand cDNA synthesis was initiated by the addition of 7 µL of the Mastermix to the reaction tube, as specified in Table 3.17. Subsequently, incubation at room temperature for 10 min and at 42ºC for 1 h was carried out. Finally, the RT was inactivated at 72ºC for 10 min.

Table 3.17 – Components required for cDNA synthesis. Designation of the component with the correspondent volume applied per sample.

Component	Volume (µL)
5x RT buffer	4 µL
dNTPs mix (10 mM each)	2 µL
RevertAid H Minus Reverse Transcriptase	1 µL

3.2.2.4 Isolation of the extracellular RNA

From the supernatants harvested, extracellular RNA was isolated using the QIAamp Viral RNA Mini Kit according to the manufacturer's instructions. In brief, the sample was lysed and applied into a column for RNA binding. Then, the RNA was washed with two buffers and collected into 1.5 mL reaction tubes by a single elution with 60 µL of the elution buffer.

3.2.2.5 Determination of intracellular ZIKV genomes by RT-qPCR

To detect and quantify intracellular transcripts, the LightCycler 480 and 1.5 systems with the SYBR Green method were utilised. During the PCR, the fluorescent dye SYBR Green binds to the DNA, enabling its quantification. The increase of fluorescence is directly proportional to the amount of amplified DNA and measured after each PCR cycle. From these data, the n-fold expression, using the $2^{-\Delta\Delta Cp}$ method was calculated. For normalisation of the measured values, the house-keeping gene hRPL27 was analysed. For each reaction, 3 µL of cDNA diluted 1:10 was added to 7 µL of the Mastermix (5 µL of 2x SYBR Green, 0.25 µL of each oligonucleotide [10 µM] and 1.5 µL nuclease-free-water) into FrameStar® 96 PCR Plate for LC480 or LightCycler capillaries. The plates/capillaries were placed into the instrument and the RT-qPCR program was executed, as described in Table 3.18.

Table 3.18 – RT-qPCR program used for quantification of intracellular genomes. Designation of the parts of the program with the respective temperature, hold time, slope and number of cycles.

Program	Temperature (ºC)	Hold time (s)	Slope (ºC/s)	Cycles
Initial denaturation	95	600	20	1
Denaturation	95	15	20	45
Annealing	56	30	20	
Elongation	72	30	5	
Melting	95	60	20	1
	60	30	20	
	95	0	0.1	
Cooling	40	30	20	

3.2.2.6 Determination of extracellular ZIKV genomes by RT-qPCR

Quantification of extracellular ZIKV genomes was performed by RT-qPCR analysis. For the reaction, the components from the LightCycler Multiplex RNA Virus Master Kit were utilised according to the instructions of the manufacturer. 5 µL of the Mastermix (components from the kit) were added to 5 µL of undiluted RNA sample into FrameStar® 96 PCR Plate for LC480 or LightCycler capillaries. The plates/capillaries were placed into the instrument and the RT-qPCR program was executed, as detailed in Table 3.19. From these data, the n-fold expression, using the $2^{-\Delta Cp}$ method was calculated.

Table 3.19 – RT-qPCR program used for quantification of extracellular genomes. Designation of the parts of the program with the respective temperature, hold time, slope and number of cycles.

Program	Temperature (ºC)	Hold time (s)	Slope (ºC/s)	Cycles
RT	50	600	4.4	1
Initial denaturation	95	30	4.4	1
Amplification	95 60	5 30	4.4 2.2	45
Melting	95 60	10 10	4.4 2.2	1
Cooling	40	2	2.2	

3.2.3 Protein biochemistry

3.2.3.1 Protein quantification by Bradford assay

The total protein amount of cell lysates was quantified using the Bradford reagent.[148] This reagent contains the dye Coomassie Brilliant Blue G-250, which shifts its absorbance from red to blue after contact with proteins (from 465 to 595 nm). To perform this assay, 5 µL of the cell lysates were mixed with 100 µL of Bradford reagent in 96 well plates. After 5 min of incubation at room temperature and protected from light, the well-plate was placed in the Infinite 1000 (Tecan reader) to measure the absorbance at 595 nm. Protein concentrations were calculated using a standard curve generated with BSA.

3.2.3.2 SDS-PAGE

Protein mixtures were separated by SDS-PAGE depending on their molecular weight.[149] Since it is a discontinuous system, this gel is composed of a stacking gel and a separation gel. The first one allows proteins to get concentrated by choosing a polymer density of 4%. This is followed by a separation gel, whose density varies according to the expected size of the protein of interest, in which the SDS-denatured proteins are separated.

10% and 14% of bisacrylamide concentrations were chosen for detection of the proteins of interest. These concentrations were mixed with TEMED and APS and applied between glass plates for polymerisation. After polymerisation of the separating gel has concluded, 4% of bisacrylamide for the stacking gel was poured on top of this gel and then polymerised. SDS gels were set into chambers filled with 1x SDS running buffer. On every gel, equal amount of protein (100 µg) were denatured in 1x SDS-

PAGE loading buffer by heating for 10 min at 95ºC, and subsequently separated in a vertical chamber at 100-160 V.

3.2.3.3 Western blot

Proteins separated by SDS-PAGE were transferred onto a methanol-activated PVDF-membrane, via a semi-dry blotting chamber and a discontinuous system (1.3 mA/cm^2 for 1 h)[150], as illustrated in Fig 3.1.

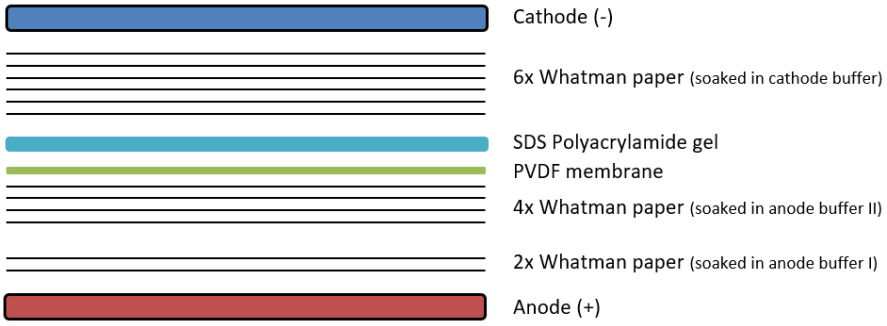

Figure 3.1 – Schematic representation of a semi-dry blot stack. Negatively charged proteins are transferred from the gel to the membrane, in direction to the cathode (+). From bottom to top: two layers of *Whatman* paper, soaked in anode buffer I; four layers *Whatman* papers, soaked in anode buffer II; one methanol-activated PVDF membrane; SDS gel with separated proteins; six layers *Whatman* paper, soaked in cathode buffer.

In order to prevent unspecific interactions, the membrane was blocked using 5% (w/v) BSA in TBST or 10% (w/v) skim milk powder in TBST for 1 h at room temperature. The blocking solution was chosen depending on the primary antibody used. Later on, the membrane was incubated with the primary antibody, diluted in the blocking solution, for 1 h at room temperature or overnight at 4ºC. Unspecific bounded antibody was removed by washing 3x 10 min in TBST, followed by incubation of the membrane with the secondary antibody against the species of the primary antibody for 1 h, at room temperature. As secondary antibodies, either a horseradish peroxidase (HRP)-coupled antibody, diluted in the blocking solution or a fluorophore-coupled antibody, diluted in 1x Roti®-Block were used. Unbound antibody was again removed by washing 3x 10 min with TBST. Proteins bands were detected with peroxidase substrate reagent and scientific imaging films or, as alternative, by using the LICOR-Odyssey System.

3.2.4 Microscopy

3.2.4.1 Indirect immunofluorescence microscopy

Determination of intracellular localisation and distribution of proteins, as well as the estimation of the number of ZIKV-positive cells were achieved by immunostaining of permeabilized cells with fluorophore-coupled antibodies. Therefore, A549 cells were grown on coverslips in 12-well plates. Prior fixation, medium was removed and cells were washed with PBS. The fixation solution was chosen according to the antibodies used. Thus, cells were either fixed with ice-cold ethanol:acetone (1:1) or in 4% formaldehyde in PBS for 10 min and 20 min at room temperature, respectively. Afterwards, cells were washed twice with PBS. According to the fixation solution, different protocols were followed, as summarised in Table 3.20.

Table 3.20 – Different protocols used in IF. Designation of each step and the respective treatment according to the fixation method, either ethanol:acetone or 4% formaldehyde. Unless indicated otherwise, 1 mL of the solutions was used per well. All steps, except antibody incubations, were performed while shaking. All steps were executed in room temperature.

Step	Ethanol:acetone	4% Formaldehyde
Permeabilisation	TBST for 10 min	PBST for 10 min
Washing	3x 5 min with TBST	3x 5 min with PBS
Blocking	10% BSA in TBST	1% BSA in PBS
Primary antibody incubation	50 µL per coverslip for 1 h (antibodies diluted in blocking solution)	50 µL per coverslip for 1 h (antibodies diluted in blocking solution)
Washing	3x 5 min with TBST	3x 5 min with PBS
Secondary antibody incubation (fluorophore-conjugated) + fluorescent dye	50 µL per coverslip for 1 h, protected from light (antibodies diluted in blocking solution) + DAPI	50 µL per coverslip for 1 h, protected from light (antibodies diluted in blocking solution) + filipin complex
Washing	3x 5 min with TBST	3x 5 min with PBS

Subsequently, the coverslips were mounted on microscope slides with 10 µl Mowiol and analysed by confocal laser scanning microscopy (CLSM).

3.2.4.2 Confocal laser scanning microscopy (CLSM)

The confocal laser scanning microscopy allows the detection of fluorescent-tagged proteins in a defined plane of the cell, as well as the investigation of their possible co-localisation. For this purpose, the sample is illuminated with focused laser beams of a specific wavelength to excite the antibody coupled fluorophore. A dichroic filter is used to direct a chosen wavelength of the laser onto the sample, while the emitted light travels back to the dichroic mirror, passing the pinhole to the detector. The pinhole serves to increase the focus of the sample plane, preventing light, which did not originate from the focal point, to pass to the detector. The detector itself is a photomultiplier, enabling detection of low signals. The LSM-510 microscope was used for analysis.

3.2.4.3 Transmission electron microscopy (TEM)

To create ultra-thin sections, A549 cells were seeded in Petri dishes and infected with the French Polynesia strain with a MOI of 0.1. Before infection, the cells were treated with 2 µg/mL of U18. After 48 hpi, the cells were fixed with 2,5% glutaraldehyde in DMEM complete for 45 min at room temperature. Subsequently, two washing steps with PBS were carried out and cells were scraped off the culture disk. After addition of a warmed agarose solution of 2%, small agarose blocks containing the cells were cut. These blocks were post-fixed with 2% osmium tetroxide in PBS and treated with 1% tannic acid, improving visibility of viral surface proteins. Afterwards, cells were dehydrated by usage of increasing ethanol concentrations and, embedded into liquid epoxy resin. Following this, the resin was incubated at 60°C for 48 h for polymerisation and cut into ultrathin sections via a ultramicrotome. These sections were fixed on glow-discharged carbon-coated nickel grids and treated with 2% uranyl acetate for 15 min, followed by 2% lead citrate for 5 min. Ultrathin sections were analysed by EM 109 Transmission Electron Microscope.

This experiment was kindly performed by Dr. Regina Eberle.

3.2.5 Statistical analysis

Results are described as mean ± SEM from 3 independent experiments, except when indicated otherwise. Error bars in the figures represent SEM. Student's t-test was used to compare two different samples in GraphPad Prism software. Statistical significance is represented in the graphs, as described in Table 3.21.

Table 3.21 – Statistical significance indicated in the graphs. Thresholds of p-values and the significance (*) they represent. More stars depicted in the graphs indicate higher significance.

Significance	p-value
Non-significant (ns)	> 0.05
*	≤ 0.05
**	≤ 0.01
***	≤ 0.001
****	≤0.0001

4. RESULTS

4.1 Determination of cell viability and cytotoxicity of autophagy modulators on A549 cells

To determine the optimal working concentration and to exclude side effects from toxicity of each autophagy modulator on A549 cells, PrestoBlue and lactate dehydrogenase (LDH) assays were performed as described in Chapter 3.2.1.4. From the multiple concentrations tested **(Appendix I)**, 10 nM of Bafilomycin A1 (BFLA), 2 µg/mL of U18666A (U18), 5 mM of 3-Methyladenine (3-MA), and 100 nM of Rapamycin (Rapa) were chosen to modulate autophagy for 24, 48, and 72 h. DMSO 1:1000 was included as a vehicle control for BFLA and Rapa **(Appendix I)**. The concentrations were selected based on toxic effect and previous studies.[151–154] Potential toxicity from the modulators was considered when interpreting further results.

As mentioned previously, the PrestoBlue assay is an indicator of cell proliferation and viability. In other words, this assay reflects the number of metabolic active cells. For BFLA and U18, only at 72 h after treatment, the viability decreased thereabout 0.35 and 0.3, respectively **(Fig. 4.1 A, B)**. 3-MA does not affect cell viability, even after 72 h of treatment **(Fig 4.1 C)**. On the other hand, Rapa reduces the viability of this cell line over time **(Fig 4.1 D)**.

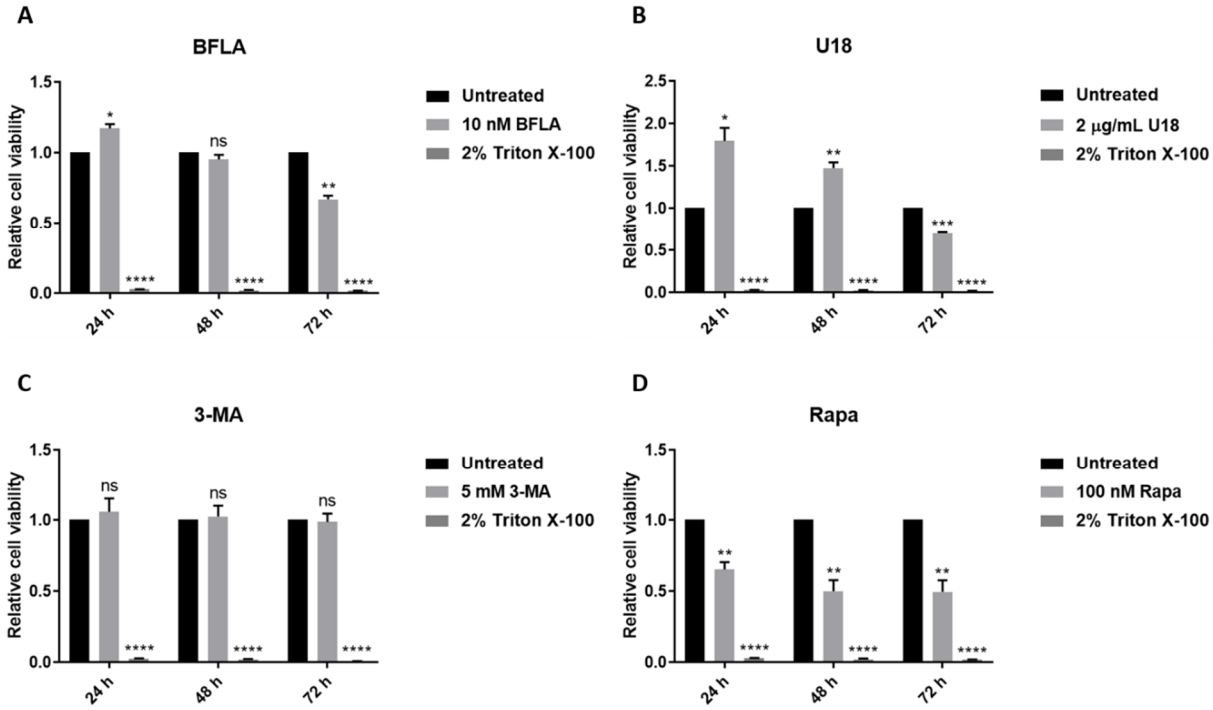

Figure 4.1 – Cell viability assays after treatment with autophagy modulators. A549 cells were treated with 10 nM of BFLA **(A)**, 2 µg/mL of U18 **(B)**, 5 mM of 3-MA **(C)**, and 100 nM of Rapa **(D)** during 24, 48, and 72 h. Relative cell viability was determined by comparing treated to untreated cells. Cells treated with 2% Triton X-100 were included as positive control. As negative control, cells were not treated (only DMEM complete).

As a complementary assay to PrestoBlue, the cytotoxicity of the modulators was also tested. The LDH colorimetric assay measures the LDH released into the cell culture medium from damaged cells quantitatively. Therefore, it is commonly used as a biomarker for cytotoxicity and cytolysis, allowing the estimation of the number of dead cells.

BFLA and U18 were found not to be toxic for A549 cells at the concentrations used after 24 h of treatment **(Fig. 4.2**). However, around 20% of cells were dead within 24 h of Rapa treatment. Determination of the cytotoxicity for later time points was not possible due to the instability of free LDH in the medium after being released from dead cells.

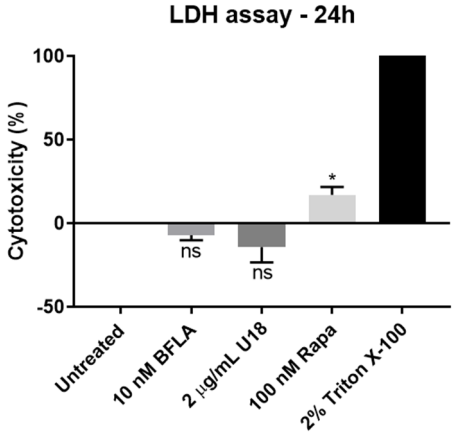

Figure 4.2 – Cytotoxicity assay of autophagy modulators. The cytotoxicity of 10 nM of BFLA, 2 µg/mL of U18, and 100 nM of Rapa was measured after 24 h of treatment by LDH assay. The measurement of LDH activity is an indicator of cell death. The cytotoxicity was calculated by setting cells treated with 2% Triton X-100 to 100% (positive control) and untreated cells to 0% (negative control).

Two more autophagy modulators were tested by these assays, but no further studies were pursued **(Appendix II)**.

4.2 Modulation of autophagy on ZIKV-infected cells

The relationship between virus and autophagy is not yet fully understood. In fact, autophagy can not only have antiviral activity, but can also be triggered upon virus infection to promote different stages of the viral life cycle.[155] Several reports suggest that flaviviruses lead to an increase of autophagic activity to enhance viral replication on mammalian cells.[156–158] The same holds true for ZIKV, which was shown to induce autophagy on fibroblasts.[22] To verify this effect on another line of ZIKV-permissive cells and to further characterize ZIKV infection and the mechanism behind this hijack of the autophagy machinery, autophagy was modulated. This modulation on ZIKV-infected cells was carried out by BFLA, U18, 3-MA and Rapa during 24, 48, and 72 hours post-infection (hpi). French Polynesia (PF13/251013-18) and Uganda (MR766) strains of ZIKV were used to infect A549 cells with a multiplicity of infection (MOI) of 0.1.

4.2.1 Relevance of endosomal-lysosomal acidification for the ZIKV life cycle

To investigate the influence of acidification of endosomal-lysosomal compartments on ZIKV infection, infected cells were treated with 10 nM of BFLA and harvested at 24, 48, and 72 hpi. Furthermore, to understand the impact of this inhibitor, not only on the spreading of infection and release of infectious viral particles, but also on the entry of the virus, post- and pre-infection treatment was applied, respectively. Pre-infection treatment means that A549 cells were treated with the modulator and 2 h later, infected with ZIKV. On the other hand, post-infection treatment consists of treating the cells 2 h after infection. The modulator was present during the whole experiment.

4.2.1.1 Determination of intra- and extracellular ZIKV genomes

To determine the amount of intra- and extracellular ZIKV genomes, intra- and extracellular ZIKV RNA was converted to cDNA by reverse transcriptase and analysed by RT-qPCR. For pre-infection treatment, no significant amount of intracellular ZIKV genomes was detected for all time points and for both strains **(Fig 4.3)**. Meanwhile, Polynesia-infected cells, which were treated post-infection, showed a significant decrease on the amount of intracellular ZIKV genomes within 24 hpi, diminishing even more after 48 and 72 hpi **(Fig 4.3 A)**. A similar outcome was noticed for the Uganda strain, although, no significant effect was evident after 24 hpi **(Fig 4.3 B)**.

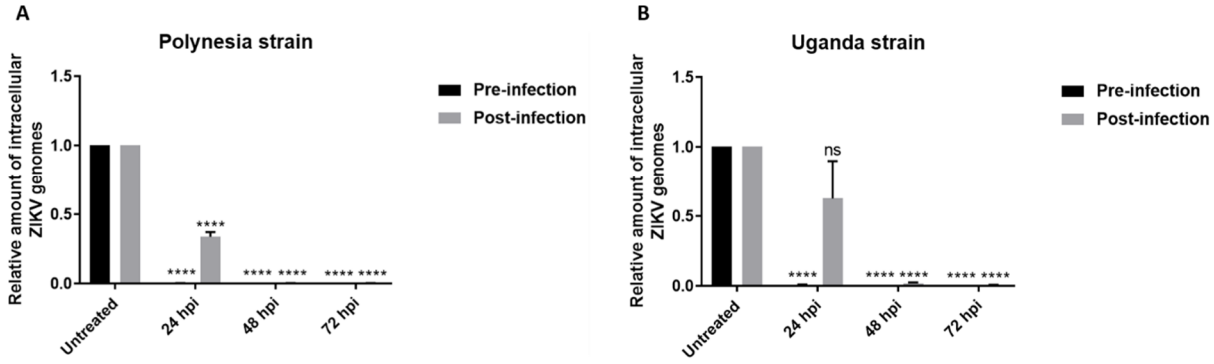

Figure 4.3 – Reduction of the amount of intracellular ZIKV genomes after BFLA treatment. Determination of the amount of intracellular ZIKV genomes in Polynesia- **(A)**, and Uganda-infected cells **(B)** was performed by RT-qPCR. A549 cells were treated with 10 nM of BFLA before (pre-) or after (post-) infection, as indicated in the graphs. As control, infected-untreated cells were used to normalise the values of 24, 48, and 72 hpi-treated cells. Although only one bar for the control is represented, each normalisation was effectuated with the respective control for each time point.

A comparable effect of BFLA on the extracellular amount of ZIKV genomes was observed by RT-qPCR analysis. Indeed, no relevant amount was measured for pre-infection treatment for both strains **(Fig 4.4)**. Post-infection treatment on ZIKV-infected cells revealed a significant decline of the amount of extracellular ZIKV genomes within 24 hpi for the Polynesia strain **(Fig 4.4 A)** and after 48 hpi for the Uganda strain **(Fig 4.4 B)**.

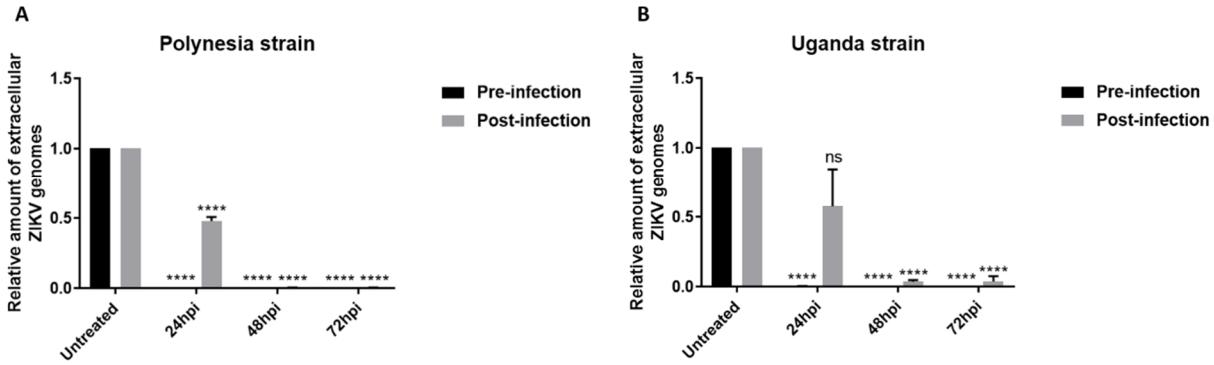

Figure 4.4 – BFLA reduces the amount of extracellular ZIKV genomes. Determination of the amount of ZIKV genomes in supernatants from Polynesia- **(A)**, and Uganda-infected cells **(B)** was performed by RT-qPCR. A549 cells were treated with 10 nM of BFLA before (pre-) or after (post-) infection, as indicated in the graphs. As control, infected-untreated cells were used to normalise the values of 24, 48, and 72 hpi-treated cells. Although only one bar for the control is represented, each normalisation was effectuated with the respective control for each time point.

4.2.1.2 Determination of intra- and extracellular infectious viral particles

In addition to ZIKV genomes, the number of intra- and extracellular infectious viral particles was assessed by plaque forming assay. In brief, plaque assay measures the concentration of infectious virus in a sample (virus titer) by the number of plaques formed after infection, as detailed in Chapter 3.2.1.5.

BFLA pre-infection treatment significantly lessened the intracellular virus titers for both strains **(Fig 4.5 A, C)**. As matter of fact, absence or a reduced number of plaques were found after treatment. Unlike pre-infection, several plaques were formed after BFLA treatment for post-infection. Still an impairment of the number of intracellular infectious viral particles was recognised **(Fig 4.5 B, D)**. Focusing on just untreated cells, Polynesia strain titers appear to increase, reaching a peak at 48 hpi, followed by a drop-down at 72 hpi **(Fig 4.5 A, B)**. Nonetheless, a different outcome was perceived for Uganda strain pre- and post-infection **(Fig 4.5 C, D)**. Despite that variation, a pattern analogous to the data of the Polynesia strain was noticed for Uganda strain pre-infection, where a rise in the number of infectious viral particles was distinguished. Likewise, it has its higher point at 48 hpi, succeeded by a small diminution of the intracellular virus titers at 72 hpi **(Fig 4.5 C)**. Contrary, for Uganda post-infection, a progressive increment of the number of infectious viral particles was discernible **(Fig 4.5 D)**. Even though, the virus titers were lower than for pre-infection **(Fig 4.5 C)**.

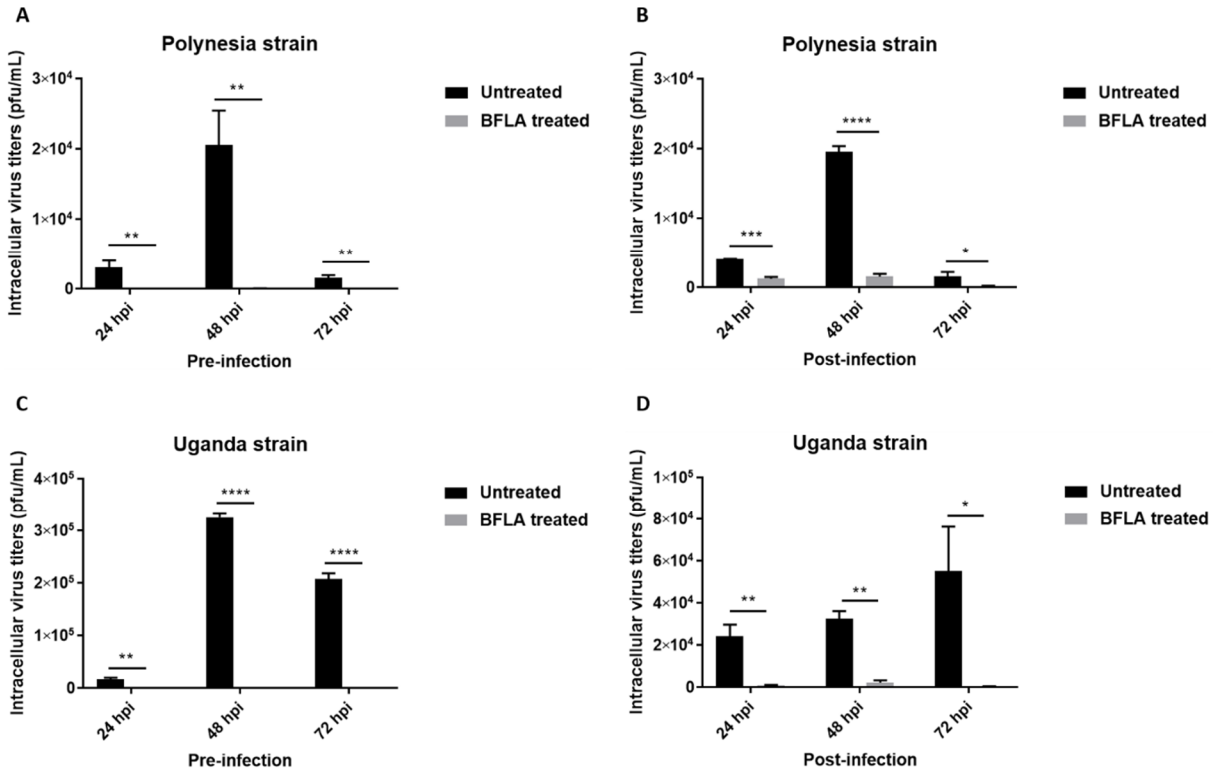

Figure 4.5 – Decline of intracellular ZIKV titers subsequent BFLA treatment. Determination of the intracellular ZIKV titers of Polynesia- **(A, B)**, and Uganda-infected cells **(C, D)** was performed by plaque forming assay in Vero cells. A549-infected cells were treated with 10 nM of BFLA before (pre-) or after (post-) infection, as indicated in the graphs. The intracellular virus titers are expressed in plaque-forming units per mL (pfu/mL). Infected-untreated cells were used for direct comparison with the values of 24, 48, and 72 hpi-treated cells. In some bars, the error bars represent mean ± SEM (n=2). The outliers from untreated cells were excluded for visualisation of the impact of the treatment.

These results were also supported by the number of extracellular ZIKV titers measured. Correspondingly, BFLA treatment leads to a significant reduction of the extracellular virus titers. In fact, no plaques were visible for pre-infection treatment **(Fig 4.6 A, C)**, whereas only a few plaques

developed post-infection **(Fig 4.6 B, D)**. As for untreated cells, discrepancies in the number of infectious viral particles were detected. However, the same tendency as the intracellular virus titers was observed, for post-infection and for both strains, with an augmentation of the virus titers, achieving the maximum values at 48 hpi **(Fig 4.6 B, D)**. In opposition to intracellular infectious viral particles, for post-infection, the Uganda strain exhibited a sudden decrease of the viral titers at 72 hpi **(Fig 4.6 D)**. For pre-infection, whilst the extracellular Polynesia titers undergo a progressive diminution **(Fig 4.6 A)**, the Uganda strain showed almost no differentiation of the virus titers over time **(Fig 4.6 C).**

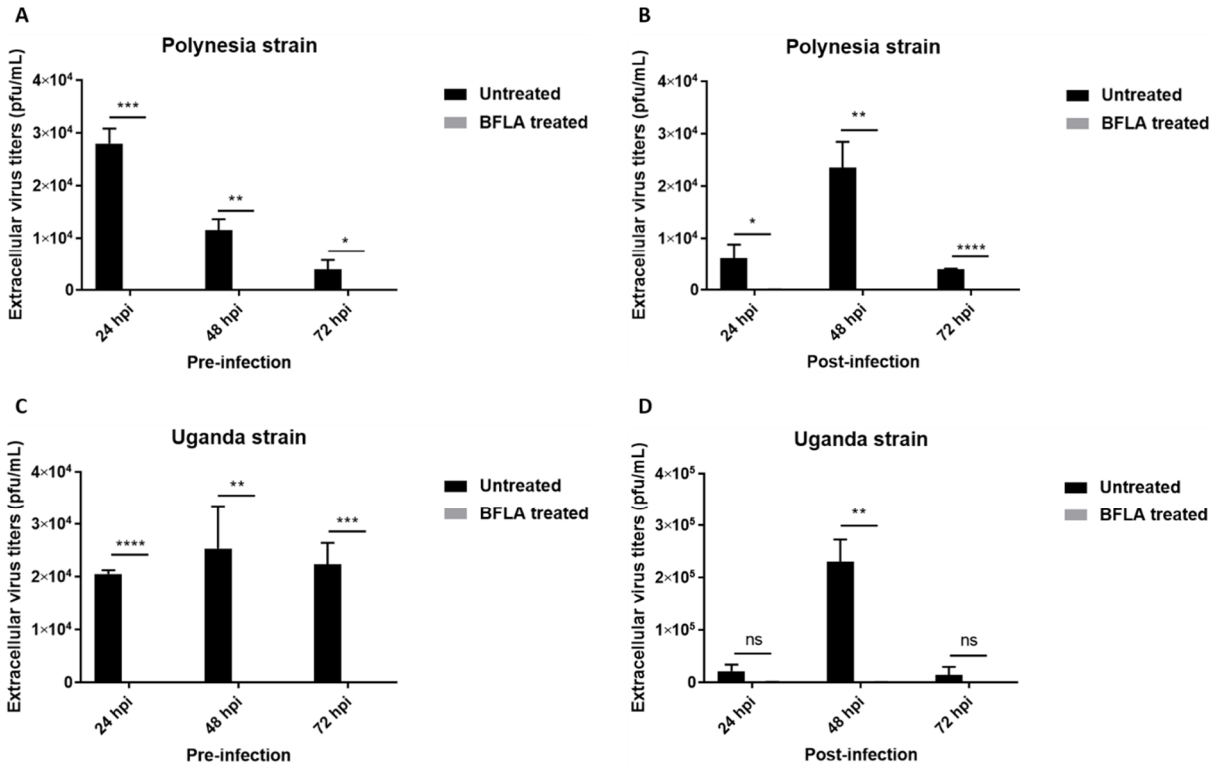

Figure 4.6 – BFLA minimises the extracellular ZIKV titers. Extracellular ZIKV titers of Polynesia- **(A, B)**, and Uganda-infected cells **(C, D)** were assessed by plaque forming assay in Vero cells. A549-infected cells were treated with 10 nM of BFLA before (pre-) or after (post-) infection, as indicated in the graphs. The extracellular virus titers are expressed in plaque-forming units per mL (pfu/mL). Infected-untreated cells were used for direct comparison with the values of 24, 48, and 72 hpi-treated cells. In some bars, the error bars represent mean ± SEM (n=2). The outliers from untreated cells were excluded for visualisation of the impact of the treatment.

4.2.1.3 Determination of the amount of ZIKV and autophagy proteins

Moreover, to examine the effect of BFLA on the amount of ZIKV and autophagy proteins, western blot analysis was performed, as explained in Chapter 3.2.3.3. The 44 kDa ZIKV-NS1 protein was detected together with p62 (62 kDa), LC3-I (14 kDa) and LC3-II (16 kDa), as well as the loading control, β-actin (42 kDa). Detection of LC3-II and p62 was carried out in uninfected cell lysates to investigate the influence of the treatment on autophagy markers. Gradual accumulation of these proteins was recognised after BFLA treatment over time **(Appendix III and Fig 4.7 F)**. Yet, densitometric quantification of LC3-II levels showed the opposite **(Appendix III A, B).** In infected cell lysates, a continuous elevation of p62 amount was perceptible, while LC3-II levels fluttered **(Appendix III and Fig 4.7 A, C, E)**. Regarding ZIKV, no accumulation of NS1 protein was observed after pre-infection treatment for both strains. On the other hand, post-infection treatment with BFLA lessened the amount of NS1 **(Fig 4.7 A, B, C, D, E).** It was uniquely detected at 24 hpi, revealing more NS1 accumulation for Uganda than for the Polynesia strain **(Fig 4.7 A, B, D)**.

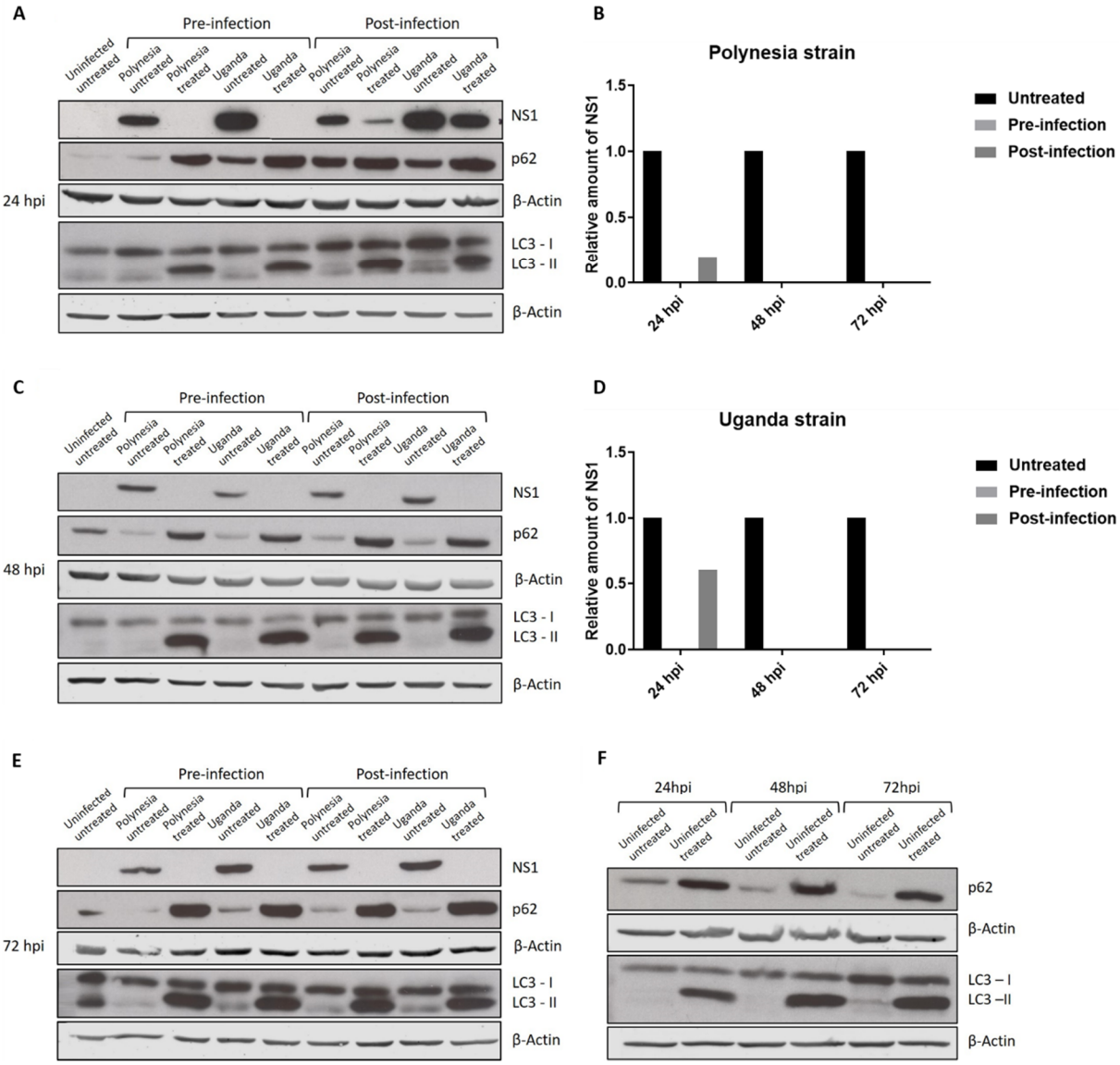

Figure 4.7 – BFLA treatment leads to a diminished ZIKV-NS1 level and to an accumulation of p62 and LC3-II proteins. Preparation of cell lysates was achieved by RIPA buffer and detection of ZIKV-NS1, p62, LC3, and β-Actin by consecutive western blot analysis. The protein levels were detected after 24 **(A)**, 48 **(C)**, and 72 hpi **(E)** for Polynesia-, and Uganda-infected cells. A549-infected cells were either untreated or treated with 10 nM of BFLA before (pre-) or after (post-) infection. p62 and LC3-II were used as autophagy markers, while β-Actin was included as loading control. Beyond that, uninfected-untreated cell lysates were utilised as negative control. As a control of the effect of BFLA on autophagy protein markers, p62 and LC3 were detected in uninfected-treated cell lysates **(F)**. Furthermore, densitometric quantification of ZIKV-NS1 protein after BFLA treatment for Polynesia **(B)** and Uganda **(D)** strains was accomplished by Image Studio Lite software. The values were first normalised to the loading control and then to infected-untreated cells. Antibody dilutions are indicated in Chapter 3.1.3

4.2.1.4 Determination of the amount of ZIKV and its intracellular localisation and distribution

To further gain insight in the amount of ZIKV proteins and number of ZIKV-positive cells, indirect immunofluorescence microscopy was performed, as mentioned in Chapter 3.2.4.1. The flavivirus E protein was detected by a specific antibody (4G2, green). For pre-infection treatment, no envelope protein of ZIKV was noticed at any time point for both strains. Looking at post-infection treatment, a reduction of the amount of E protein over time was visible. In addition, due to the cytopathic effect of ZIKV, progressively less infected A549 cells were observed over the time frame **(Fig 4.8)**.

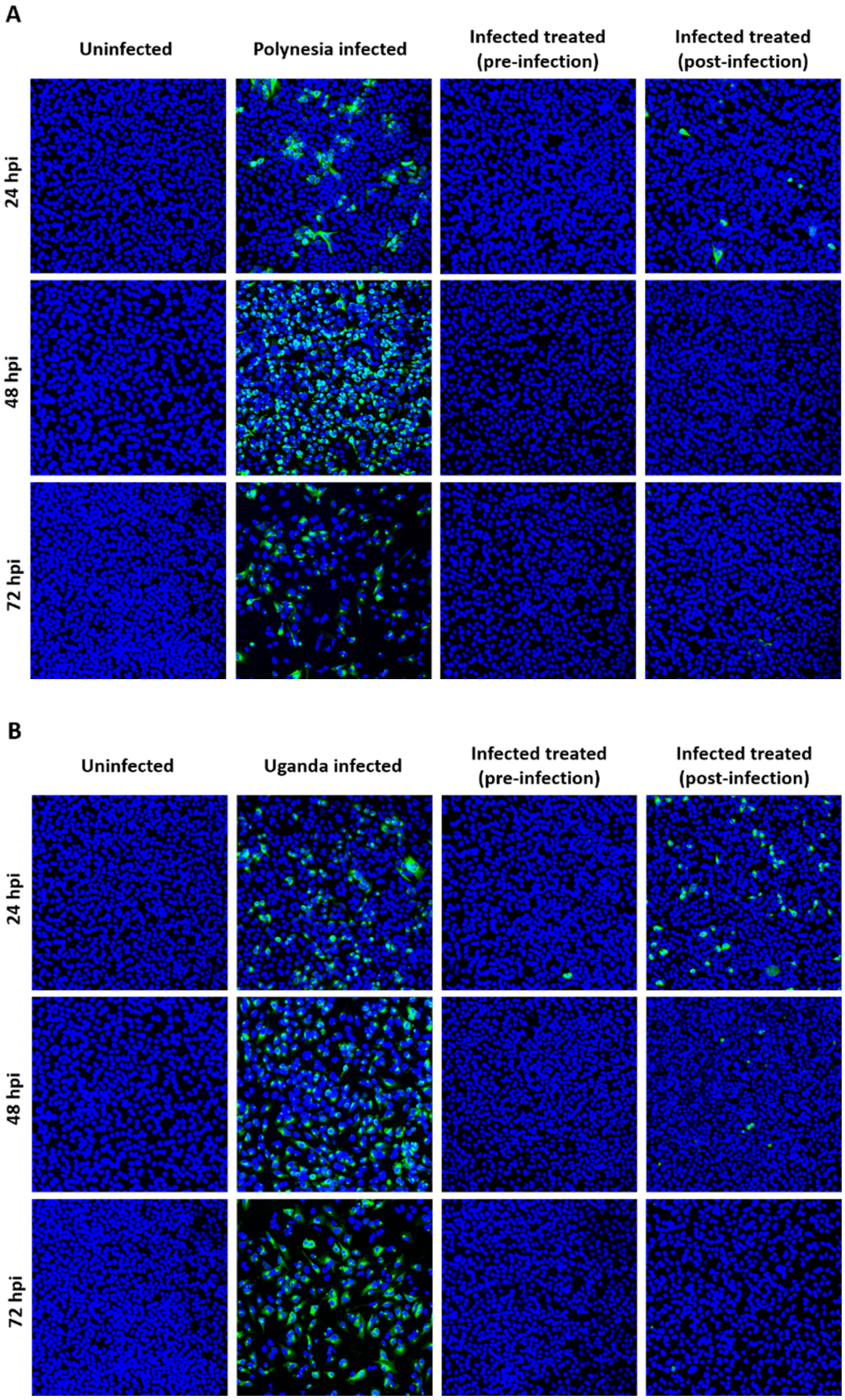

Figure 4.8 – Reduction of ZIKV-infected cells after BFLA treatment. Fluorescence analysis of Polynesia- **(A)**, and Uganda-infected cells **(B)** after 24, 48, and 72 hpi. Infected cells were treated with 10 nM of BFLA before (pre-) or after (post-) infection. Uninfected cells were included as a negative control. A549 cells were fixed with ethanol:acetone (1:1) and analysed by confocal laser scanning microscopy (CLSM). Cells nuclei and E protein were stained with DAPI (blue) and 4G2 antibody (green), respectively. The pictures were taken with the 16x objective.

To investigate the intracellular localisation and distribution of ZIKV-specific proteins, the same samples were analysed at higher magnification. Since the number of infected cells declined dramatically after 48 and 72 hpi, only cells harvested at 24 hpi were shown. At early stages of infection different localisation of ZIKV proteins were exhibited, such as a dispersion throughout the cell **(Fig 4.9 Ac, Bb)** or perinuclear **(Fig 4.9 Aa, Ab, Ad, Ba, Bc, Bd)**. The most predominant distribution is the dot-like staining **(Fig 4.9 Aa, Ab, Bc, Bd)**, being more evident and frequent in late stages of infection (not shown) and for the Uganda strain **(Fig 4.9 Bc)**. The distribution of ZIKV-specific proteins and its intracellular localisation were modified after BFLA treatment. Besides, the typical dot-like staining and strong cytosolic dots **(Fig 4.9 Ag, Bh)** appeared together with a reticular structure **(Fig 4.9 Ae, Be)**. The reticular staining and the cytosolic dots were found on infected cells at 48 and 72 hpi as well (not shown).

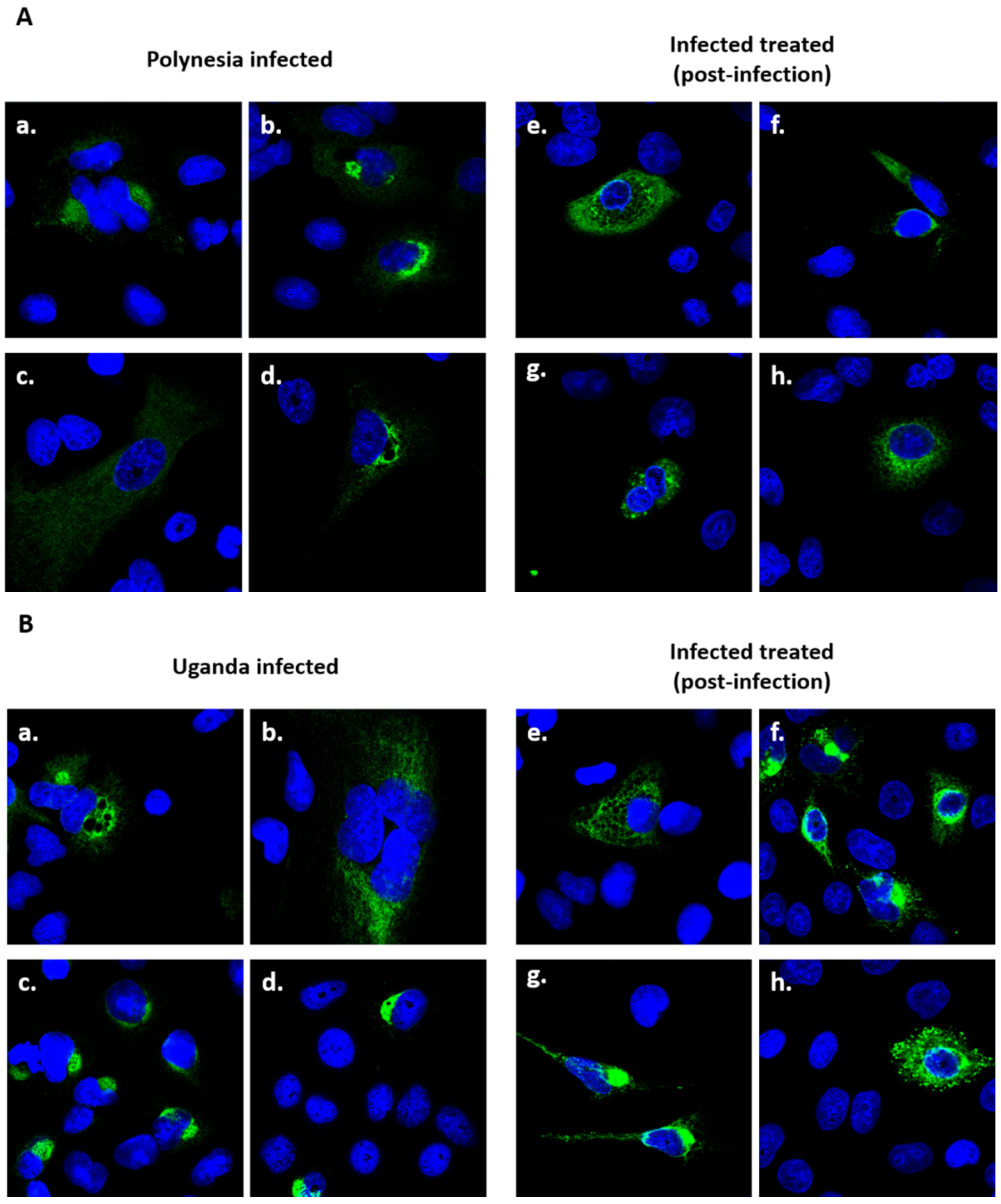

Figure 4.9 – BFLA treatment changes intracellular distribution and localisation of ZIKV-specific proteins. Fluorescence analysis of Polynesia- **(A)**, and Uganda-infected cells **(B)** after 24 hpi. Different intracellular distribution and localisation was discernible in untreated and treated cells with 10 nM of BFLA **(a. - g.)**. A549 cells were fixed with Ethanol:Acetone (1:1) and analysed by confocal laser scanning microscopy (CLSM). Cells nuclei and E protein were stained with DAPI (blue) and 4G2 antibody (green), respectively. The pictures were taken with the 100x objective.

4.2.2 Effect of cholesterol trafficking inhibition and relevance of endosomal maturation for ZIKV life cycle

To understand the role of cholesterol transportation and the importance of endosomal maturation on the evolution of ZIKV infection, infected cells were treated with 2 µg/mL of U18 and harvested after 24, 48, and 72 hpi. For the same reasons mentioned in Chapter 4.2.1, a pre- and post-infection treatment was applied.

4.2.2.1 Determination of intra- and extracellular ZIKV genomes

Likewise, quantification of the amount of intra- and extracellular ZIKV genomes was accomplished by RT-qPCR. Contrary to BFLA treatment, no substantial discrepancies were measured on the intracellular amount between pre-and post-infection treatment. Indeed, both strains revealed a similar pattern for all time points analysed. U18 treatment seems to decrease the amount of intracellular ZIKV genomes over time **(Fig 4.10)**.

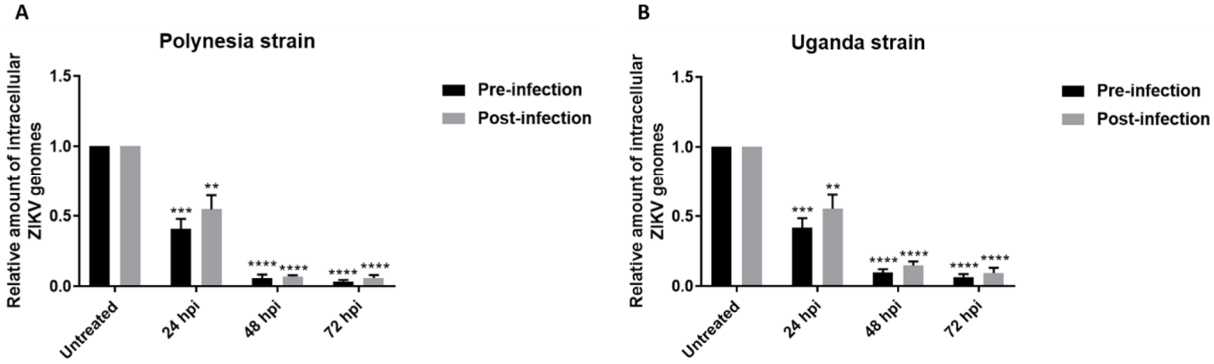

Figure 4.10 – Diminution of the amount of intracellular ZIKV genomes after U18 treatment. Determination of the amount of intracellular ZIKV genomes in Polynesia- **(A)**, and Uganda-infected cells **(B)** was performed by RT-qPCR. A549 cells were treated with 2 µg/mL of U18 before (pre-) or after (post-) infection, as indicated in the graphs. As control, infected-untreated cells were used to normalise the values of 24, 48, and 72 hpi-treated cells. Although only one bar for the control is represented, each normalisation was effectuated with the respective control for each time point.

A gradual downtrend in the amount of extracellular ZIKV genomes was noticed. The observed tendency was comparable to the intracellular Uganda genomes (**Fig 4.11 B)**. Nonetheless, the Polynesia strain showed slight variations at 72 hpi, where an elevation of genomes was distinguished **(Fig 4.11 A)**.

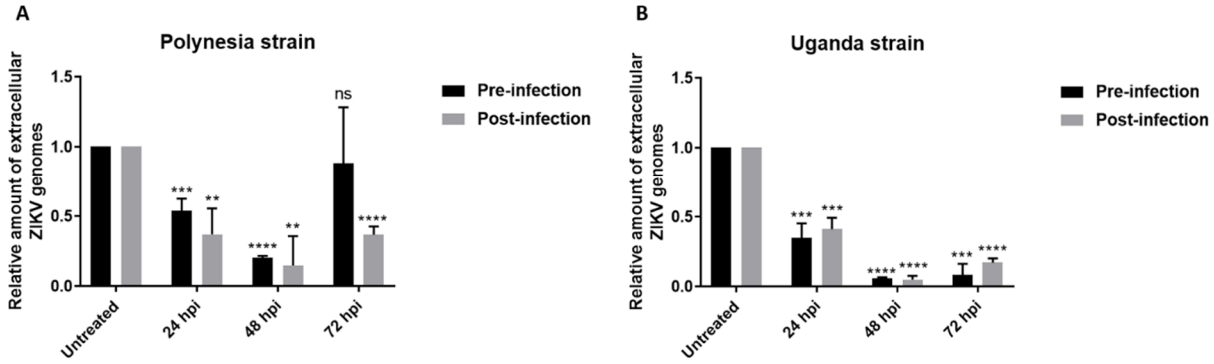

Figure 4.11 – U18 decreases the amount of extracellular ZIKV genomes. Determination of the amount of ZIKV genomes in supernatants from Polynesia- **(A)**, and Uganda-infected cells **(B)** was performed by RT-qPCR. A549 cells were treated with 2 µg/mL of U18 before (pre-) or after (post-) infection, as indicated in the graphs. As control, infected-untreated cells were used to normalise the values of 24, 48, and 72 hpi-treated cells. Although only one bar for the control is represented, each normalisation was effectuated with the respective control for each time point. In some bars, the error bars represent mean ± SEM (n=2). The outliers from were excluded for visualisation of the impact of the treatment.

4.2.2.2 Determination of intra- and extracellular infectious viral particles

To assess the amount of intra- and extracellular infectious viral particles, plaque forming assay was performed. In general, a reduction on the intracellular virus titers was visible after U18 treatment, displaying no relevant changes between pre- and post-infection treatment **(Fig 4.10)**. Regarding the Polynesia strain, only at 24 hpi (pre-infection) and at 48 hpi (post-infection) a significant decline of the number of infectious viral particles was perceptible after treatment **(Fig 4.12 A, B)**. Contrariwise, intracellular virus titers lessened for the Uganda strain at all time points **(Fig 4.12 C, D)**.

As for the intracellular titers of untreated cells, innumerable differences were exhibited for both strains. For the Polynesia strain, a distinct number of intracellular infectious viral particles was identified between the experiments, with inferior virus titers for post-infection. Nevertheless, the same trend as previously described in Chapter 4.2.1 was recognised here, with a maximum of infectious viral particles at 48 hpi **(Fig 4.12 A, B)**. On top of that, this tendency was also presented by the Uganda strain for the pre-infection experiment **(Fig 4.12 C)**. With respect to the post-infection experiment, the Uganda strain demonstrated a progressive increase of the intracellular virus titers **(Fig 4.12 D)**.

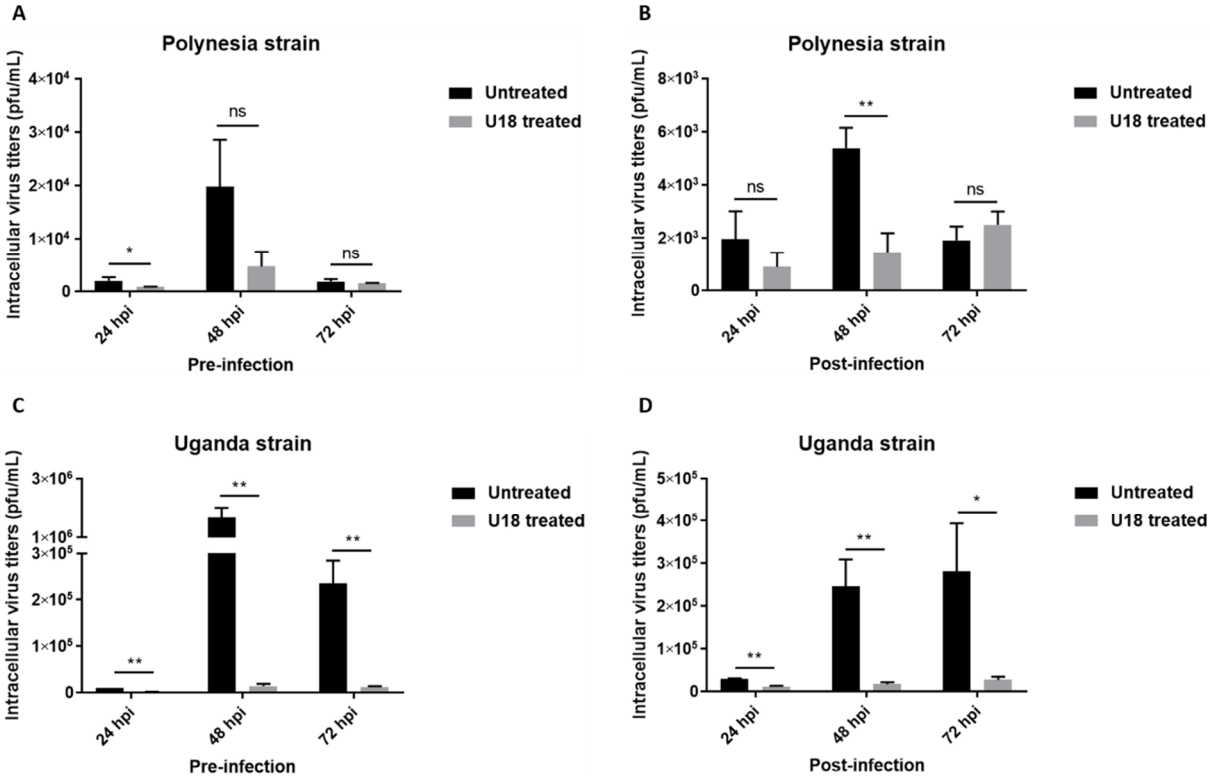

Figure 4.12 – Intracellular ZIKV titers are diminished by subsequent U18 treatment. Determination of the intracellular ZIKV titers of Polynesia- **(A, B)**, and Uganda-infected cells **(C, D)** was performed by plaque forming assay in Vero cells. A549-infected cells were treated with 2 µg/mL of U18 before (pre-) or after (post-) infection, as indicated in the graphs. The intracellular virus titers are expressed in plaque-forming units per mL (pfu/mL). Infected-untreated cells were used for direct comparison with the values of 24, 48, and 72 hpi-treated cells. In some bars, the error bars represent mean ± SEM (n=2). The outliers from untreated cells were excluded for visualisation of the impact of the treatment.

An identical effect was also observed on the amount of extracellular infectious viral particles after U18 treatment, without deviations between pre- and post-infection for both strains. On average, the virus titers of Polynesia and Uganda strains decreased after U18 treatment at all time points analysed **(Fig 4.13)**. However, at 24 hpi for pre-infection (Polynesia) and post-infection (Uganda) experiments, no distinction was found between untreated and cells treated with U18 **(Fig 4.13 A, D)**. Concerning the extracellular viral titers of untreated cells, approximately equal amounts of infectious viral particles were

exhibited by the Polynesia strain for pre- and post-infection experiments. Additionally, the same tendency as reported before in Chapter 4.2.1 was also perceived, with the highest virus titers at 48 hpi, followed by a diminution to almost the same level as shown for 24 hpi **(Fig 4.13 A, B)**. Besides that, in general, an augmentation of the virus titers was measured by comparison to the ones presented for BFLA in the previous chapter **(Fig 4.6 B)**. On the other hand, the Uganda strain revealed different extracellular virus titers for pre- and post-infection. In the post-infection experiment, a continuous rise of the number of infectious viral particles was discernible **(Fig 4.13 D)**, while in the pre-infection experiment a considerable increase was yielded from 24 to 48 hpi, with a constant level until 72 hpi **(Fig 4.13 C)**.

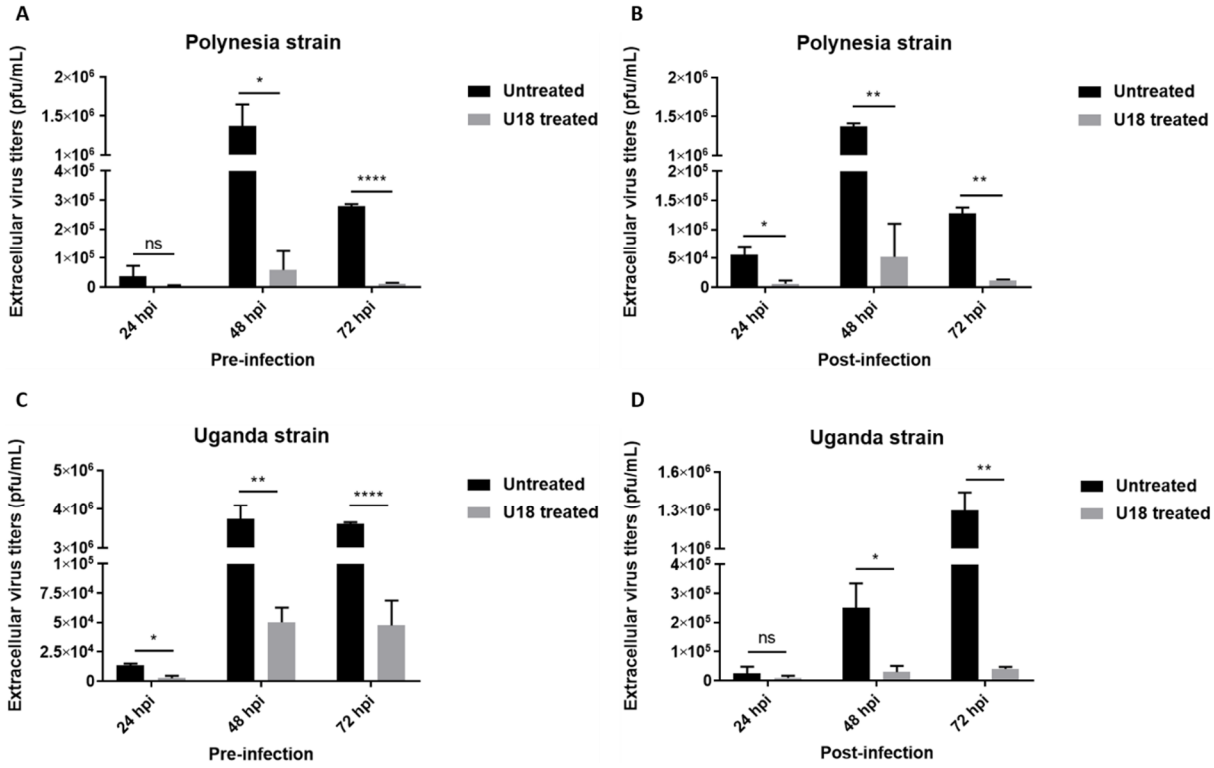

Figure 4.13 – U18 treatment lowers the extracellular ZIKV titers. Extracellular ZIKV titers of Polynesia- **(A, B)**, and Uganda-infected cells **(C, D)** were assessed by plaque forming assay in Vero cells. A549-infected cells were treated with 2 µg/mL before (pre-) or after (post-) infection, as indicated in the graphs. The extracellular virus titers are expressed in plaque-forming units per mL (pfu/mL). Infected-untreated cells were used for direct comparison with the values of 24, 48, and 72 hpi-treated cells. In some bars, the error bars represent mean ± SEM (n=2). The outliers from untreated cells were excluded for visualisation of the impact of the treatment.

4.2.2.3 Determination of the amount of ZIKV and autophagy proteins

Moreover, to investigate the effect of U18 treatment on the amount of ZIKV-specific proteins, western-blot analysis was performed. Apart from the ZIKV-NS1 protein and the autophagy markers (p62 and LC3-II), the lysosome-associated membrane protein 2 (LAMP2) was also detected in this study. LAMP2 is a protein with a molecular weight of 120 kDa in its glycosylated form.[159] Detection of LC3-II and p62 was carried out in uninfected cell lysates to investigate the influence of the treatment on autophagy markers. A gradual accumulation of these proteins appeared after U18 treatment **(Fig 4.14 F)**. Still, the densitometric quantification of LC3-II indicates the contrary. The same changes were observed for p62 and LC3-II in infected cell lysates after treatment **(Fig 4.14 A, C, E)**, with some irrelevant exceptions for the Uganda strain after densitometric quantification. **(Appendix IV E, F).** As for ZIKV protein, both strains expressed a downtrend of NS1 level after post-infection treatment, which levelled off from

48 to 72 hpi **(Fig 4.14 B, D)**. Meanwhile, for pre-infection treatment, the Polynesia strain displayed an even more drastic reduction, with a constant low amount of NS1 protein for all time points **(Fig 4.14 B)**.

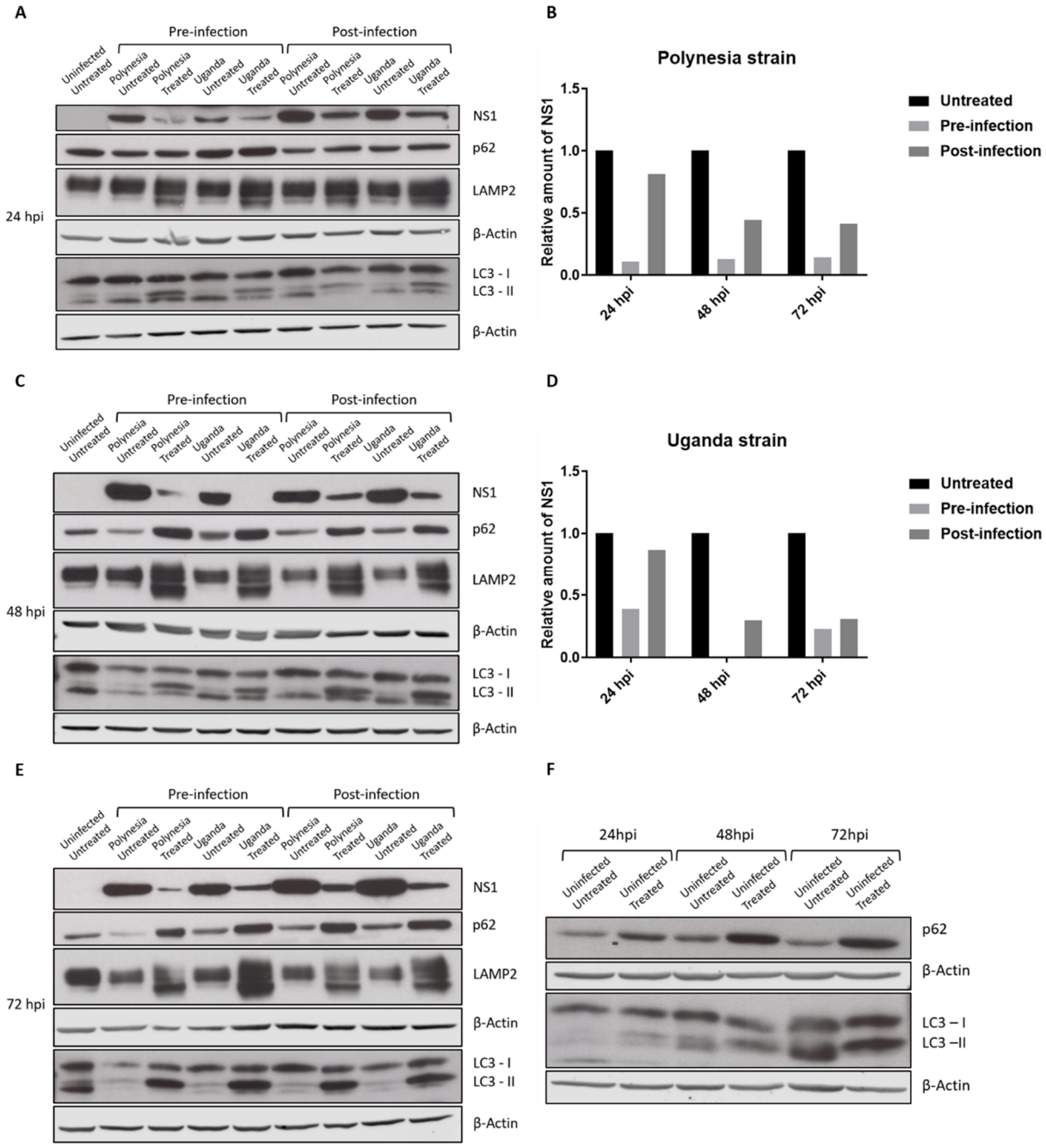

Figure 4.14 – **Reduction of ZIKV-NS1 levels and accumulation of LAMP2, p62 and LC3-II levels after U18 treatment.** Preparation of cell lysates was achieved by RIPA buffer and detection of ZIKV-NS1, p62, LC3, LAMP2, and β-Actin by consecutive western blot analysis. The protein levels were detected after 24 **(A)**, 48 **(C)**, and 72 hpi **(E)** for Polynesia-, and Uganda-infected cells. A549-infected cells were either untreated or treated with 2 µg/mL of U18 before (pre-) or after (post-) infection. LAMP2, p62 and LC3-II were used as lysosomal and autophagy markers, respectively, while β-Actin was included as loading control. Beyond that, uninfected-untreated cell lysates were utilised as negative control. As a control of the effect of U18 on autophagy markers, p62 and LC3 were detected in uninfected-treated cell lysates **(F)**. Furthermore, densitometric quantification of ZIKV-NS1 protein after U18 treatment for Polynesia **(B)** and Uganda **(D)** strains was accomplished by Image Studio Lite software. The values were first normalised to the loading control and then to infected-untreated cells. Antibody dilutions are indicated in Chapter 3.1.3

4.2.2.4 Determination of the amount of ZIKV proteins and its intracellular localisation and distribution

To further gain insight about the effect of U18 on the amount of ZIKV and autophagy specific proteins, indirect immunofluorescence was performed. Monitorisation of autophagic activity was achieved by detection of p62 (red) and ZIKV-infected cells were identified with the 4G2 antibody (green). In this experiment, samples from pre- and post-infection treatment were analysed, but due to a comparable outcome only post-infection data was presented here. A progressive intensification of the filipin complex and p62 signal was visible over time after treatment with U18 **(Fig 4.15 – cyan, red)**. With respect to ZIKV, lessened E protein amount was found after treatment for both strains **(Fig 4.15 - green)**. Even though a decline of the number of ZIKV-positive cells after U18 treatment was always seen between untreated and treated cells. The same outcome was not perceptible for treated cells, where the amount of positive cells went up at 48 hpi and dropped again at 72 hpi **(Fig 4.15 - green)**. On top of that, the cytopathic effect of ZIKV and the peak of infection at 48 hpi could be observed here.

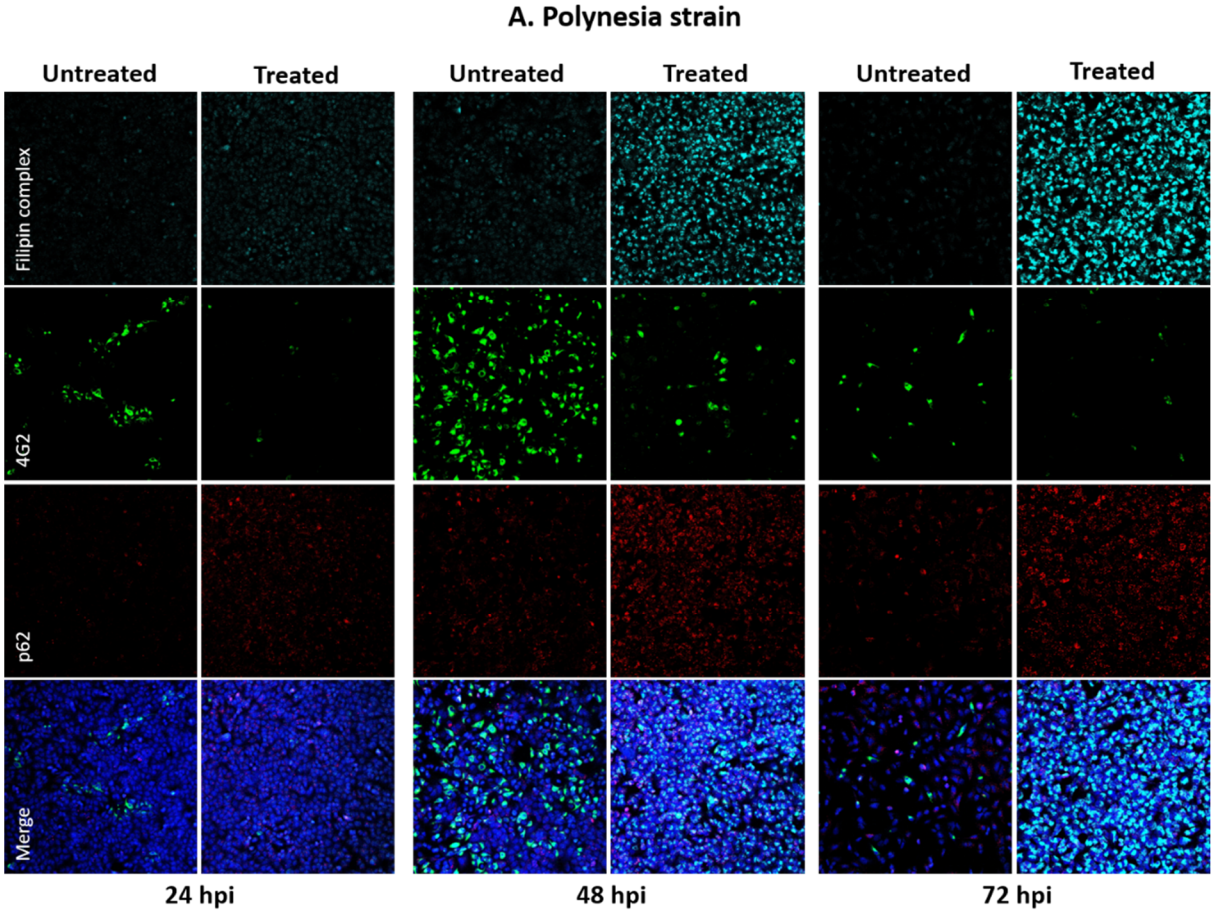

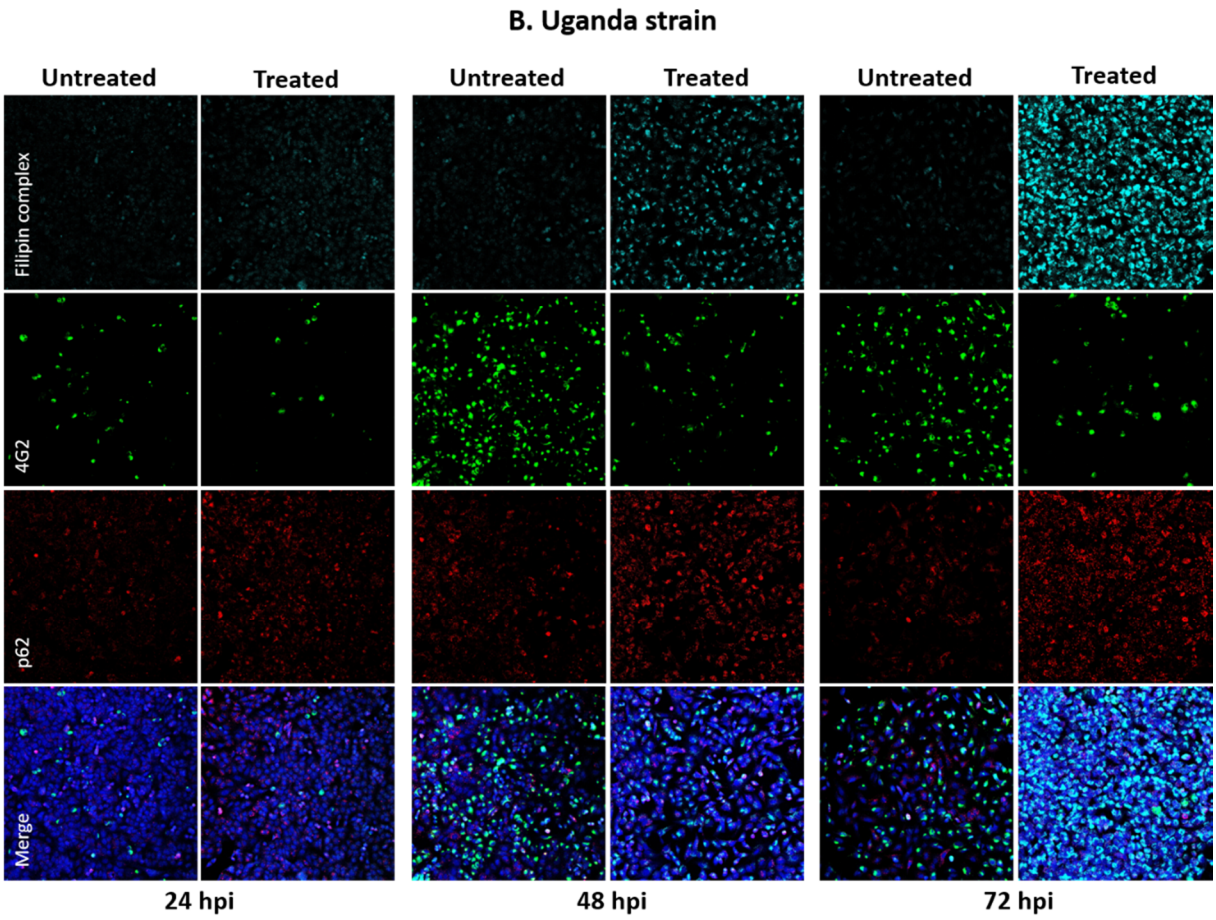

Figure 4.15 – U18 treatment decreases the number ZIKV-infected cells and intensifies of p62 and filipin complex signal. Fluorescence analysis of Polynesia- **(A)**, and Uganda-infected cells **(B)** after 24, 48, and 72 hpi. Infected cells were treated post-infection with 2 µg/mL of U18. A549 cells were fixed in 4% formaldehyde and analysed by confocal laser scanning microscopy (CLSM). Cholesterol, E protein, p62 and the nuclear envelope were stained with filipin complex (cyan), 4G2 antibody (green), p62 antibody (red) and lamin A (blue), respectively. The pictures were taken with the 16x objective.

To investigate the intracellular localisation and distribution of ZIKV-specific proteins, the same samples were analysed at higher magnification. At early stages of infection, a major type of protein localisation was recognised for Polynesia and Uganda strains: the perinuclear localisation with a dot-like staining **(Fig 4.16 left panel)**. The latter was even more prevalent in late stages of infection, especially for the Uganda strain **(Fig 4.16 B left panel)**. As an overall for both strains, a dispersion throughout the cell of the envelope protein was evident after U18 treatment **(Fig 4.16 right panel)**. Though, the dot-like staining appeared as well in the presence of this modulator (not shown).

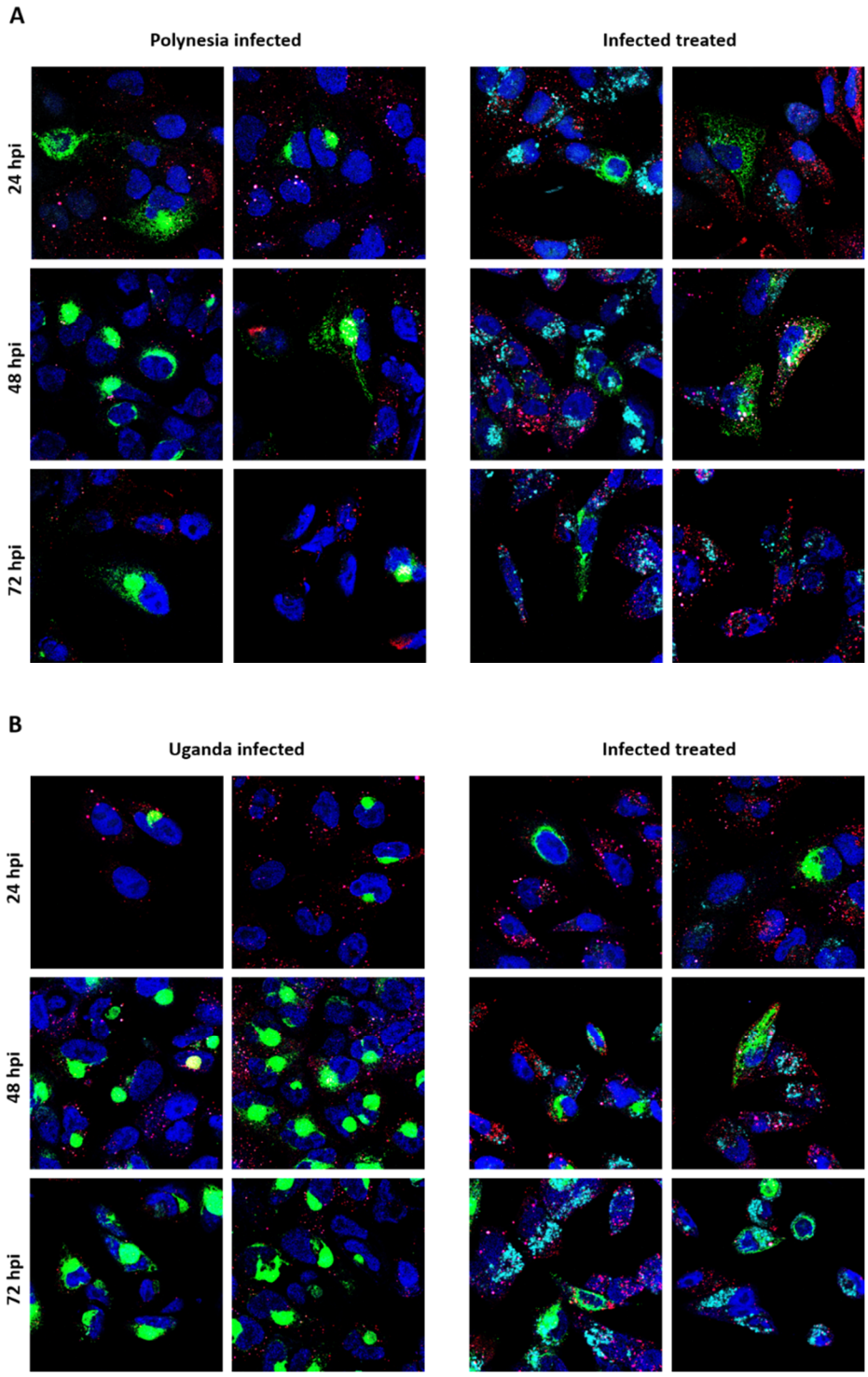

Figure 4.16 – U18 treatment promotes cytoplasmic dispersion of ZIKV-specific proteins. Fluorescence analysis of Polynesia- **(A)**, and Uganda-infected cells **(B)** after 24, 48, and 72 hpi. The left panel shows infected untreated cells and infected cells treated with 2 µg/mL of U18 on the right panel. A549 cells were fixed in 4% formaldehyde and analysed by confocal laser scanning microscopy (CLSM). Cholesterol, E protein, p62 and the nuclear envelope were stained with filipin complex (cyan), 4G2 antibody (green), p62 antibody (red) and lamin A (blue), respectively. The pictures were taken with the 100x objective.

4.2.2.5 Cellular changes after ZIKV infection and U18 treatment

For a better understanding and characterisation of ZIKV infection and to further comprehend the impact of U18 treatment on a cellular level, transmission electron microscopy (TEM) was performed. For this purpose, Polynesia-infected cells were either treated with U18 or untreated, and harvested after 48 hpi, followed by preparation of microscopic samples, as described in Chapter 3.4.2.3. The electron microscopy revealed the presence of large and small vacuoles in the cytoplasm of infected cells **(Fig 4.17 C)**. In addition, pyknosis (irreversible condensation of chromatin), cytoplasmic fragments and cell shrinkage were also distinguished **(Fig 4.17 B)** when compared to uninfected cells **(Fig 4.17 A)**. On top of that, vesicle packets (VPs) **(Fig 4.17 D)** and displacement of cellular organelles **(Fig 4.17 G)** were observed, close to the ER. Potential virus particles were detected in association with these membranous RFs **(Fig 4.17 E)** and in vacuoles **(Fig 4.17 F)**. Furthermore, multilamellar bodies (MLBs) and lipid droplets (LDs) were identified in cells treated with U18 **(Fig 4.17 H)**.

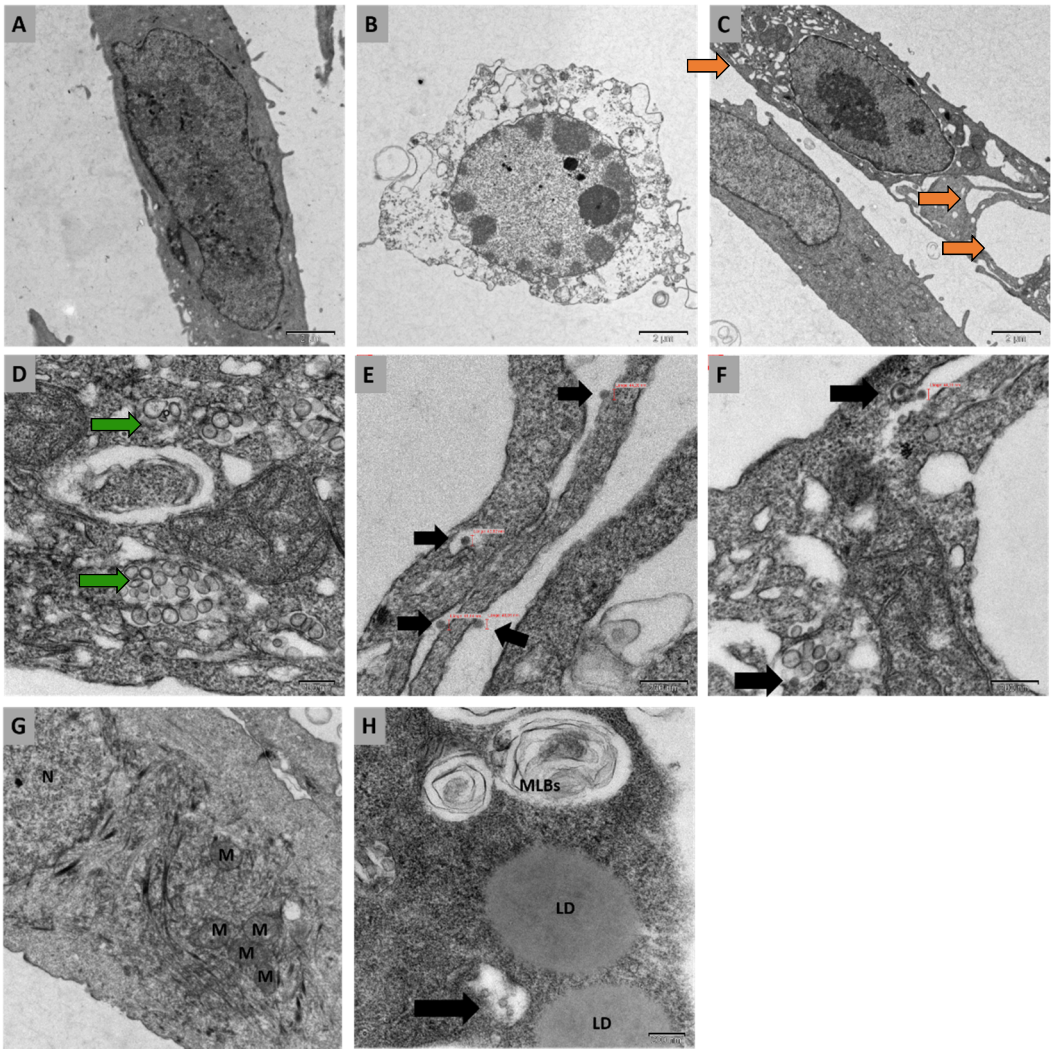

Figure 4.17 – Effects of ZIKV and U18 treatment on A549 cells. Transmission electron microscopy images of Polynesia-infected cells after 48 hpi. Effects of ZIKV infection on A549 **(B - G)** were directly compared with the morphology of uninfected cells **(A)**. Vacuoles, RFs, and viral particles are marked with orange, green and black arrows, respectively. Formation of MLBs and LDs after U18 treatment **(H)**. (LD – lipid droplet; M – mitochondria; N – nucleus, MLBs – multilamellar bodies)

4.2.3 Impact of autophagy inhibition and activation on ZIKV life cycle

Lastly, to gain further insight regarding the relevance of autophagy for the ZIKV life cycle, infected cells were harvested at 24, 48, and 72 hpi and treated, either with 5 mM of the inhibitor 3-MA or 100 nM of the activator Rapa. Unlike the preceding experiments, autophagy was directly blocked or activated using exclusively post-infection treatment, since these modulators do not interfere with steps related to the entry of the virus.

4.2.3.1 Determination of intra- and extracellular ZIKV genomes

To determine the amount of intra- and extracellular ZIKV genomes, RT-qPCR was performed. In relation to 3-MA treatment, the amount of intracellular ZIKV genomes were impaired for both strains **(Fig 4.18 A, B)**. More specifically, a noteworthy downtrend of the intracellular Polynesia genomes was revealed within 24 hpi after treatment, succeeded by slight decreases until 72 hpi **(Fig 4.18 A)**. As for the Uganda strain, the same fold reduction was visible within 24 hpi, proceeded from a hardly noticeable increase, and once more, a decrement at 72 hpi **(Fig 4.18 B)**. On the other hand, Rapa treatment enhanced the amount of intracellular genomes for all time points and for both strains, with the exception at 72 hpi for the Uganda strain **(Fig 4.18 D)**. Moreover, the effect of Rapa on the Uganda strain was undoubtedly lost over the time frame **(Fig 4.18 D),** while the Polynesia strain underwent some fluctuations **(Fig 4.18 C)**.

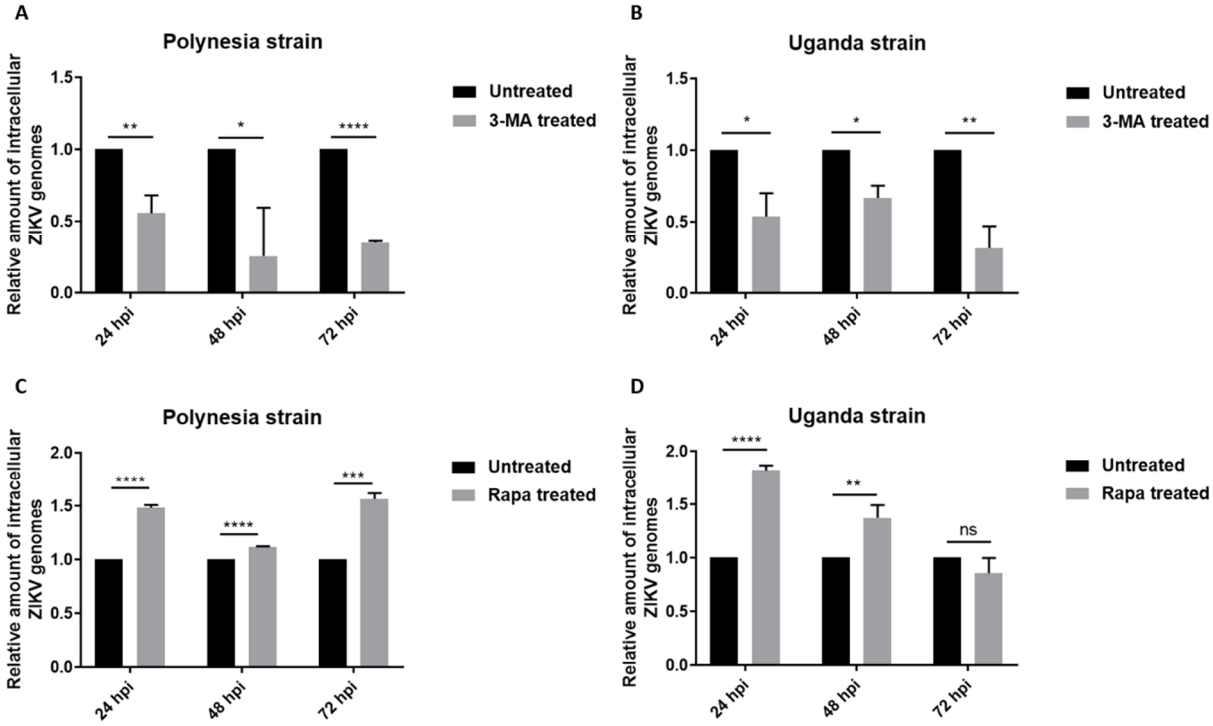

Figure 4.18 – 3-MA treatment lowers the amount of intracellular ZIKV genomes, while Rapa causes an upregulation of ZIKV genomes. Determination of the amount of intracellular ZIKV genomes in Polynesia- **(A, C)**, and Uganda-infected cells **(B, D)** was performed by RT-qPCR. A549 cells were treated with 5 mM of 3-MA, and 100 nM of Rapa after (post-) infection. As control, infected-untreated cells were used to normalise the values of 24, 48, and 72 hpi-treated cells. The error bars represent mean ± SEM (n=2). A replicate was excluded for visualisation of the impact of the treatment.

Regarding the extracellular ZIKV genomes, the Polynesia strain displayed a significant diminution of the genomes within 24 hpi after 3-MA treatment, followed by an increment over time until 72 hpi, reaching the control level **(Fig 4.19 A)**. Comparable results were observed for the Uganda strain, but at a later time point, the amount of extracellular ZIKV genomes remained approximately stable **(Fig 4.19 B)**. Concerning the Rapa treatment, an elevation of the amount of extracellular Polynesia genomes was perceived from 48 to 72 hpi. Measurement of 24 hpi resulted in higher standard deviation, leading to a not meaningful result **(Fig 4.19 C)**. On the contrary, extracellular Uganda genomes went down steadily over time, with an irregularity at 48 hpi **(Fig 4.19 D)**.

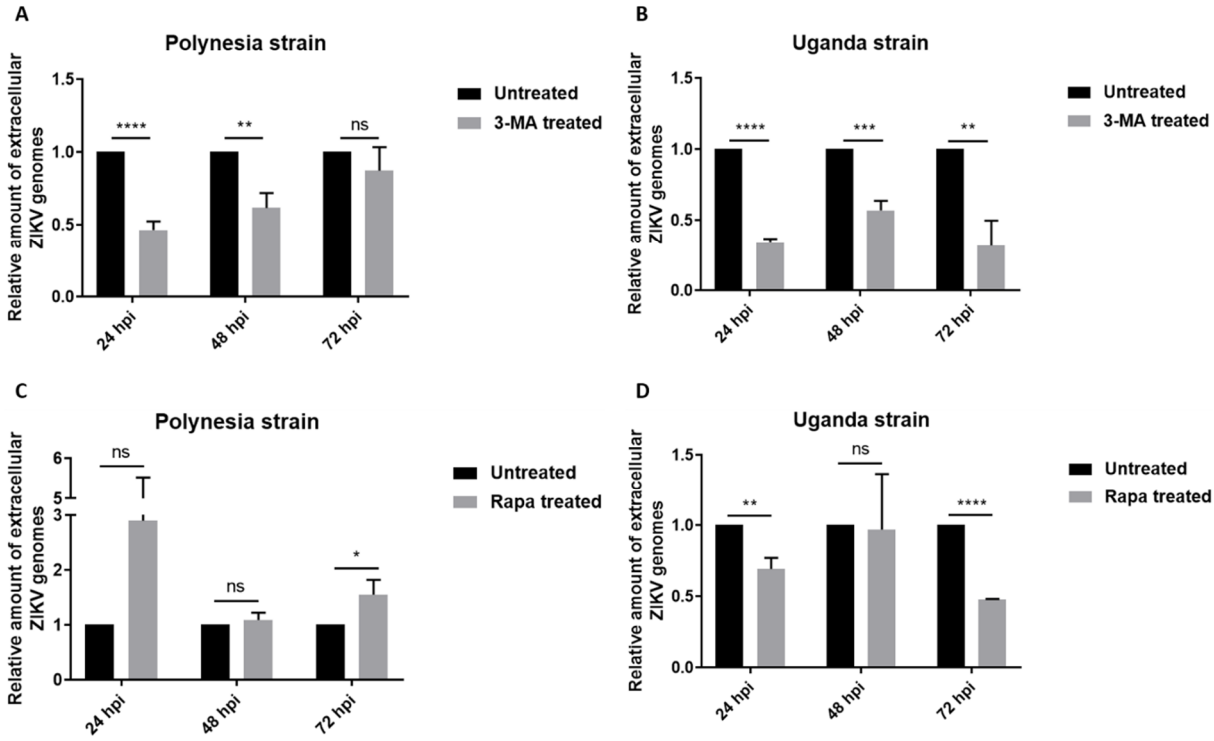

Figure 4.19 – The amount of extracellular ZIKV genomes is lessened by 3-MA treatment and undergoes different effects by Rapa treatment. Determination of the amount of ZIKV genomes in supernatants from Polynesia- **(A, C)**, and Uganda-infected cells **(B, D)** was performed by RT-qPCR. A549 cells were treated with 5 mM of 3-MA, and 100 nM of Rapa after (post-) infection. As control, infected-untreated cells were used to normalise the values of 24, 48, and 72 hpi-treated cells. In some bars, the error bars represent mean ± SEM (n=2). The outliers were excluded for visualisation of the impact of the treatment.

4.2.3.2 Determination of intra- and extracellular infectious viral particles

To assess the number of intra- and extracellular infectious viral particles, plaque forming assay was conducted. 3-MA led to a decline of the intracellular viral titers only at 24 hpi for the Polynesia strain, while the Uganda strain showed a decreasing effect measured for all time points **(Fig 4.20 A, B)**. Contrarywise, Rapa treatment promoted a significant augmentation of the virus titers for the Uganda strain. **(Fig 4.20 D)**. The number of Polynesia-infectious viral particles went up only at 48 hpi after treatment **(Fig 4.20 C)**.

Overall, the intracellular virus titers of untreated cells resembled the ones already presented in Chapter 4.2.1 and 4.2.2. However, some differences in the number of infectious viral particles for the Polynesia strain were discernible. For the 3-MA experiment, a variation was found at 24 and 48 hpi, and only at 24 hpi for Rapa experiment **(Fig 4.20 A, C)**. These higher and lower titers, at 24 and 48 hpi, respectively, led to a disappearance of the peak at 48 hpi **(Fig 4.20 A)**. With respect to the Uganda strain, minimal

changes were distinguished between experiments. In other words, comparable progression of infection was recognised, with a peak of infection at 48 hpi, followed by an unsubstantial decrease at 72 hpi **(Fig 4.20 B, D)**. The intracellular Uganda titers were higher for the 3-MA experiment at all time points **(Fig 4.20 B)**.

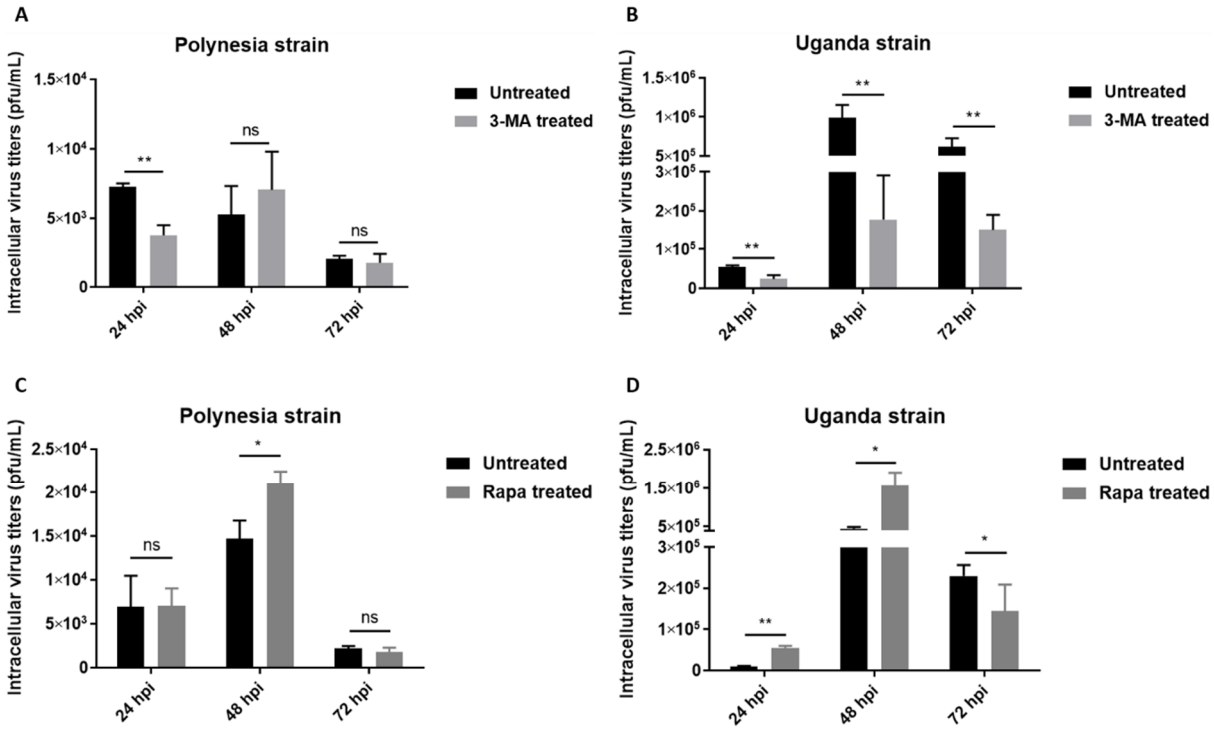

Figure 4.20 – 3-MA and Rapa treatment have impact on the intracellular Uganda titers and almost no effect on intracellular Polynesia titers, respectively. Extracellular ZIKV titers of Polynesia- **(A, C)**, and Uganda-infected cells **(B, D)** were assessed by plaque forming assay in Vero cells. A549-infected cells were treated with 5 mM of 3-MA, and 100 nM of Rapa after (post-) infection. The intracellular virus titers are expressed in plaque-forming units per mL (pfu/mL). Infected-untreated cells were used for direct comparison with the values of 24, 48, and 72 hpi-treated cells. In some bars, the error bars represent mean ± SEM (n=2). The outliers were excluded for visualisation of the impact of the treatment.

As for the extracellular virus titers, no significant effect was detected for Polynesia and Uganda strains after 3-MA and Rapa treatment, respectively. (**Fig 4.21 A, D)**. The same holds true for the Polynesia strain after Rapa treatment, with the exception at 72 hpi where an impairment of the number of infectious viral particles was visible **(Fig 4.21 C)**. Meanwhile, 3-MA treatment reduced the number of extracellular infectious viral particles for 24 and 48 hpi **(Fig 4.21 B)**.

The same tendency for the extracellular virus titers, as reported in the previous chapters, was noticed. As matter of fact, Polynesia titers reached its maximum at 48 hpi and went down at 72 hpi **(Fig 4.21 A, C)**. The number of Uganda infectious viral particles went up for the 3-MA experiment until 48 hpi and stayed the same from 48 to 72 hpi **(Fig 4.21 B)**. For the Rapa experiment, the Uganda titers continued to increase until 72 hpi **(Fig 4.21 D)**.

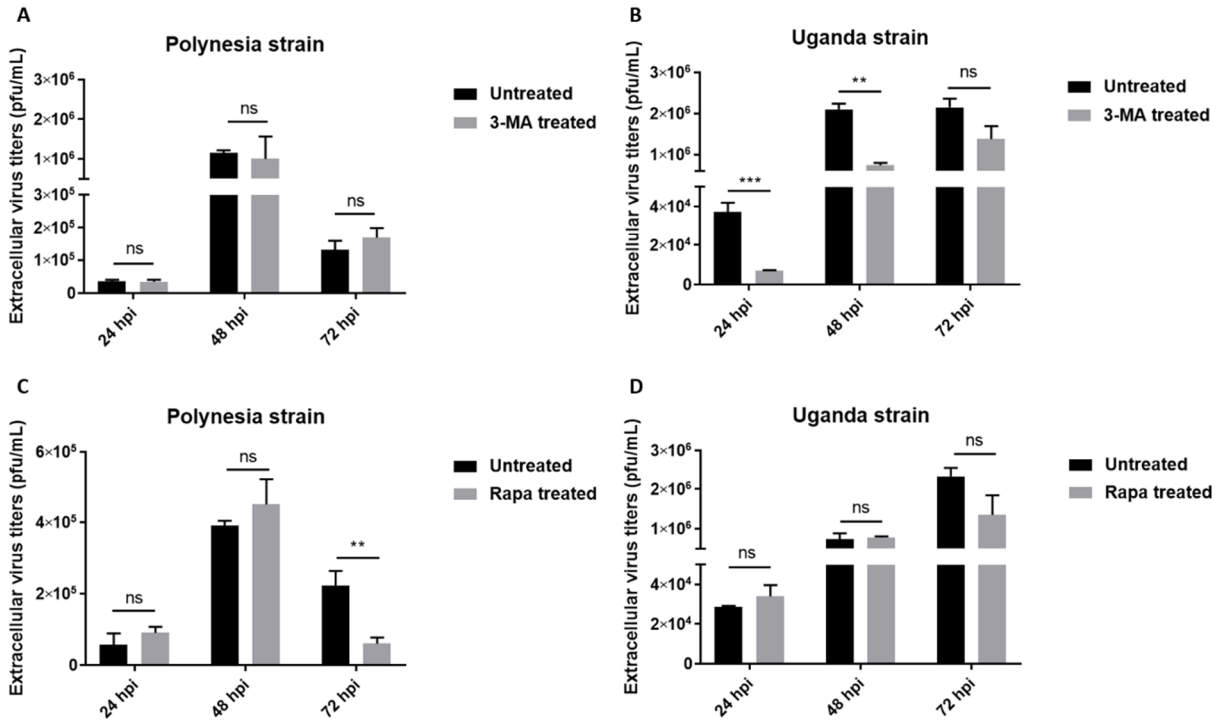

Figure 4.21 – The extracellular virus titers are mostly not affected by 3-MA or Rapa treatment. Extracellular ZIKV titers of Polynesia- **(A, C)**, and Uganda-infected cells **(B, D)** were assessed by plaque forming assay in Vero cells. A549-infected cells were treated with 5 mM of 3-MA, and 100 nM of Rapa after (post-) infection. The extracellular virus titers are expressed in plaque-forming units per mL (pfu/mL). Infected-untreated cells were used for direct comparison with the values of 24, 48, and 72 hpi-treated cells. In some bars, the error bars represent mean ± SEM (n=2). The outliers were excluded for visualisation of the impact of the treatment.

4.2.3.3 Determination of the amount of ZIKV and autophagy proteins

To study the effect of 3-MA on the amount of autophagy and ZIKV proteins, western blot analysis was performed. Detection of LC3-II and p62 was carried out in uninfected cell lysates to investigate the influence of the treatment on autophagy markers. Densitometric quantification revealed an increment of p62 and LC3-II after 3-MA treatment **(Appendix V A, B)**. In infected cell lysates, an augmentation of p62 levels was observed for both strains **(Fig 4.22 A, C, E and Appendix V D, F)**. On the other hand, LC3-II amount decreased for the Polynesia strain and increased for the Uganda strain **(Appendix C, E)**. Regarding ZIKV-NS1 protein, a marginal decline was perceived for the Polynesia strain, with an exception at 72 hpi **(Fig 4.22 B)**. Still, lower NS1 levels were present for the Uganda strain **(Fig 4.22 D)**.

The same study was conducted for Rapa. In uninfected cell lysates, a downtrend of p62 and LC3-II levels was discerned after treatment, with an irregularity at 48 hpi for the LC3-II **(Appendix VI A, B)**. Likewise, these proteins were detected in infected cell lysates. In the same manner, less amount of p62 and LC3-II was found after treatment **(Fig 4.23 A, C, E and Appendix VI C, D, E, F)**. But, small accumulation was perceptible for the Uganda strain at 24 hpi **(Appendix VI E)**. With reference to ZIKV-NS1 protein, Rapa treatment induced an accumulation over time for the Polynesia strain **(Fig 4.23 B)**. An opposed effect was detected for the Uganda strain, with an abrupt decrement from 24 to 48 hpi **(Fig 4.23 D)**.

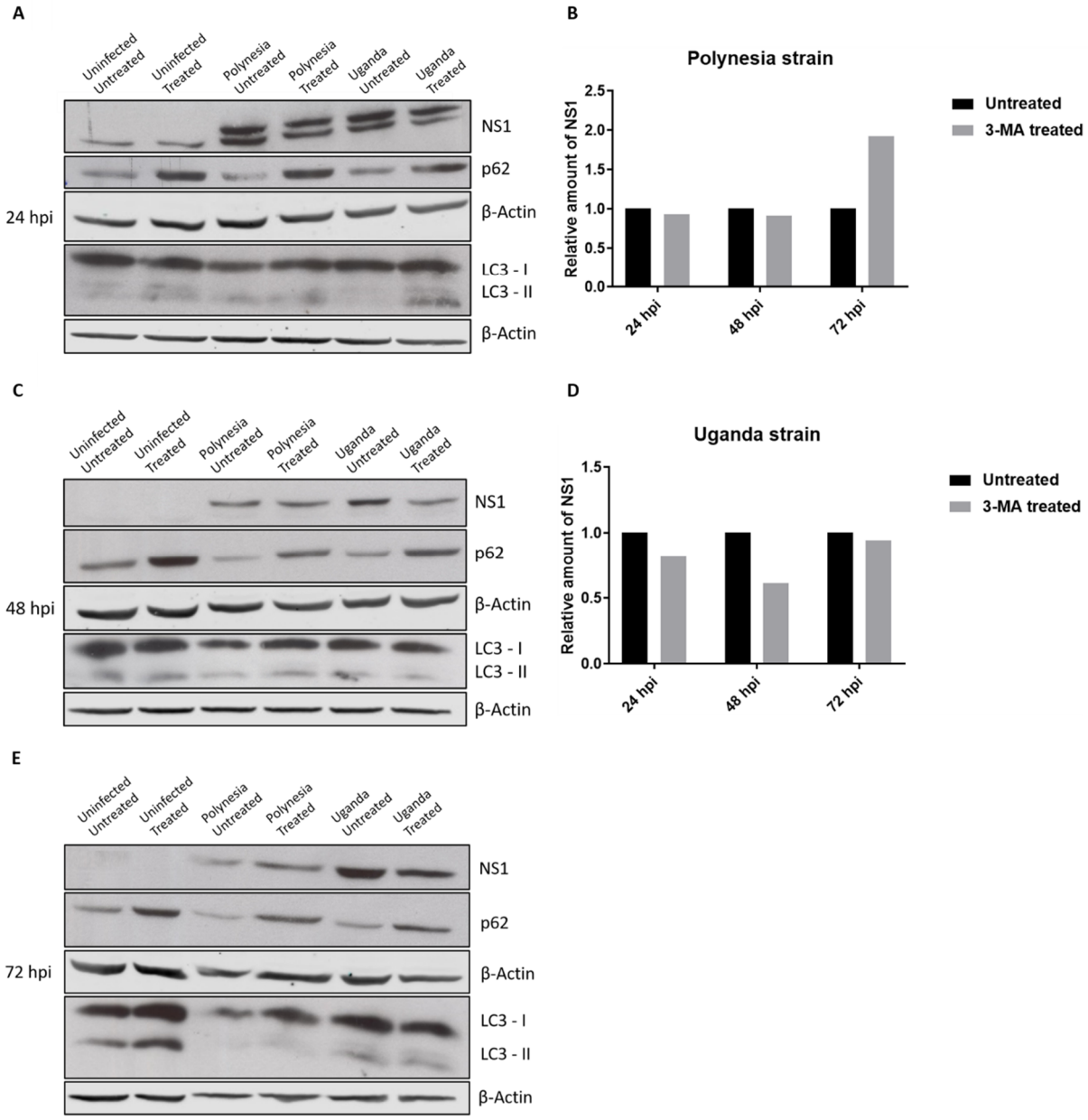

Figure 4.22 – 3-MA treatment lessened the amount of ZIKV-NS1 protein. Preparation of cell lysates was achieved by RIPA buffer and detection of ZIKV-NS1, p62, LC3, and β-Actin by consecutive western blot analysis. The protein levels were detected after 24 **(A)**, 48 **(C)**, and 72 hpi **(E)** for Polynesia-, and Uganda-infected cells. A549-infected cells were treated with 5 mM of 3-MA after (post-) infection. LC3-II and p62 were used as autophagy markers, while β-Actin was included as loading control. In **(A),** two bands were detected, with NS1 being the upper one. Beyond that, uninfected-untreated cell lysates were utilised as negative control. Furthermore, densitometric quantification of ZIKV-NS1 protein after 3-MA treatment for Polynesia **(B)** and Uganda **(D)** strains was accomplished by Image Studio Lite software. The values were first normalised to the loading control and then to infected-untreated cells. Antibody dilutions are indicated in Chapter 3.1.3

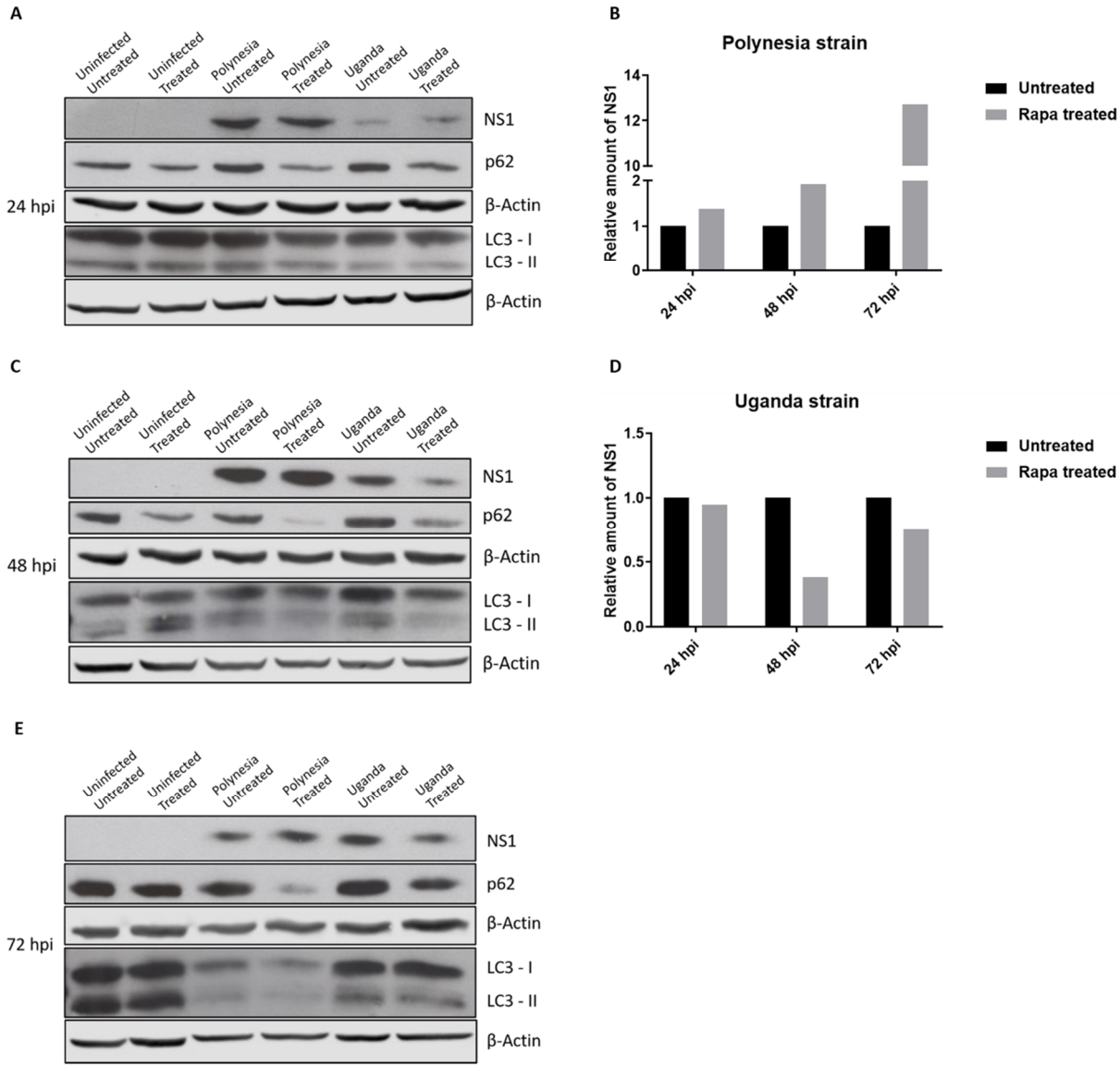

Figure 4.23 – Rapa treatment augments and reduces ZIKV-NS1 protein for Polynesia and Uganda strains, respectively. Preparation of cell lysates was achieved by RIPA buffer and detection of ZIKV-NS1, p62, LC3, and β-Actin by consecutive western blot analysis. The protein levels were detected after 24 **(A)**, 48 **(C)**, and 72 hpi **(E)** for Polynesia-, and Uganda-infected cells. A549-infected cells were treated with 100 nM of Rapa after (post-) infection. LC3-II and p62 were used as autophagy markers, while β-Actin was included as loading control. Beyond that, uninfected-untreated cell lysates were utilised as negative control. Furthermore, densitometric quantification of ZIKV-NS1 protein after Rapa treatment for Polynesia **(B)** and Uganda **(D)** strains was accomplished by Image Studio Lite software. The values were first normalised to the loading control and then to infected-untreated cells. Antibody dilutions are indicated in Chapter 3.1.3

4.2.3.4 Determination of the number of ZIKV-positive cells

To further gain insight about the effect of 3-MA and Rapa on the number of ZIKV and autophagy specific proteins, indirect immunofluorescence was performed. Monitorisation of autophagic activity was achieved by detection of p62 (red) and ZIKV-infected cells were identified with the 4G2 antibody (green). An accumulation of p62 was observed after 3-MA treatment. Concerning the E protein amount, comparable results were detected between treated and untreated cells for both strains **(Fig 4.24 A, B)**. In other words, 3-MA does not seem to affect the number of ZIKV-infected cells. As for the Rapa experiment, the laser intensity was reduced due to the high background of p62 channel in order to better discern protein present. A decline of p62 signal was revealed after treatment, but no significant differences on the amount of E protein were recognised for both strains **(Fig 4.24 C, D)**. Although, a

slight increase of Uganda-infected cells at 72 hpi after treatment was spotted **(Fig 4.24 D)**. On top of that, the cytopathic effect of ZIKV could be observed here.

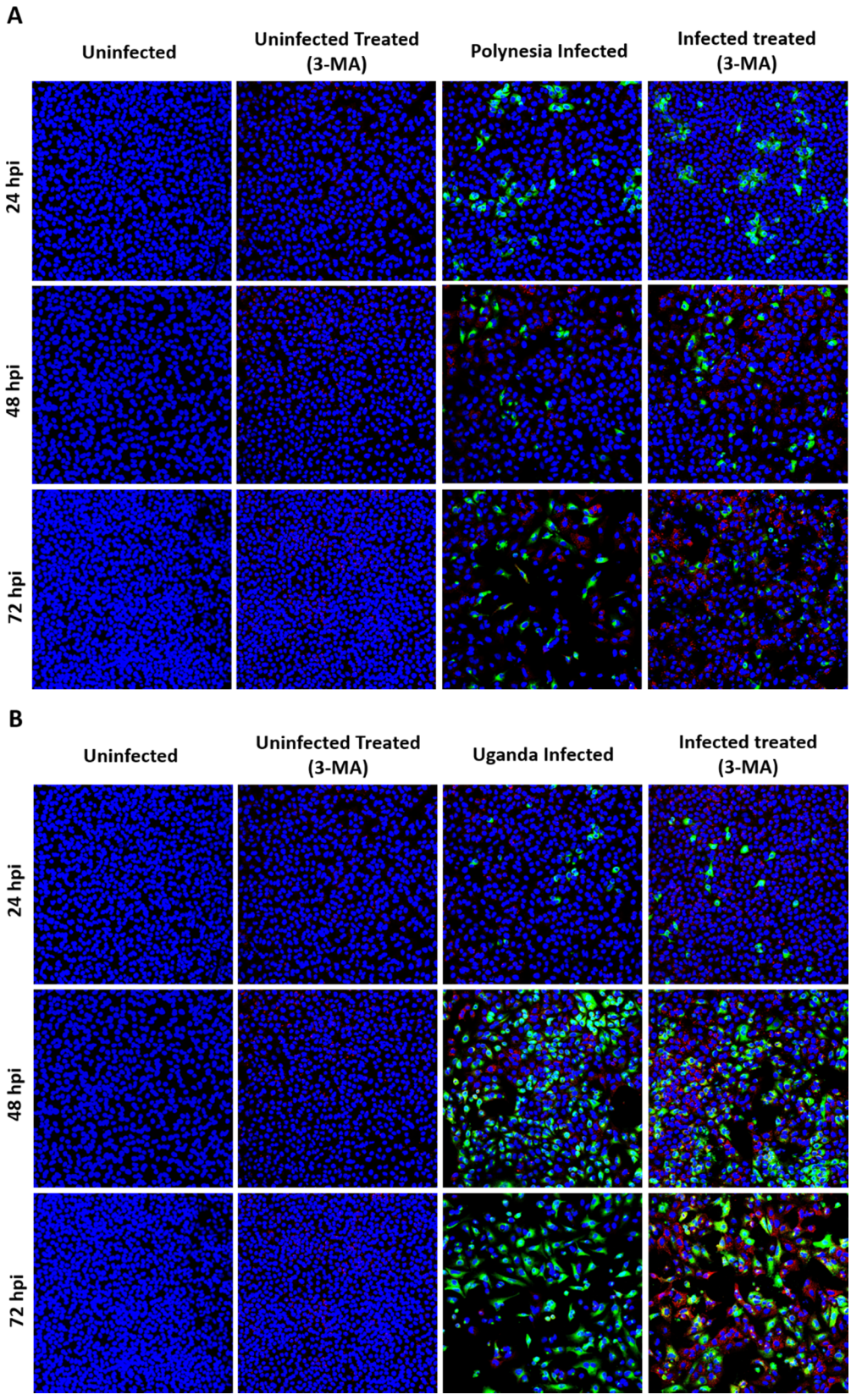

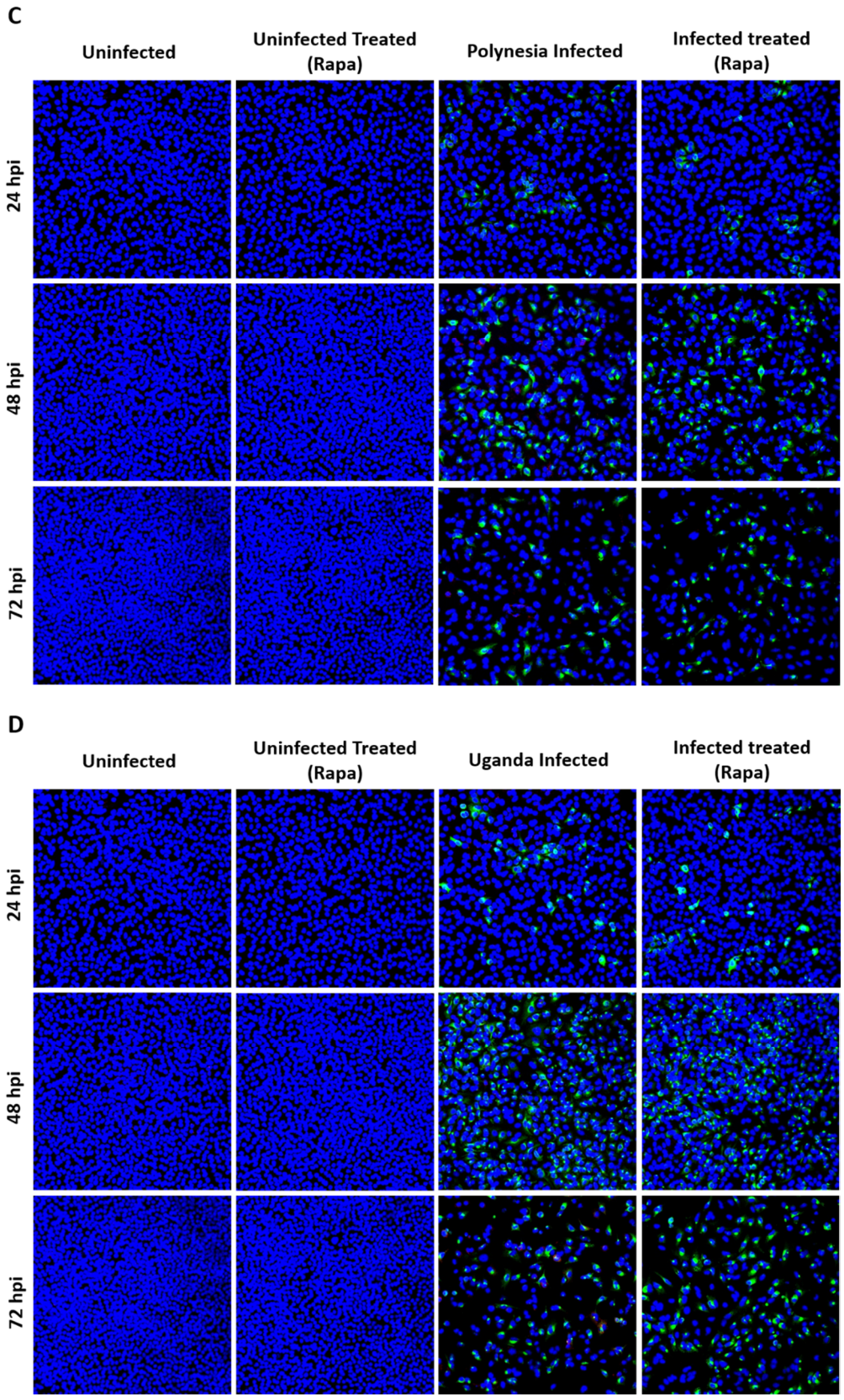

Figure 4.24 – No significant changes in the amount of E protein after treatment with 3-MA, and Rapa. Fluorescence analysis of Polynesia- **(A, C)**, and Uganda-infected cells **(B, D)** after 24, 48, and 72 hpi. Infected cells were treated post-infection with 5 mM of 3-MA **(A, B)**, and 100 nM of Rapa **(C, D)**. A549 cells were fixed with ethanol:acetone (1:1) and analysed by confocal laser scanning microscopy (CLSM). E protein, p62 and the nuclei were stained with 4G2 antibody (green), p62 antibody (red) and DAPI (blue), respectively. The pictures were taken with the 16x objective.

5. DISCUSSION

5.1 A549 cell viability after treatment with autophagy modulators and the cytotoxicity of these compounds

PrestoBlue and LDH assays were performed to inspect the cell viability of A549 after treatment with autophagy modulators and to evaluate the cytotoxicity of these chemicals, respectively. These assays allowed the discrimination between unspecific toxic effects and specific effects by the treatment, required for the interpretation of the results.

In the cell viability assay, the PrestoBlue reagent is metabolically reduced by viable cells from resazurin to resofurin.[144] An increase of relative cell viability was detected for BFLA within 24 h and for U18, after 24 and 48 h of treatment. Regarding U18, this elevation was also reported by Elgner *et al.*, 2016 in Huh 7.5 cells.[152] It can be speculated that this inhibitor hampers the function of proteases involved in the degradation of oxidoreductases. Thus, the PrestoBlue reagent undergoes an augmentation of its reduction by active cells. As for BFLA, the cellular stress caused by the impairment of autophagy could lead to an increment of the metabolism of cells to compensate the induced stress. Another plausible explanation can be the fact that by inhibiting autophagy, the lysosomal degradation of oxidoreductases could be affected, leading to an enhancement of the reduction of the reagent. Contrariwise, BFLA can also diminish the relative cell viability, as observed at 72 h, due to its role on both inhibition of cell growth and activation of apoptosis.[160,161] The about same drop of cell viability was shown for U18 at 72 h. This observation might be related to the induction of cell death in response to the accumulation of cholesterol in MVBs and lysosomes.[162] The relative cell viability went down for Rapa likely because it activates caspase-3 expression on human lung cancer cells (A549).[163,164] Caspase-3 is an endoprotease that promotes apoptosis, thereby Rapa lessens the amount of viable cells.[165]

On the other hand, the LDH assay estimates the number of dead cells by quantitatively measuring the LDH released into the cell culture medium from damaged cells.[145] No significant cytotoxicity for BFLA and U18 was revealed after 24 h of treatment. In fact, negative values were calculated because the absorbance of the treated samples was inferior to the untreated ones. This observation suggests that the compounds tested might interfere with the measurement or they could trigger pro-survival effects on A549. By contrast, Rapa caused around 20% of death cells within 24 h of treatment. This cytotoxicity, as already explained above, derive from the fact that Rapa upregulates caspase-3 expression.

5.2 Acidification of endosomal-lysosomal compartments plays a role on ZIKV life cycle

BFLA is a late autophagy inhibitor that blocks V-ATPases, preventing the acidification of the lumen of organelles such as lysosomes and endosomes.[129,130] Therefore, lysosomal degradation is impeded.[131] BFLA pre- and post-infection treatment was applied to study the relevance of endosomal-lysosomal acidification on the ZIKV entry and on the spreading of infection, respectively.

Determination of the amount of intra- and extracellular ZIKV genomes was accomplished by RT-qPCR analysis to assess the influence of the treatment at viral RNA levels. For pre-infection treatment, no significant amount of intracellular ZIKV genomes was visible for all time points analysed and for both strains. This fact indicates that BFLA might hinder receptor-mediated endocytosis, probably by precluding pH-dependent conformation changes necessary for the viral entry process. Consequently, no

new viral particles were produced and released to the supernatant, justifying the nonexistence of extracellular ZIKV genomes. As for post-infection treatment, the viral RNA was translated and replicated, but after the introduction of BFLA, the produced viral particles, even if they were exported, they would not be able to repeat their life cycle in other cells. Hence, a significant decline of the amount of intracellular ZIKV genomes was discernible within 24 hpi for the Polynesia strain. Due to a high standard deviation, no conclusion could be drawn for the Uganda strain at the same time point. However, at 48 and 72 hpi, no significant amount of intracellular ZIKV genomes was found for both strains because, even if newly assembled viral particles egressed the cell, they can no longer establish an infection in the neighbouring cells. Additionally, the infected cells will die over time, as a result of ZIKV cytopathic effect, releasing the viral genomes into the supernatant.[22,166,167] The high standard deviation for the Uganda strain at 24 hpi can most likely be attributed to an error. Possible errors can be an elevated MOI or a lower concentration of the modulator. A comparable outcome was noticed for the amount of extracellular ZIKV genomes. Once more, a high standard deviation was perceptible for the Uganda strain at 24 hpi. A noteworthy decrease of the extracellular ZIKV genomes was recognised at this time point. From these data, it can be concluded that the acidification of endosomal-lysosomal compartments is essential for the secretion of viral RNA. Furthermore, death of infected cells leads to the egress of the intracellular viral RNA into the extracellular space. Even though, this should promote an increase of detected RNA at 48 hpi, most of it seems to be removed by the included washing step between 24 and 48 hpi. This observation suggests that cell death occurs around 24 hpi. Thereupon, no significant amount of extracellular ZIKV genomes was evident at 48 and 72 hpi.

Even though RT-qPCR is an effective tool to detect viral genomic RNA, it measures RNA fragments, immature viral genomic RNA, naked capsids loaded with RNA, and unpackaged genomes. For those reasons, plaque forming assay was carried out to determine the number of actual intra- and extracellular infectious viral particles. This method provides insight on the amount of virions that are capable to execute the life cycle. Lethal mutations in the viral genomes, as well as incorrect packaging or loss of envelope can result in lack of infectivity or capability to establish infection. For pre-infection treatment, no significant number of intra- and extracellular infectious viral particles was perceived for both strains and for all time points analysed. These data are in agreement with the results of RT-qPCR analysis. The fate of the infectious viral particles which entered the cells during the initial input remained unknown. Since the MOI used to infect cells was too low, the internalised particles might not be easily detected by intracellular plaque assay. Despite that, another explanation for the lack of intracellular infectious viral particles might be that there is still some activity in the endosomes. Therefore, the viral envelope could be partial degraded and the genomic RNA is solubilised. An alternative to this, the virus particles that reside inside the compartments, might exit the cell by sorting in the endosomal pathway.[168] Then, the washing step removes the released infectious particles, preventing their detection. Meanwhile, for post-infection treatment, some intracellular infectious viral particles were produced within 24 hpi, but in a less number when compared to the untreated ones. The infection is established, but after the introduction of BFLA the receptor-mediated endocytosis is disturbed, thus the intracellular virus titers went down after treatment. As for the extracellular infectious viral particles, no plaques were formed for both strains, indicating that viral maturation requires conformational changes at low pH and, consequently, spreading of infection is impaired. Hence, the extracellular viral RNA detected by the RT-qPCR does not seem to be included in infectious viral particles.

The effect of BFLA on the protein level was also investigated. For this purpose, western blot analysis was performed and ZIKV-NS1, p62, and LC3 were detected in cell lysates. First, detection of the autophagy markers, p62 and LC3, was carried out in uninfected cell lysates to analyse the impact of the treatment itself. Densitometric quantification revealed an accumulation of p62 over the time frame. The

same outcome was observed in infected cell lysates. These findings were expected due to the fact that p62 degradation is autophagy-dependent.[121] On top of that, the LC3-II/LC3-I ratio was higher at all time points for uninfected cells treated with BFLA than for the untreated ones. This fact stems from an accumulation of LC3-II, resulted from an impairment of lysosomal degradation. Despite that, the ratio decreased with the time, as a consequence from a rise of LC3-I amount. Possible reasons could be the delipidation of LC3-II from the outer membrane of the autophagosome or a compensatory upregulation of LC3-I. Nevertheless, an increment of LC3-II/LC3-I ratio was quantified in infected cell lysates, suggesting that ZIKV infection interferes with the mechanism behind this augmentation of LC3-I. With respect to ZIKV-NS1 detection, the results were shown to support the RT-qPCR data. For pre-infection treatment, NS1 was absent for all time points and for both strains, demonstrating that by disrupting receptor-mediated endocytosis, the translation of the viral polyprotein was impeded. As for post-infection treatment, a notable diminution of the NS1 amount at 24 hpi was visible for both strains, confirming the indirect influence of BFLA on viral proteins translation. Still, the reduction of NS1 was less evident for the Uganda strain, substantiating the higher infectivity for this strain as measured in plaque forming assay. This elevated amount of NS1 for the Uganda strain was also verified by Liu *et al.*, 2017, in Vero cells, when compared to Asian strains.[169]

Confirmation of these findings was accomplished by indirect immunofluorescence microscopy. This method allowed to further gain insight on the impact of this modulator on ZIKV infection and to determine the intracellular localisation and distribution of ZIKV-specific proteins as well. As expected, no E protein was detected for pre-infection treatment, whereas for post-infection, a significant decline of the E protein amount was noticed. A reticular structure appeared after BFLA treatment that might derived from an accumulation of the E protein in the ER and Golgi compartments. In addition, cytosolic dots were also discernible, which could indicate that virus particles might get trapped in heavily enlarged endosomes/lysosomes or that the viral polyprotein undergoes an uncorrected processing.

In conclusion, BFLA affects the receptor-mediated endocytosis and, once the infection is established, the acidification of endosomal-lysosomal compartments is crucial for both early and late steps of the ZIKV life cycle. A similar effect of the acidification inhibition of these compartments in ZIKV infection was also reported by Delvecchio *et al.*, 2016 through the use of Chloroquine.[81]

5.3 Intracellular cholesterol trafficking inhibition hinders ZIKV infection

U18 is a chemical compound that affects the trafficking of the intracellular cholesterol, leading to its accumulation in late endosomes/MVBs and lysosomes.[136] Subsequently, their biogenesis is impaired. Pre- and post-infection treatment was applied to study the influence of U18 on the ZIKV entry and on the spreading of infection, respectively.

RT-qPCR analysis was performed to inspect the impact of U18 on viral RNA levels by the determination of ZIKV genomes. The number of intracellular ZIKV genomes were found to be almost identical for both strains, without substantial variations between pre- and post-infection treatment. The minor changes at 24 hpi reflects the longer duration of treatment for pre-infection compared to post-infection. Overall, a downtrend was perceptible over time after treatment, with remarkably low amount of genomes at 48 and 72 hpi. The intracellular cholesterol accumulation could interfere with the virus entry process, as it was demonstrated by Lee *et al.*, 2008 for JEV and DENV.[170] The excess cholesterol changes the rigidity of the cellular membranes, possibly affecting uncoating of the genomic RNA.[170] Additionally, viral replication might be hampered by the reduction of cholesterol in the ER, which could have

repercussions on the replication complex formation.[136] Similar results were obtained for the extracellular ZIKV genomes for both strains. From this outcome, it can be presumed that the decrease of the extracellular genomes stems from the decrement of the intracellular ones. Nonetheless, the fact that the export of viral RNA could be compromised as well cannot be excluded. Particularly, an increase of genomes at 72 hpi compared to 48 hpi, was recognised after treatment. It was more pronounced for the Polynesia strain, which might be attributed to its higher cytopathic effect. Moreover, a strong deviation was observed for the Polynesia strain at 72 hpi pre-infection treatment. The origin of this discrepancy can be ascribed to sample contamination or errors in the execution of the experiment.

Furthermore, the number of intra- and extracellular infectious viral particles was assessed by plaque forming assay. Apart from the statistical tests, intra- and extracellular viral titers were reduced for all time points and both strains. These findings could be the result of interference in viral entry, replication or release. The mechanistic influence of U18 was investigated by Elgner *et al.*, 2016 for HCV, and for DENV by Poh *et al.*, 2011.[152,171] These reports demonstrated the inhibition of DENV entry and replication, and also HCV viral particles release by U18.

The impact of U18 on viral and cellular protein level was determined as well. For this purpose, western blot analysis was performed and ZIKV-NS1, LAMP2, p62, and LC3 were detected in cell lysates. Densitometric quantification revealed an accumulation of p62 levels in uninfected and infected cell lysates over time. This might be explained by the impairment of the biogenesis of MVBs and lysosomes and thus, degradation via autophagy is blocked. For the same reasons, the LC3-II/LC3-I ratio increased, but this ratio dropped over the time frame, which might be caused by a compensatory upregulation of LC3-I or delipidation of LC3-II, as suggested for BFLA. Looking at LAMP2, a lysosomal marker included in this study, an accumulation was evident after U18 treatment, as clearly shown by Elgner *et al.*, 2016.[152] Since the intracellular accumulation of cholesterol impedes the biogenesis of MVBs and lysosomes, these organelles promote the formation of non-functional lysosomal MLBs, which are also positive for LAMP2. As for the ZIKV-NS1, its amount was minimised for pre-infection treatment, proposing an effect of U18 on viral translation or entry. On the other hand, a gradual decline of NS1 amount was visible for post-infection treatment. The viral translation or entry was also disturbed, but with the difference of a previous establishment of infection before the introduction of U18.

To further gain insight about the influence of U18 on ZIKV infection, indirect immunofluorescence was performed. As a verification of the intracellular cholesterol accumulation due to U18 treatment, filipin complex was required in this experiment, since it binds to free cholesterol.[172] Comparable augmentation of cholesterol after treatment was stated by Poh *et al.*, 2011 and Elgner *et al.*, 2016.[152,171] In addition, the disruption of the autophagic activity, as a result of the defective biogenesis of lysosomes, was monitored by the increment of p62. Regarding ZIKV-specific protein, the E protein amount diminished in the presence of U18, corroborating its intervention on the viral entry, replication or release. However, a gradual elevation of the number of positive cells from 24 to 48 hpi after treatment was perceived for both strains, indicating a kind of lag-phase in the life cycle of treated cells. Using the same method, the intracellular distribution and localisation of these proteins was also inspected. U18 induced a dispersion of the E protein throughout the cytoplasm which could reflect an effect on membrane fluidity and, consequently, on the formation of the RFs or release of viral particles.

To better understand ZIKV infection and the impact of the treatment on a cellular level, transmission electron microscopy was performed. The ZIKV cytopathic effect was clearly observed after 48 hpi for the Polynesia strain by the presence of pyknosis, cytoplasmic fragments and cell shrinkage. All this indicate imminent cell death. Moreover, ZIKV induces cytoplasmic vacuole formation derived from the ER, as reported by Monel *et al.*, 2017.[173] This cytoplasmic vacuolisation together with the swelling of

the ER and mitochondria characterises a specific type of cell death, paraptosis.[174] Displacement of swollen mitochondria and of other cellular organelles was also discernible, suggesting possible cytoskeletal rearrangement, as proposed by Cortese *et al.*, 2017.[85] This conjunct of modifications favours the formation of the RFs. In fact, VPs were easily identified. Potential viral particles were found in close association with the RFs and the large vacuoles, reinforcing the importance of these cellular alterations for viral replication and assembly. Treatment with U18 revealed MLBs and lipid droplets formation. Besides the inhibition of the trafficking of cholesterol, U18 blocks the trafficking of lipids, leading to its accumulation in these lipid droplets.[136] As suggested for HCV, the viral particles might get trapped inside of the MLBs, since U18 seems to affect exocytosis. However, no direct association between ZIKV viral particles and MLBs were visible.

To sum up, U18 could have an effect of different stages of the ZIKV life cycle. On one hand, it might interfere with early steps since viral replication to assembly and/or interfere with late steps, namely exocytosis of the viral particles. Thus, further experiments are required to clarify this.

5.4 Autophagy is involved in ZIKV replication

3-MA and Rapa are directly involved in the initiation of autophagy. 3-MA inhibits the PI3KC3 and, as a consequence the PI3P production is impaired, thereby the phagophore is unable to be formed.[126,127] On the other hand, Rapa blocks the kinase activity of mTOR, activating the ULK1/2 complex and thus, contributing to the phagophore creation.[138] Therefore, 3-MA and Rapa constitutes autophagy inhibitor and activator, respectively. In this study, only post-infection treatment was applied since these modulators do not affect steps related to the entry of the virus.

The effect of the treatment at viral RNA levels was investigated by RT-qPCR analysis of the ZIKV genomes. A meaningful diminution of the intracellular ZIKV genomes was detected after 3-MA treatment within 24 hpi, suggesting that autophagy plays a role in the virus replication. Thereupon, less viral RNA was secreted, as shown for the extracellular ZIKV genomes. Similar results were reported by Hamel *et al.*, 2015 and Liang *et al.*, 2016.[22,140] However, it is important to consider that the inhibitory effect of 3-MA in the PI3KC3 is transient.[175] Additionally, 3-MA inhibits the class I PI3K, which indirectly promotes autophagy induction. That being said, after the effect of 3-MA on the PI3KC3 is concluded, autophagy is induced. From 24 to 48 hpi, the relative amount of intracellular genomes stayed constant for both strains. Interestingly, for 72 hpi the amount of intracellular ZIKV genomes went down. This could indicate an overlapping effect of 3-MA, where renewing of the medium refreshes the blocking ability of 3-MA, causing the relative values to grow apart. However, the extracellular number of genomes revealed an increase over time for the Polynesia strain and a reduction for the Uganda strain at 72 hpi. While these data correlate for the Uganda strain, it is surprising to detect an elevation in extracellular genomes, while the intracellular amount decreases for the Polynesia strain. If refreshing the medium induced inhibition of autophagy anew, a slowed production of viral RNA would be expected for both strains, making it impossible to deduce reasons for the observed increase in extracellular RNA for Polynesia without further experiments. Nonetheless, the influence of 3-MA might differ between the two strains and promote certain parts of the life cycle. In relation to Rapa, the two ZIKV strains behaved differently over time in response to the treatment. As a matter of fact, the influence of the treatment on the amount of intracellular Uganda genomes caused a gradual decline over time, while the impact varied for the Polynesia strain, with a deviation at 48 hpi. Overall, Rapa significantly elevated the amount of intracellular genomes for 24 hpi, supporting the role of autophagy on ZIKV replication. The decrease at 48 hpi could be explained by the unfolding of the toxic effect of Rapa and therefore, lowering the relative values. Since the cell viability of Rapa-treated cells has been shown to stay more or less constant from

48 to 72 h, an incline of intracellular RNA was observed at 72 hpi for the Polynesia strain. On the other hand, the intracellular number of genomes continued to decrease for the Uganda strain until 72 hpi. Concerning the amount of extracellular ZIKV genomes, Rapa treatment supports the data for the intracellular number of genomes for the Polynesia strain, exhibiting similar changes at the same time points. However, the Uganda strain displayed a decline in extracellular genomes for 24 and 48 hpi, when compared to the untreated ones, while the amount was elevated for the intracellular genomes. Even though the intracellular number of genomes was reduced from 24 to 48 hpi, the level of the extracellular amount remained more or less constant for those two-time points. Lastly, the amount of extracellular Uganda genomes decreased at 72 hpi. This indicates, that while Rapa induces autophagy, it exposes different impacts on the strains. The induction of autophagy seems to promote viral replication, leaving the export of RNA unaffected for the Polynesia strain. As for the Uganda strain, induction of autophagy causes an initial augmentation of the intracellular ZIKV genomes, after which a steady decline was evident. Furthermore, the number of extracellular genomes stayed lower than for the untreated cells, possibly indicating an adverse impact on the release.

To evaluate the impact of the modulators on the internalisation and production of infectious viral particles, plaque forming assay was performed. The inhibitory effect of 3-MA on autophagy revealed a decrease of the number on intracellular infectious viral particles for both strains. These data reinforce the possible role of autophagy on viral replication and, consequently, on viral production, as demonstrated by the decline of the extracellular virus titers. Nonetheless, the release of infectious viral particles for the Polynesia strain did not seem to be affected. Interestingly, this observation was also reported by Frumence *et al.*, 2016.[166] An elevation of the number of Uganda intra- and extracellular infectious viral particles at 48 and 72 hpi was evident when compared to 24 hpi, probably due to the overlapping effect of 3-MA. These findings are in agreement with the RT-qPCR results. However, no significant changes of the intra- and extracellular viral titers were measured for the Polynesia strain. Concerning Rapa treatment, a general rise of the number of intracellular infectious viral particles was noticed, but no changes on the amount of the extracellular ones. This fact indicate that the role of autophagy might be on viral replication, without affecting the secretion of infectious viral particles. An unexplainable decrease of the extracellular virus titers was found for the Polynesia strain at 72 hpi.

The influence of 3-MA and Rapa on viral and cellular protein levels was investigated as well through the western blot detection of ZIKV-NS1, p62, and LC3 in cell lysates. After 24 hpi, an augmentation of p62 level was detected after 3-MA treatment for uninfected and infected cell lysates due to the impairment of lysosomal degradation. Surprisingly, it seems that 3-MA can increase the p62 amount, even after the inhibitory effect of 3-MA on autophagy is over. This increment was also observed by Wu *et al.*, 2010 where they showed that upregulation of p62 by 3-MA is independent of the autophagy machinery.[175] In fact, 3-MA can elevate the transcription rate of the mRNA, leading to a rise of the protein expression.[175] Opposing this, Rapa diminished the p62 level in both uninfected and infected cells lysates, as result of the enhancement of the autophagic activity. With respect to LC3, LC3-II keeps the about same level after treatment with 3-MA, since the conversion of LC3-I to LC3-II is impeded. Looking at the LC3-II/LC3-I ratio, no conclusion can be drawn due to quantification errors, as well as detection problems. As for Rapa, the LC3-II/LC3-I ratio underwent some fluctuation, but a general decrease can be discernible. This decline traduces in a reduction of LC3-I level when compared to the untreated one. This observation is a consequence of the increment of the autophagic activity. Regarding ZIKV-NS1, a gradual elevation was visible for both treatments, whereas slight reduction was noticed. As shown for the number of genomes, the amount of ZIKV-NS1 between the two strains was different. This fact proposes a diverse effect of autophagy on ZIKV infection depending on the strain.

To further understand the importance of autophagy on ZIKV infection and to determine the impact of these modulators on the number of ZIKV-positive cells, indirect immunofluorescence was performed. As demonstrated for western blot analysis, an accumulation and reduction of p62 was discernible after 3-MA and Rapa treatment, respectively. Regarding the E protein amount, similar results were obtained for untreated and treated cells for both strains. This observation suggests that autophagy does not affect the spreading of infection and the influence might be only facilitating the viral replication.

As a conclusion, the impact of 3-MA and Rapa seems to be mainly on ZIKV replication, supporting the proposed role of autophagy on providing membranes for the replications sites.[140]

6. FUTURE PERSPECTIVES

Currently, there is no vaccine or specific antiviral drug available for ZIKV infection. Together with the increase of microcephaly cases, discovering a way to reduce or eradicate the infection has become urgent. Therefore, further studies should be pursued to better understand the ZIKV life cycle.

In the framework of this thesis, the relevance of the acidification of endosomal-lysosomal compartments and the trafficking of intracellular cholesterol, as well as the role of autophagy on ZIKV infection were under investigation.

An effect of BFLA on the viral entry and maturation was discernible. However, the exact mechanism how the augmentation of pH can impair these processes is not fully clear by the experiments that were performed. Thereupon, more experiments should be carried out as an attempt to elucidate this. Another interesting aspect would be the study in detail the composition of the reticular structure and the cytosolic dots formed after BFLA treatment. This could be achieved by co-staining with ER/Golgi markers such as, PDI, TGN46 or GM130, and with autophagy/lysosomal markers like, p62, LC3 or LAMP-2, respectively.

The exact steps of the ZIKV life cycle that are affected by U18 are still unclear. Thus, further experiments need to be performed, focusing especially on viral replication and on the release of viral particles. Since the TEM experiments were inconclusive regarding the determination of possible viral particles inside MLBs, immunogold labelling could be performed to address this question. This method allows the identification of organelles and viral particles by using specific antibodies. Moreover, the dispersion of the E protein induced by U18 is an interesting topic to be further investigated and may clarify the impact of the modulator. Co-staining with cytoskeletal markers such as, β-Actin, α- and β-Tubulin, and Cytokeratin 8 might be performed.

Additionally, a major asset in the comprehension of the higher pathogenesis of the Asian strain, when compared to the African strain relies on comprehending the differences presented by the two strains during autophagy modulation. Different inhibitors should be used to further investigate these variations.

This work provided insights into the relationship between autophagy and ZIKV, which can be helpful for ongoing studies on other flaviruses. Furthermore, the knowledge gained from the results of this thesis can be used to the development of new compounds with antiviral activity against ZIKV.

7. REFERENCES

1. International Committee on Taxonomy of Viruses (ICTV). Available at: https://talk.ictvonline.org/taxonomy/. (Accessed: 6th September 2017)

2. Kuno, G. *et al.* Phylogeny of the Genus Flavivirus. **72,** 72–83 (1998).

3. Cook, S. & Holmes, E. C. A multigene analysis of the phylogenetic relationships among the flaviviruses (Family: Flaviviridae) and the evolution of vector transmission. *Arch Virol* **151,** 309–325 (2006).

4. Pierson, T. C. & Diamond, M. S. Chapter 26 Flaviviruses. in *Fields Virology* **1,** 748–795 (Lippincott Williams & Wilkins, 2013).

5. Heinz, F. X. & Stiasny, K. The Antigenic Structure of Zika Virus and Its Relation to Other Flaviviruses: Implications for Infection and Immunoprophylaxis. *Microbiol. Mol. Biol. Rev.* **81,** e00055-16 (2017).

6. Kuno, G. & Chang, G. J. J. Full-length sequencing and genomic characterization of Bagaza, Kedougou, and Zika viruses. *Arch. Virol.* **152,** 687–696 (2007).

7. Baronti, C. *et al.* Complete Coding Sequence of Zika Virus from a French Polynesia. *Genome Announc.* **2,** 2013–2014 (2014).

8. Zhu, Z. *et al.* Comparative genomic analysis of pre-epidemic and epidemic Zika virus strains for virological factors potentially associated with the rapidly expanding epidemic. *Emerg. Microbes Infect.* **5,** e22 (2016).

9. Ng, W., Soto-Acosta, R., Bradrick, S., Garcia-Blanco, M. & Ooi, E. The 5′ and 3′ Untranslated Regions of the Flaviviral Genome. *Viruses* **9,** 137 (2017).

10. Chambers, T. J., Hahn, C. S., Galler, R. & Rice, C. M. Flavivirus Genome Organization, Expression, and Replication. *Annu. Rev. Microbiol.* **44,** 649–688 (1990).

11. Stadler, K., Allison, S. L., Schalich, J. & Heinz, F. X. Proteolytic Activation of Tick-Borne Encephalitis Virus by Furin. *J. Virol.* **71,** 8475–8481 (1997).

12. Elshuber, S., Allison, S. L., Heinz, F. X. & Mandl, C. W. Cleavage of protein prM is necessary for infection of BHK-21 cells by tick-borne encephalitis virus. *J. Gen. Virol.* **84,** 183–191 (2003).

13. Lindenbach, B. D. & Rice, C. M. Molecular biology of flaviviruses. **59,** 23–61 (2003).

14. Chambers, T. J. Flaviviruses: General Features. in *Encyclopedia of Virology* 241–252 (Elsevier, 2008). doi:10.1016/B978-012374410-4.00621-X

15. Martín-Acebes, M. A. West Nile virus: A re-emerging pathogen revisited. *World J. Virol.* **1,** 51 (2012).

16. Apte-Sengupta, S., Sirohi, D. & Kuhn, R. J. Coupling of replication and assembly in flaviviruses. *Curr. Opin. Virol.* **9,** 134–142 (2014).

17. Viralzone - Expasy. Available at: http://viralzone.expasy.org/6756?outline=all_by_species. (Accessed: 6th September 2017)

18. Sirohi, D. *et al.* The 3.8 Å resolution cryo-EM structure of Zika virus. *Science* **352,** 467–70 (2016).

19. Kostyuchenko, V. A. *et al.* Structure of the thermally stable Zika virus. *Nature* **533,** 425–8 (2016).

20. Dick, G. W. A. Pathogenicity and Physical Properties. *Trans. R. Soc. Trop. Med. Hyg.* **46,** 521–534 (1952).

21. Bell, T. M., Field, E. J. & Narang, H. K. Zika virus infection of the central nervous system of mice. *Arch. Gesamte Virusforsch.* **35,** 183–193 (1971).

22. Hamel, R. *et al.* Biology of Zika Virus Infection in Human Skin Cells. *J. Virol.* **89,** 8880–8896 (2015).

23. Dick, G. W. . Paper: Epidemiological notes on some viruses isolated in Uganda (Yellow fever, Rift Valley fever, Bwamba fever, West Nile, Mengo, Semliki forest, Bunyamwera, Ntaya, Uganda S and Zika viruses). *Trans. R. Soc. Trop. Med. Hyg.* **47,** 13–48 (1953).

24. Dick, G. W. ., Kitchen, S. . & Haddow, A. . Zika Virus (I). Isolations and serological specificity. *Trans. R. Soc. Trop. Med. Hyg.* **46,** 509–520 (1952).

25. MacNamara, F. . Zika virus : A report on three cases of human infection during an epidemic of jaundice in Nigeria. *Trans. R. Soc. Trop. Med. Hyg.* **48,** 139–145 (1954).

26. Marchette, N., Garcia, R. & Rudnick, A. Isolation of Zika virus from Aedes aegypti mosquitoes in Malaysia. *Am J Trop Med Hyg* **18,** 411–415 (1969).

27. Fagbami, A. H. Zika virus infections in Nigeria: virological and seroepidemiological investigations in Oyo State. *J. Hyg. (Lond).* **83,** 213–219 (1979).

28. Moore, D. L. *et al.* Arthropod-borne viral infections of man in Nigeria, 1964–1970. *Ann. Trop. Med. Parasitol.* **69,** 49–64 (1975).

29. Olson, J. G., Ksiazek, T. G., Suhandiman & Triwibowo. Zika virus, a cause of fever in Central Java, Indonesia. *Trans. R. Soc. Trop. Med. Hyg.* **75,** 389–393 (1981).

30. Simpson, D. I. H. Zika virus infection in man. *Trans. R. Soc. Trop. Med. Hyg.* **58,** 339–348 (1964).

31. Duffy M. *et al.* Zika virus outbreak on Yap Island, Federated States of Micronesia. *N. Engl. J. Med.* **360,** 2536–2543 (2009).

32. Cao-Lormeau, V.-M. *et al.* Zika Virus, French Polynesia, South Pacific, 2013. *Emerg. Infect. Dis.* **20,** 1084–1086 (2014).

33. European Centre for Disease Prevention and Control. Rapid risk assessment: Zika virus infection outbreak, French Polynesia. *ECDC* 1–12 (2014).

34. Mallet, H. P., Vial, A. L. & Musso, D. Bilan de l'épidémie à virus Zika en Polynésie française, 2013-2014. Zika virus outbreak in French Polynesia, 2013-2014. *Bull. d'Information Sanit. Epidémiologique Stat.* **13,** 1–5. (In French.) (2015).

35. Cao-Lormeau, V.-M. *et al.* Guillain-Barré Syndrome outbreak associated with Zika virus infection in French Polynesia: a case-control study. *Lancet* **387,** 1531–1539 (2016).

36. Zika and Guillain-Barré Syndrome | Zika virus | CDC. Available at: https://www.cdc.gov/zika/healtheffects/gbs-qa.html. (Accessed: 7th September 2017)

37. Yuki, N. & Hartung, H.-P. Guillain–Barré Syndrome. *N. Engl. J. Med.* **366,** 2294–2304 (2012).

38. van den Berg, B. *et al.* Guillain–Barré syndrome: pathogenesis, diagnosis, treatment and prognosis. *Nat. Rev. Neurol.* **10,** 469–482 (2014).

39. Dupont-Rouzeyrol, M. *et al.* Co-infection with Zika and Dengue Viruses in 2 Patients, New Caledonia, 2014. *Emerg. Infect. Dis.* **21,** 381–382 (2015).

40. Tognarelli, J. *et al.* A report on the outbreak of Zika virus on Easter Island, South Pacific, 2014. *Arch. Virol.* **161,** 665–668 (2016).

41. Brusin, S. *et al.* Zika virus infection outbreak, Brazil and the Pacific region ECDC internal response team External experts consulted and acknowledgements Disease background information. (2015).

42. Zanluca, C. *et al.* First report of autochthonous transmission of Zika virus in Brazil. *Mem Inst Oswaldo Cruz Rio Janeiro* **110,** 569–572 (2015).

43. Campos, G. S., Bandeira, A. C. & Sardi, S. I. Zika virus outbreak, Bahia, Brazil. *Emerging Infectious Diseases* **21,** 1885–1886 (2015).

44. WHO. Zika virus outbreaks in the Americas. *Wkly. Epidemiol. Rec.* **90,** 609–610 (2015).

45. ECDC, E. C. for D. P. and C. Rapid risk assessment: Zika virus epidemic in the Americas: potential association with microcephaly and Guillain-Barré syndrome, 10 December 2015. *ECDC* 1–14 (2015).

46. Pan American Health Organization/World Health Organization (PAHO/WHO). *PAHO WHO | Zika virus infection*. (2016).

47. World Health Organization. Zika Virus, Microcephaly and Guillain-Barré Syndrome - Situation report 21 april 2016. *World Heal. Organ.* 1–15 (2016).

48. Petersen, L. R., Jamieson, D. J., Powers, A. M. & Honein, M. A. Zika Virus. *N. Engl. J. Med.* **374,** 1552–1563 (2016).

49. Musso, D. & Gubler, D. J. Zika virus. *Clin. Microbiol. Rev.* **29,** 487–524 (2016).

50. Song, B. H., Yun, S. I., Woolley, M. & Lee, Y. M. Zika virus: History, epidemiology, transmission, and clinical presentation. *Journal of Neuroimmunology* **308,** 50–64 (2017).

51. Zika virus cases. Available at: http://www.goinvo.com/features/zika/. (Accessed: 10th September 2017)

52. Victora, C. G. *et al.* Microcephaly in Brazil: How to interpret reported numbers? *The Lancet* **387,** 621–624 (2016).

53. Cauchemez, S. *et al.* Association between Zika virus and microcephaly in French Polynesia, 2013–15: a retrospective study. *Lancet* **387,** 2125–2132 (2016).

54. Passemard, S., Kaindl, A. M. & Verloes, A. Microcephaly. *Handb. Clin. Neurol.* **111,** 129–141 (2013).

55. Von der Hagen, M. *et al.* Diagnostic approach to microcephaly in childhood: A two-center study and review of the literature. *Dev. Med. Child Neurol.* **56,** 732–741 (2014).

56. WHO | World Health Organization. WHO statement on the first meeting of the International Health Regulations (2005) (IHR 2005) Emergency Committee on Zika virus and observed increase in neurological disorders and neonatal malformations. *Who* **37,** 2–5 (2016).

57. Singh, R. K. *et al.* Zika virus – emergence, evolution, pathology, diagnosis, and control: current global scenario and future perspectives – a comprehensive review. *Vet. Q.* **36,** 150–175 (2016).

58. Haddow, A. D. *et al.* Genetic characterization of zika virus strains: Geographic expansion of the asian lineage. *PLoS Negl. Trop. Dis.* **6,** (2012).

59. Enfissi, A., Codrington, J., Roosblad, J., Kazanji, M. & Rousset, D. Zika virus genome from the Americas. *The Lancet* **387,** 227–228 (2016).

60. Centers for Diesease Control and Prevention. About Zika Virus Disease. (2016). Available at: https://ecdc.europa.eu/en/zika-virus-infection/facts/factsheet. (Accessed: 8th September 2017)

61. WHO. WHO | Zika virus. *World Health Organization* (2017). Available at: http://www.who.int/mediacentre/factsheets/zika/en/. (Accessed: 12th September 2017)

62. Kraemer, M. U. G. *et al.* The global distribution of the arbovirus vectors Aedes aegypti and Ae. Albopictus. *Elife* **4,** 1–18 (2015).

63. Besnard, M., Lastère, S., Teissier, A., Cao-Lormeau, V. M. & Musso, D. Evidence of perinatal transmission of zika virus, French Polynesia, December 2013 and February 2014. *Eurosurveillance* **19,** (2014).

64. Foy, B. D. *et al.* Probable Non–Vector-borne Transmission of Zika Virus, Colorado, USA. *Emerg. Infect. Dis.* **17,** 880–882 (2011).

65. Musso, D. *et al.* Potential Sexual Transmission of Zika Virus. *Emerg. Infect. Dis.* **21,** 359–361 (2015).

66. Musso, D. *et al.* Potential for Zika virus transmission through blood transfusion demonstrated during an outbreak in French Polynesia, November 2013 to February 2014. *Eurosurveillance* **19,** (2014).

67. Kashima, S., Slavov, S. N. & Covas, D. T. Zika virus and its implication in transfusion safety. *Rev. Bras. Hematol. Hemoter.* **38,** 90–91 (2016).

68. Leung, G. H. Y., Baird, R. W., Druce, J. & Anstey, N. M. ZIKA VIRUS INFECTION IN AUSTRALIA FOLLOWING A MONKEY BITE IN INDONESIA. *Southeast Asian J. Trop. Med. Public Health* **46,** 460–464 (2015).

69. Filipe, A. R., Martins, C. M. V & Rocha, H. Laboratory infection with Zika virus after vaccination against yellow fever. *Arch. Gesamte Virusforsch.* **43,** 315–319 (1973).

70. Engla, N. E. W. Zika virus in the Americas. *Perspective* **363,** 1–3 (2010).

71. Faye, O. *et al.* One-step RT-PCR for detection of Zika virus. *J. Clin. Virol.* **43,** 96–101 (2008).

72. Lanciotti, R. S. *et al.* Genetic and serologic properties of Zika virus associated with an epidemic, Yap State, Micronesia, 2007. *Emerg. Infect. Dis.* **14,** 1232–1239 (2008).

73. Musso, D. *et al.* Detection of Zika virus in saliva. *J. Clin. Virol.* **68,** 53–55 (2015).

74. Gourinat, A. C., O'Connor, O., Calvez, E., Goarant, C. & Dupont-Rouzeyrol, M. Detection of zika virus in urine. *Emerg. Infect. Dis.* **21,** 84–86 (2015).

75. Hayes, E. B. Zika virus outside Africa. *Emerg. Infect. Dis.* **15,** 1347–1350 (2009).

76. PAHO. Epidemiological Update October 16, 2015. *Pan American Health Organization* (2015). Available at: http://www.paho.org/hq/index.php?option=com_content&view=article&id=11599&Itemid=41691&lang=pt. (Accessed: 10th September 2017)

77. Shan, C. *et al.* Zika Virus: Diagnosis, Therapeutics, and Vaccine. *ACS Infect. Dis.* **2,** 170–172 (2016).

78. Abbink, P. *et al.* Protective efficacy of multiple vaccine platforms against Zika virus challenge in rhesus monkeys. *Science (80-.).* **353,** 1129–1132 (2016).

79. Abbasi, J. First Inactivated Zika Vaccine Trial. *JAMA* **316,** 2588 (2016).

80. NIH. Phase 2 Zika vaccine trial begins in U.S., Central and South America | National Institutes of Health (NIH). *National Institutes of Health* (2017). Available at: https://www.nih.gov/news-events/news-releases/phase-2-zika-vaccine-trial-begins-us-central-south-america. (Accessed: 9th September 2017)

81. Delvecchio, R. *et al.* Chloroquine, an endocytosis blocking agent, inhibits zika virus infection in different cell models. *Viruses* **8,** (2016).

82. Gollins, S. W. & Porterfield, J. S. pH-dependent fusion between the flavivirus West Nile and liposomal model membranes. *J. Gen. Virol.* **67,** 157–166 (1986).

83. Pierson, T. C. & Diamond, M. S. Degrees of maturity: the complex structure and biology of flaviviruses. *Curr. Opin. Virol.* **2,** 168–175 (2012).

84. Hanners, N. W. *et al.* Western Zika Virus in Human Fetal Neural Progenitors Persists Long Term with Partial Cytopathic and Limited Immunogenic Effects. *Cell Rep.* **15,** 2315–2322 (2016).

85. Cortese, M. *et al.* Ultrastructural Characterization of Zika Virus Replication Factories. *Cell Rep.* **18,** 2113–2123 (2017).

86. Wengler, G., Wengler, G. & Gross, H. J. Studies on virus-specific nucleic acids synthesized in vertebrate and mosquito cells infected with flaviviruses. *Virology* **89,** 423–437 (1978).

87. Welsch, S. *et al.* Composition and Three-Dimensional Architecture of the Dengue Virus Replication and Assembly Sites. *Cell Host Microbe* **5,** 365–375 (2009).

88. Gillespie, L. K., Hoenen, A., Morgan, G. & Mackenzie, J. M. The Endoplasmic Reticulum Provides the Membrane Platform for Biogenesis of the Flavivirus Replication Complex. *J. Virol.* **84,** 10438–10447 (2010).

89. Yu, I.-M. *et al.* Structure of the Immature Dengue Virus at Low pH Primes Proteolytic Maturation. *Science (80-.).* **319,** 1834–1837 (2008).

90. Chiramel, A., Brady, N. & Bartenschlager, R. Divergent Roles of Autophagy in Virus Infection. *Cells* **2,** 83–104 (2013).

91. Kaur, J. & Debnath, J. Autophagy at the crossroads of catabolism and anabolism. *Nat. Rev. Mol. Cell Biol.* **16,** 461–472 (2015).

92. Mizushima, N., Levine, B., Cuervo, A. M. & Klionsky, D. J. Autophagy fights disease through cellular self-digestion. *Nature* **451,** 1069–1075 (2008).

93. Deretic, V. & Levine, B. Autophagy, Immunity, and Microbial Adaptations. *Cell Host and Microbe* **5,** 527–549 (2009).

94. Levine, B. & Kroemer, G. Autophagy in the Pathogenesis of Disease. *Cell* **132,** 27–42 (2008).

95. Hayashi-Nishino, M. *et al.* A subdomain of the endoplasmic reticulum forms a cradle for autophagosome formation. *Nat. Cell Biol.* **11,** 1433–1437 (2009).

96. Ylä-Anttila, P., Vihinen, H., Jokitalo, E. & Eskelinen, E. L. 3D tomography reveals connections between the phagophore and endoplasmic reticulum. *Autophagy* **5,** 1180–1185 (2009).

97. Ravikumar, B., Moreau, K., Jahreiss, L., Puri, C. & Rubinsztein, D. C. Plasma membrane contributes to the formation of pre-autophagosomal structures. *Nat. Cell Biol.* **12,** 747–757 (2010).

98. Yamamoto, H. *et al.* Atg9 vesicles are an important membrane source during early steps of autophagosome formation. *J. Cell Biol.* **198,** 219–233 (2012).

99. Hailey, D. W. *et al.* Mitochondria Supply Membranes for Autophagosome Biogenesis during Starvation. *Cell* **141,** 656–667 (2010).

100. Tooze, S. A., Abada, A. & Elazar, Z. Endocytosis and autophagy: Exploitation or cooperation? *Cold Spring Harb. Perspect. Biol.* **6,** (2014).

101. Ploen, D. Hepatitis C virus comes for dinner: How the hepatitis C virus interferes with autophagy. *World J. Gastroenterol.* **21,** 8492 (2015).

102. Eskelinen, E.-L. & Saftig, P. Autophagy: A lysosomal degradation pathway with a central role in health and disease. *Biochim. Biophys. Acta - Mol. Cell Res.* **1793,** 664–673 (2009).

103. Glick, D., Barth, S. & Macleod, K. F. Autophagy: Cellular and molecular mechanisms. *Journal of Pathology* **221,** 3–12 (2010).

104. Kroemer, G., Mariño, G. & Levine, B. Autophagy and the Integrated Stress Response. *Molecular Cell* **40,** 280–293 (2010).

105. Sengupta, S., Peterson, T. R. & Sabatini, D. M. Regulation of the mTOR Complex 1 Pathway by Nutrients, Growth Factors, and Stress. *Mol. Cell* **40,** 310–322 (2010).

106. Harnett, M. M. *et al.* From Christian de Duve to Yoshinori Ohsumi: More to autophagy than just dining at home. *Biomedical Journal* **40,** 9–22 (2017).

107. Kim, J., Kundu, M., Viollet, B. & Guan, K.-L. AMPK and mTOR regulate autophagy through direct phosphorylation of Ulk1. *Nat. Cell Biol.* **13,** 132–141 (2011).

108. Klionsky, D. J. Autophagy: from phenomenology to molecular understanding in less than a decade. *Nat. Rev. Mol. Cell Biol.* **8,** 931–937 (2007).

109. Lamb, C. A., Yoshimori, T. & Tooze, S. A. The autophagosome: origins unknown, biogenesis complex. *Nat. Rev. Mol. Cell Biol.* **14,** 759–774 (2013).

110. Nascimbeni, A. C., Codogno, P. & Morel, E. Phosphatidylinositol-3-phosphate in the regulation of autophagy membrane dynamics. *FEBS Journal* **284,** 1267–1278 (2017).

111. Axe, E. L. *et al.* Autophagosome formation from membrane compartments enriched in phosphatidylinositol 3-phosphate and dynamically connected to the endoplasmic reticulum. *J. Cell Biol.* **182,** 685–701 (2008).

112. Roberts, R. & Ktistakis, N. T. Omegasomes: PI3P platforms that manufacture autophagosomes. *Essays Biochem.* **55,** 17–27 (2013).

113. Burman, C. & Ktistakis, N. T. Regulation of autophagy by phosphatidylinositol 3-phosphate. *FEBS Lett.* **584,** 1302–1312 (2010).

114. Mizushima, N., Yoshimori, T. & Ohsumi, Y. The Role of Atg Proteins in Autophagosome Formation. *Annu. Rev. Cell Dev. Biol.* **27,** 107–132 (2011).

115. Kabeya, Y. *et al.* LC3, a mammalian homolog of yeast Apg8p, is localized in autophagosome membranes after processing. *EMBO Journal* **19,** 5720–5728 (2000).

116. Kirisako, T. *et al.* The reversible modification regulates the membrane-binding state of Apg8/Aut7 essential for autophagy and the cytoplasm to vacuole targeting pathway. *J. Cell Biol.* **151,** 263–275 (2000).

117. Ichimura, Y. *et al.* A ubiquitin-like system mediates protein lipidation. *Nature* **408,** 488–492 (2000).

118. Fujita, N. *et al.* The Atg16L complex specifies the site of LC3 lipidation for membrane biogenesis in autophagy. *Mol Biol Cell* **19,** 2092–2100 (2008).

119. Tanida, I., Ueno, T. & Kominami, E. LC3 conjugation system in mammalian autophagy. *Int. J. Biochem. Cell Biol.* **36,** 2503–2518 (2004).

120. Pankiv, S. *et al.* p62/SQSTM1 Binds Directly to Atg8/LC3 to Facilitate Degradation of Ubiquitinated Protein Aggregates by Autophagy. *J. Biol. Chem.* **282,** 24131–24145 (2007).

121. Bjørkøy, G. *et al.* p62/SQSTM1 forms protein aggregates degraded by autophagy and has a protective effect on huntingtin-induced cell death. *J. Cell Biol.* **171,** 603–614 (2005).

122. Choi, A. M. K., Ryter, S. W. & Levine, B. Autophagy in Human Health and Disease. *N. Engl. J. Med.* **368,** 651–662 (2013).

123. Yang, Y.-P. *et al.* Application and interpretation of current autophagy inhibitors and activators. *Acta Pharmacol. Sin.* **34,** 625–635 (2013).

124. Galluzzi, L., Bravo-San Pedro, J. M., Levine, B., Green, D. R. & Kroemer, G. Pharmacological modulation of autophagy: therapeutic potential and persisting obstacles. *Nat. Rev. Drug Discov.* **16,** 487–511 (2017).

125. Seglen, P. O. & Gordon, P. B. 3-Methyladenine: Specific inhibitor of autophagic/lysosomal protein degradation in isolated rat hepatocytes. *Proc. Natl. Acad. Sci.* **79,** 1889–1892 (1982).

126. Blommaart, E. F., Krause, U., Schellens, J. P., Vreeling-Sindelárová, H. & Meijer, A. J. The phosphatidylinositol 3-kinase inhibitors wortmannin and LY294002 inhibit autophagy in isolated rat hepatocytes. *Eur. J. Biochem.* **243,** 240–6 (1997).

127. Petiot, A., Ogier-Denis, E., Blommaart, E. F. C., Meijer, A. J. & Codogno, P. Distinct Classes of Phosphatidylinositol 3'-Kinases Are Involved in Signaling Pathways That Control Macroautophagy in HT-29 Cells. *J. Biol. Chem.* **275,** 992–998 (2000).

128. Werner, G., Hagenmaier, H., Drautz, H., Baumgartner, A. & Zähner, H. Metabolic products of microorganisms. 224. Bafilomycins, a new group of macrolide antibiotics. Production, isolation, chemical structure and biological activity. *J. Antibiot. (Tokyo).* **37,** 110–117 (1984).

129. Bowman, E. J., Siebers, A. & Altendorf, K. Bafilomycins: a class of inhibitors of membrane ATPases from microorganisms, animal cells, and plant cells. *Proc. Natl. Acad. Sci. U. S. A.* **85,** 7972–7976 (1988).

130. Mellman, I., Fuchs, R. & Helenius, A. Acidification of the endocytic and exocytic pathways. *Annu. Rev. Biochem.* **55,** 663–700 (1986).

131. Mindell, J. A. Lysosomal Acidification Mechanisms. *Annu. Rev. Physiol.* **74,** 69–86 (2012).

132. Villamil Giraldo, A. M., Appelqvist, H., Ederth, T. & Öllinger, K. Lysosomotropic agents: impact on lysosomal membrane permeabilization and cell death. *Biochem. Soc. Trans.* **42,** 1460–1464 (2014).

133. Ohkuma, S. & Poole, B. Fluorescence probe measurement of the intralysosomal pH in living cells and the perturbation of pH by various agents. *Proc. Natl. Acad. Sci. U. S. A.* **75,** 3327–31 (1978).

134. Homewood, C. a, Warhurst, D. C., Peters, W. & Baggaley, V. C. Lysosomes, pH and the anti-malarial action of chloroquine. *Nature* **235,** 50–2 (1972).

135. Morgan, M. J. *et al.* Regulation of autophagy and chloroquine sensitivity by oncogenic RAS in vitro is context-dependent. *Autophagy* **10,** 1814–1826 (2014).

136. Cenedella, R. J. Cholesterol Synthesis Inhibitor U18666A and the Role of Sterol Metabolism and Trafficking in Numerous Pathophysiological Processes. *Lipids* **44,** 477–487 (2009).

137. Vézina, C., Kudelski, A. & Sehgal, S. N. Rapamycin (AY-22,989), a new antifungal antibiotic. I. Taxonomy of the producing streptomycete and isolation of the active principle. *J. Antibiot. (Tokyo).* **28,** 721–6 (1975).

138. Ballou, L. M. & Lin, R. Z. Rapamycin and mTOR kinase inhibitors. *J. Chem. Biol.* **1,** 27–36 (2008).

139. Jackson, W. T. Viruses and the autophagy pathway. *Virology* **479–480,** 450–456 (2015).

140. Liang, Q. *et al.* Zika Virus NS4A and NS4B Proteins Deregulate Akt-mTOR Signaling in Human Fetal Neural Stem Cells to Inhibit Neurogenesis and Induce Autophagy. *Cell Stem Cell* **19,** 663–671 (2016).

141. Cao, B., Parnell, L. A., Diamond, M. S. & Mysorekar, I. U. Inhibition of autophagy limits vertical transmission of Zika virus in pregnant mice. *J. Exp. Med.* **214,** 2303–2313 (2017).

142. Giard, D. J. *et al.* In Vitro Cultivation of Human Tumors: Establishment of Cell Lines Derived From a Series of Solid Tumors2. *JNCI J. Natl. Cancer Inst.* **51,** 1417–1423 (1973).

143. Yasumura, Y. & Kawakita, Y. Studies on SV40 in tissue culture - preliminary step for cancer research in vitro. *Nihon Rinsho* **21,** 1201–1215 (1963).

144. PrestoBlue Cell Viability Reagent - Thermo Fisher Scientific. Available at: https://www.thermofisher.com/order/catalog/product/A13261?ICID=cvc-prestoblue-c1t1. (Accessed: 1st October 2017)

145. Takara Bio Inc. LDH Cytotoxicity Detection Kit Product Manual.

146. Koley, D. & Bard, A. J. Triton X-100 concentration effects on membrane permeability of a single HeLa cell by scanning electrochemical microscopy (SECM). *Proc. Natl. Acad. Sci.* **107,** 16783–16787 (2010).

147. peqLab. TriFast ™ - Data Sheet. 1–10 (2010).

148. Bradford, M. M. A rapid and sensitive method for the quantitation of microgram quantities of protein utilizing the principle of protein-dye binding. *Anal. Biochem.* **72,** 248–54 (1976).

149. Laemmli, U. K. Cleavage of structural proteins during the assembly of the head of bacteriophage T4. *Nature* **227,** 680–5 (1970).

150. Towbin, H., Staehelin, T. & Gordon, J. Electrophoretic transfer of proteins from polyacrylamide gels to nitrocellulose sheets: procedure and some applications. *Proc. Natl. Acad. Sci. U. S. A.* **76,** 4350–4 (1979).

151. Redmann, M. *et al.* Inhibition of autophagy with bafilomycin and chloroquine decreases mitochondrial quality and bioenergetic function in primary neurons. *Redox Biol.* **11,** 73–81 (2017).

152. Elgner, F. *et al.* The Intracellular Cholesterol Transport Inhibitor U18666A Inhibits the Exosome-Dependent Release of Mature Hepatitis C Virus. *J. Virol.* **90,** 11181–11196 (2016).

153. Cheng, P.-H. *et al.* Combination of autophagy inducer rapamycin and oncolytic adenovirus improves antitumor effect in cancer cells. *Virol. J.* **10,** 293 (2013).

154. Medvedev, R. *et al.* HCV-induced oxidative stress by inhibition of Nrf2 triggers autophagy and favors release of viral particles. *Free Radic. Biol. Med.* **110,** 300–315 (2017).

155. Kudchodkar, S. B. & Levine, B. Viruses and autophagy. *Reviews in Medical Virology* **19,** 359–378 (2009).

156. Lee, Y.-R. *et al.* Autophagic machinery activated by dengue virus enhances virus replication. *Virology* **374,** 240–248 (2008).

157. Blázquez, A.-B., Martín-Acebes, M. A. & Saiz, J.-C. Amino acid substitutions in the non-structural proteins 4A or 4B modulate the induction of autophagy in West Nile virus infected cells independently of the activation of the unfolded protein response. *Front. Microbiol.* **5,** 797 (2014).

158. Li, J.-K., Liang, J.-J., Liao, C.-L. & Lin, Y.-L. Autophagy is involved in the early step of Japanese encephalitis virus infection. *Microbes Infect.* **14,** 159–168 (2012).

159. Carlsson, S. R., Roth, J., Piller, F. & Fukuda, M. Isolation and characterization of human lysosomal membrane glycoproteins, h-lamp-1 and h-lamp-2. Major sialoglycoproteins carrying polylactosaminoglycan. *J. Biol. Chem.* **263,** 18911–18919 (1988).

160. Yuan, N. *et al.* Bafilomycin A1 targets both autophagy and apoptosis pathways in pediatric B-cell acute lymphoblastic leukemia. **100,** 345–356 (2015).

161. Yan, Y. *et al.* Bafilomycin A1 induces caspase-independent cell death in hepatocellular carcinoma cells via targeting of autophagy and MAPK pathways. *Sci. Rep.* **6,** 37052 (2016).

162. Huang, Z., Hou, Q., Cheung, N. S. & Li, Q. Neuronal cell death caused by inhibition of intracellular cholesterol trafficking is caspase dependent and associated with activation of the mitochondrial apoptosis pathway. *J. Neurochem.* **97,** 280–291 (2006).

163. Jiang, R.-Y., Pei, H.-L., Gu, W.-D., Huang, J. & Wang, Z.-G. Autophagic inhibitor attenuates rapamycin-induced inhibition of proliferation in cultured A549 lung cancer cells. *Eur. Rev. Med. Pharmacol. Sci.* **18,** 806–10 (2014).

164. Wang, L. & Wang, R. Effect of rapamycin (RAPA) on the growth of lung cancer and its mechanism in mice with A549. *Int. J. Clin. Exp. Pathol.* **8,** 9208–9213 (2015).

165. Porter, A. G. & Jänicke, R. U. Emerging roles of caspase-3 in apoptosis. *Cell Death Differ.* **6,** 99–104 (1999).

166. Frumence, E. *et al.* The South Pacific epidemic strain of Zika virus replicates efficiently in human epithelial A549 cells leading to IFN-β production and apoptosis induction. *Virology* **493,** 217–226 (2016).

167. Ghouzzi, V. El *et al.* ZIKA virus elicits P53 activation and genotoxic stress in human neural progenitors similar to mutations involved in severe forms of genetic microcephaly and p53. *Cell Death Dis.* **7,** (2016).

168. Hu, Y.-B., Dammer, E. B., Ren, R.-J. & Wang, G. The endosomal-lysosomal system: from acidification and cargo sorting to neurodegeneration. *Transl. Neurodegener.* **4,** 18 (2015).

169. Liu, Y. *et al.* Evolutionary enhancement of Zika virus infectivity in Aedes aegypti mosquitoes. *Nature* **545,** 482–486 (2017).

170. Lee, C., Lin, H., Liao, C. & Lin, Y. Cholesterol Effectively Blocks Entry of Flavivirus. **82,** 6470–6480 (2008).

171. Poh, M. K. *et al.* U18666A, an intra-cellular cholesterol transport inhibitor, inhibits dengue virus entry and replication. *Antiviral Res.* **93,** 191–198 (2012).

172. Schroeder, F., Holland, J. & Bieber, L. Fluorometric evidence for the binding of cholesterol to the filipin complex. *J. Antibiot. (Tokyo).* **24,** 846–849 (1971).

173. Monel, B. *et al.* Zika virus induces massive cytoplasmic vacuolization and paraptosis□like death in infected cells. *EMBO J.* **36,** 1653–1668 (2017).

174. Sperandio, S., de Belle, I. & Bredesen, D. E. An alternative, nonapoptotic form of programmed cell death. *Proc. Natl. Acad. Sci. U. S. A.* **97,** 14376–81 (2000).

175. Wu, Y.-T. *et al.* Dual Role of 3-Methyladenine in Modulation of Autophagy via Different Temporal Patterns of Inhibition on Class I and III Phosphoinositide 3-Kinase. *J. Biol. Chem.* **285,** 10850–10861 (2010).

8. APPENDICES

8.1 Appendix I – Cell viability assays

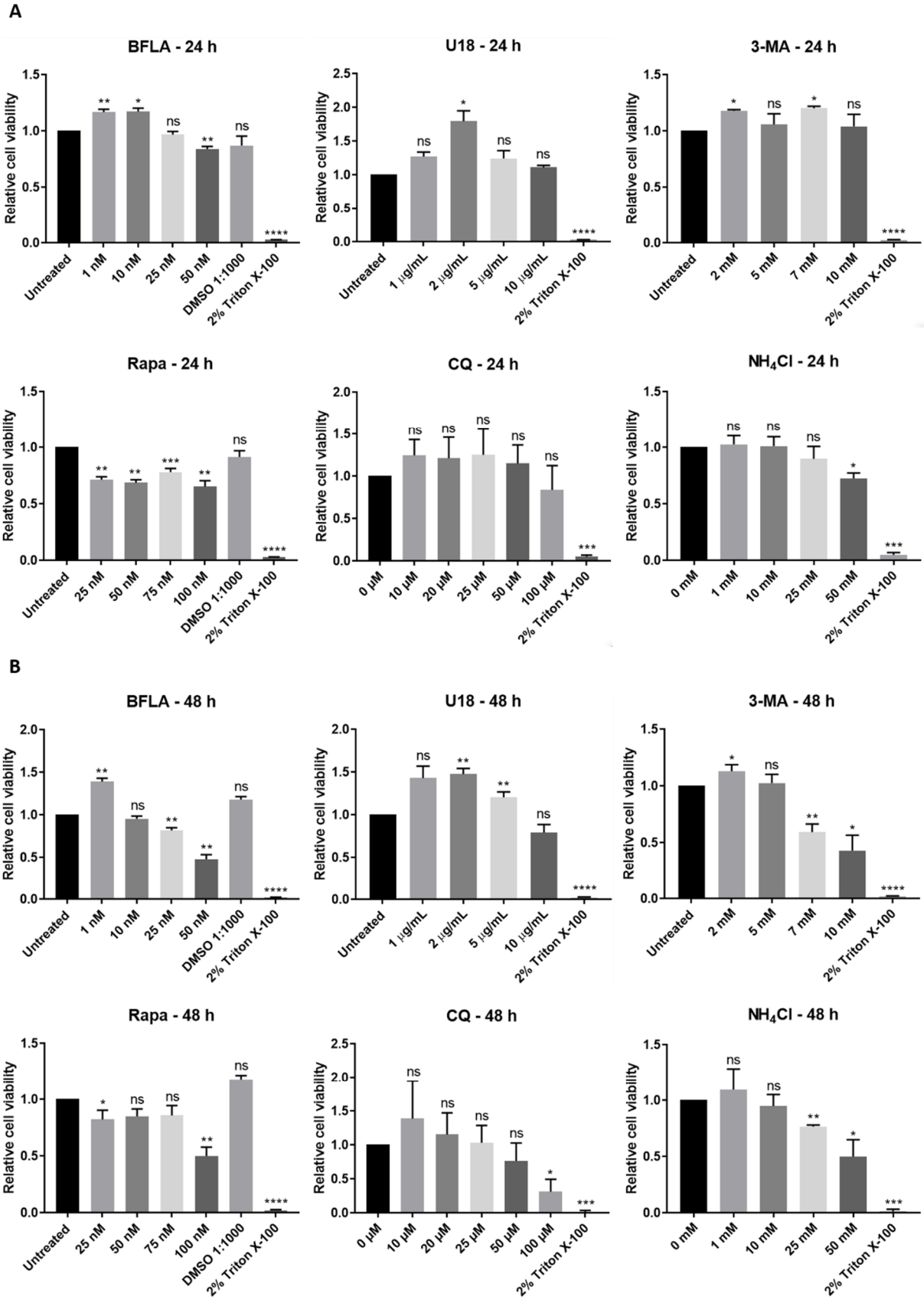

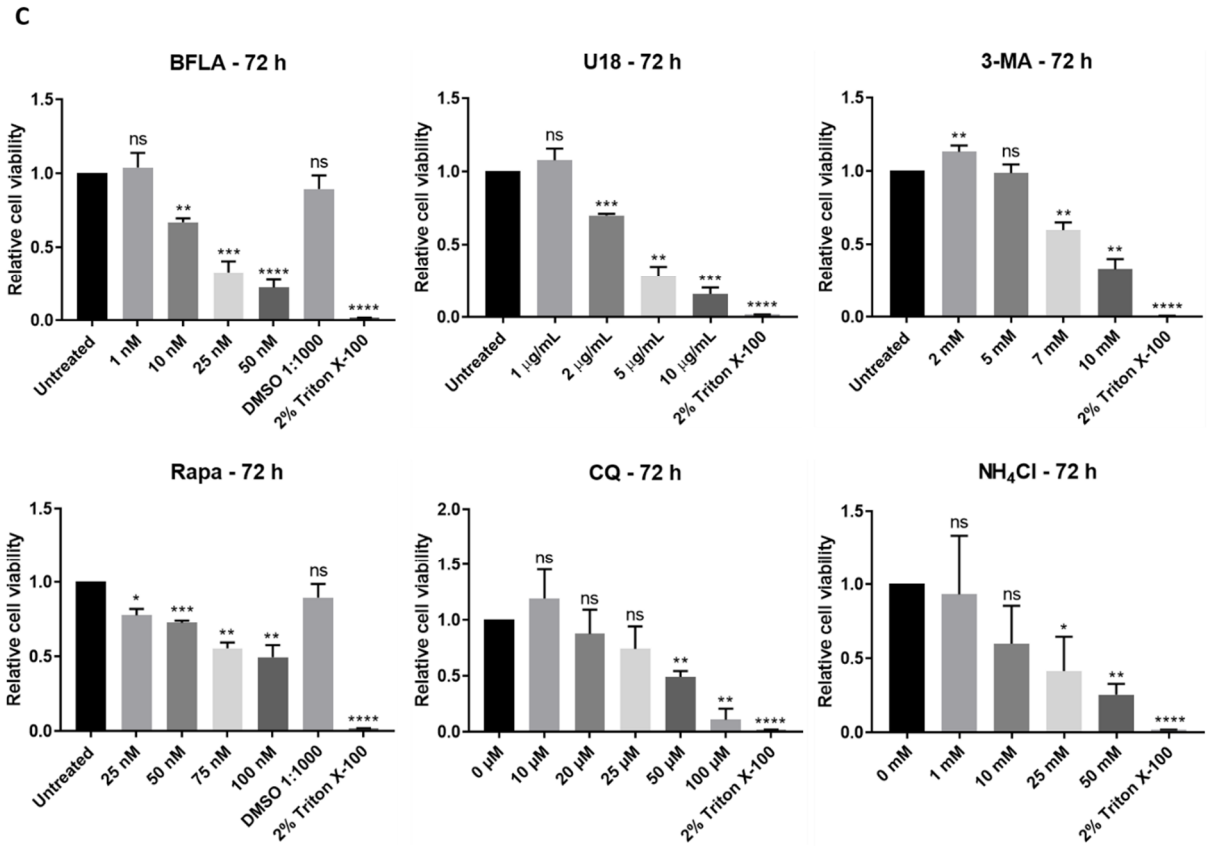

Figure 8.1 – Cell viability assays of A549 cells treated with autophagy modulators. A549 cells were treated with multiple concentrations of BFLA, U18, Rapa, 3-MA, CQ and NH_4Cl during 24 **(A)**, 48 **(B)**, and 72 h **(C)**. Relative cell viability was determined by comparing treated to untreated cells. Cells treated with 2% Triton X-100 were included as positive control. As negative control, cells were not treated (only DMEM complete). DMSO 1:1000 was included as vehicle control for BFLA and Rapa.

8.2 Appendix II – Cytotoxicity assays

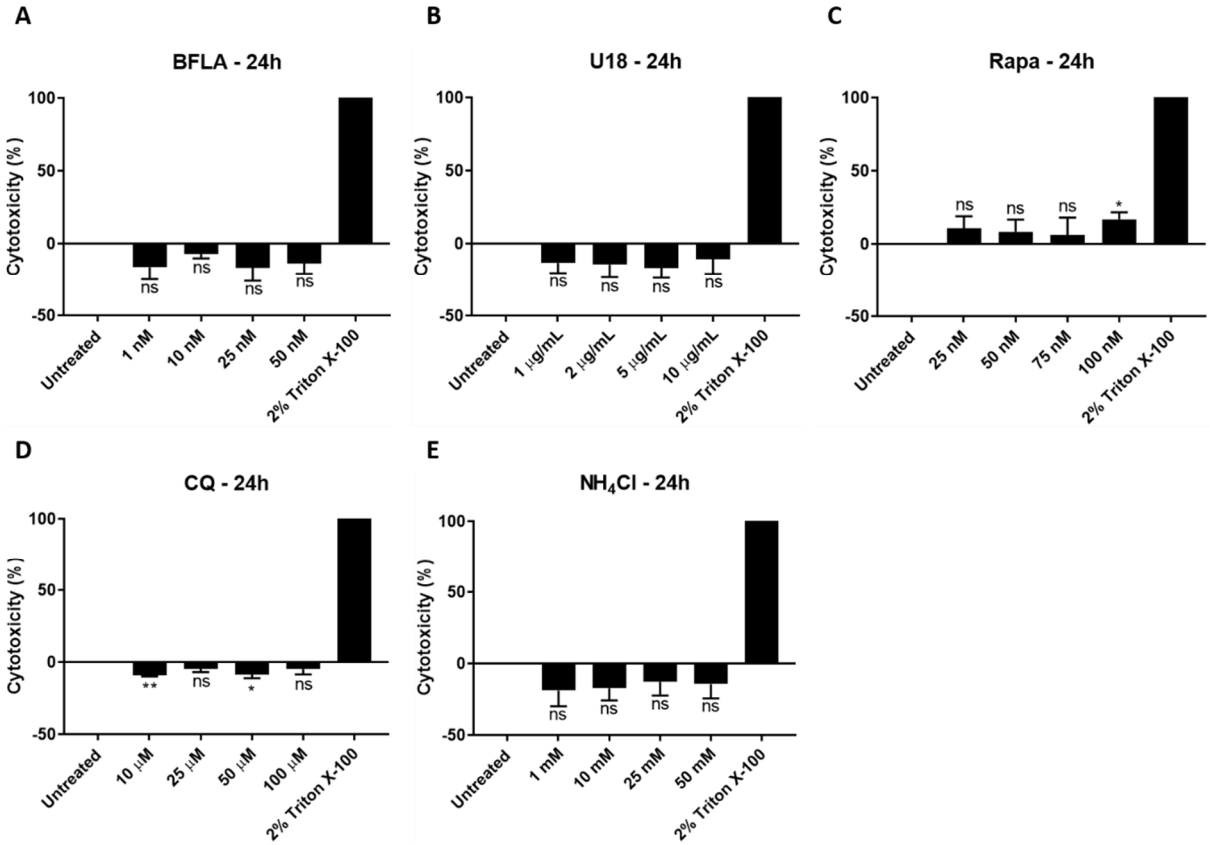

Figure 8.2 – Cytotoxicity assays of autophagy modulators. The cytotoxicity of BFLA **(A)**, U18 **(B)**, Rapa **(C)**, CQ **(D)**, and NH_4Cl **(E)** was measured after 24 h of treatment by LDH assay. The measurement of LDH activity is an indicator of cell death. The cytotoxicity was calculated by setting 2% Triton X-100 as maximum LDH released (100% - positive control) and only DMEM complete (untreated) as minimum LDH released (0% - negative control).

8.3 Appendix III – Densitometric quantification of cell lysates from BFLA-treated cells

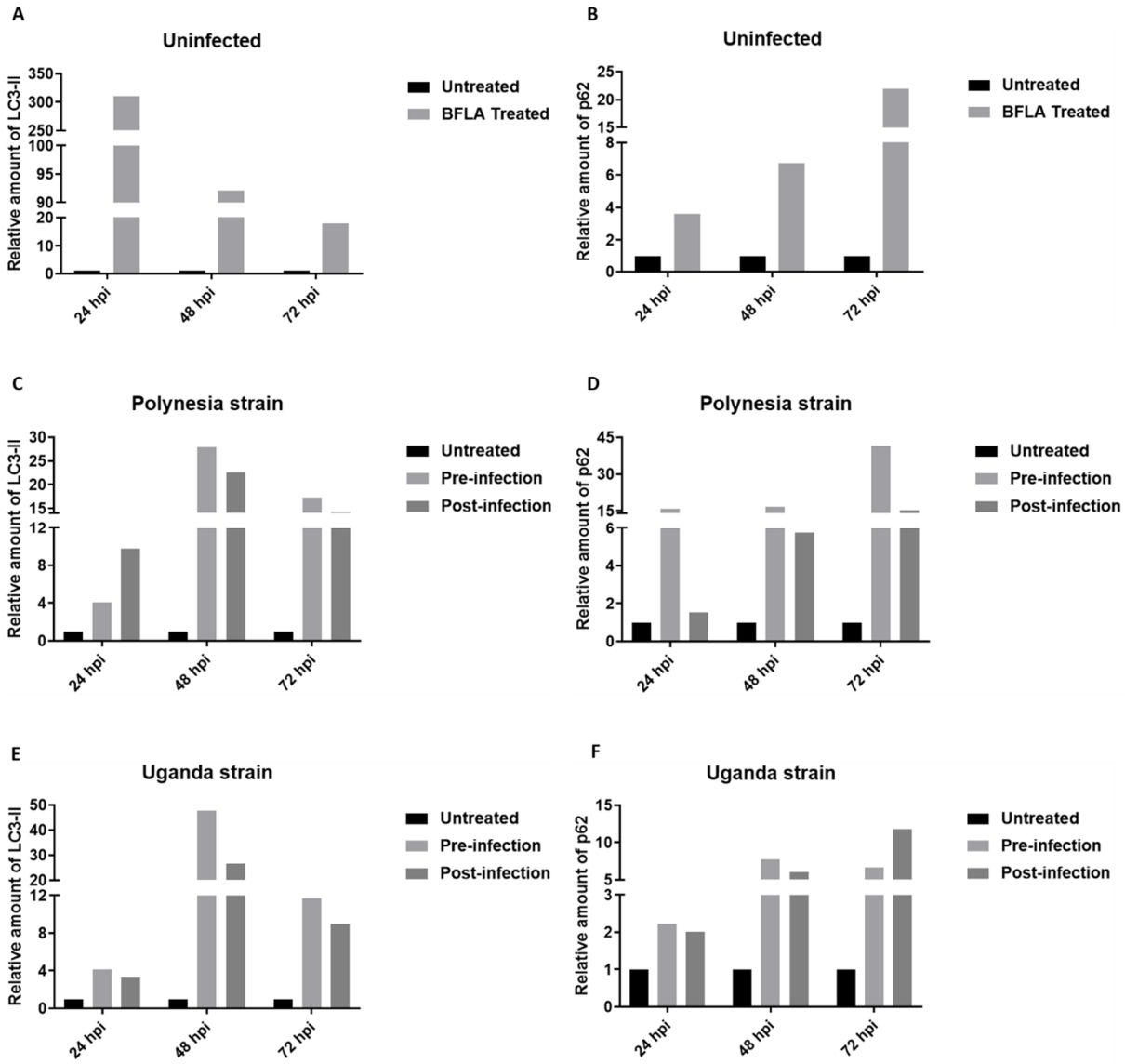

Figure 8.3 – Densitometric quantification of p62 and LC3-II of cell lysates from BFLA-treated cells. Densitometric quantification of p62 and LC3-II after 24, 48, and 72 hpi was accomplished by Image Studio Lite software. Polynesia- **(C, D)** and Uganda-infected cells **(E, F)** were treated before (pre-) and after (post-) infection with BFLA. Moreover, the effect of BFLA on p62 and LC3-II levels was evaluated in uninfected cell lysates **(A, B)**. The values were first normalised to the loading control and then to untreated cell lysates. The relative amount of LC3-II corresponds to the ratio LC3-II/LC3-I.

8.4 Appendix IV – Densitometric quantification of cell lysates from U18-treated cells

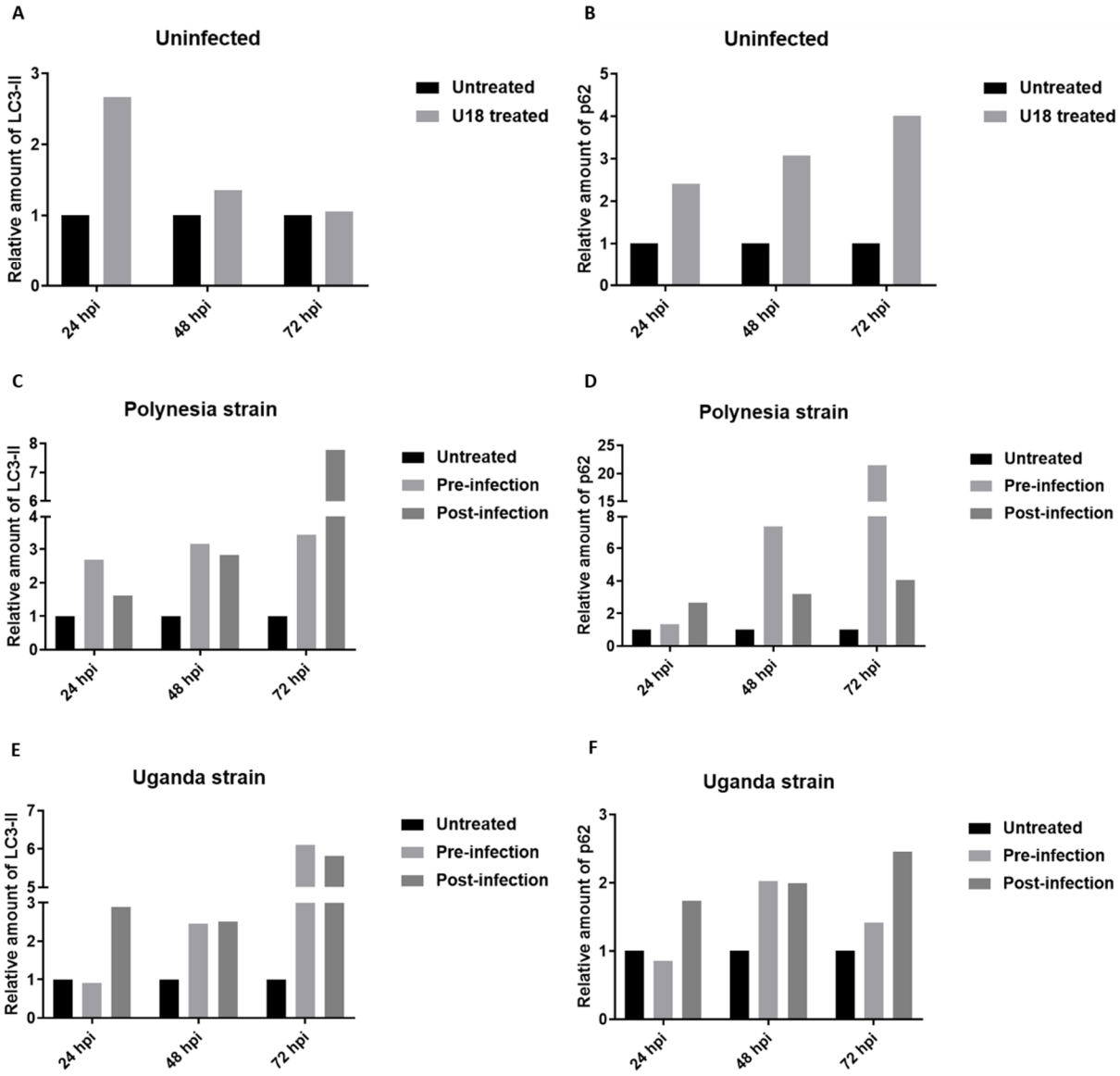

Figure 8.4 – Densitometric quantification of p62 and LC3-II of cell lysates from U18-treated cells. Densitometric quantification of p62 and LC3-II after 24, 48, and 72 hpi was accomplished by Image Studio Lite software. Polynesia- **(C, D)** and Uganda-infected cells **(E, F)** were treated before (pre-) and after (post-) infection with U18. Moreover, the effect of U18 on p62 and LC3-II levels was evaluated in uninfected cell lysates **(B, D)**. The values were first normalised to the loading control and then to untreated cell lysates. The relative amount of LC3-II corresponds to the ratio LC3-II/LC3-I.

8.5 Appendix V – Densitometric quantification of cell lysates from 3-MA-treated cells

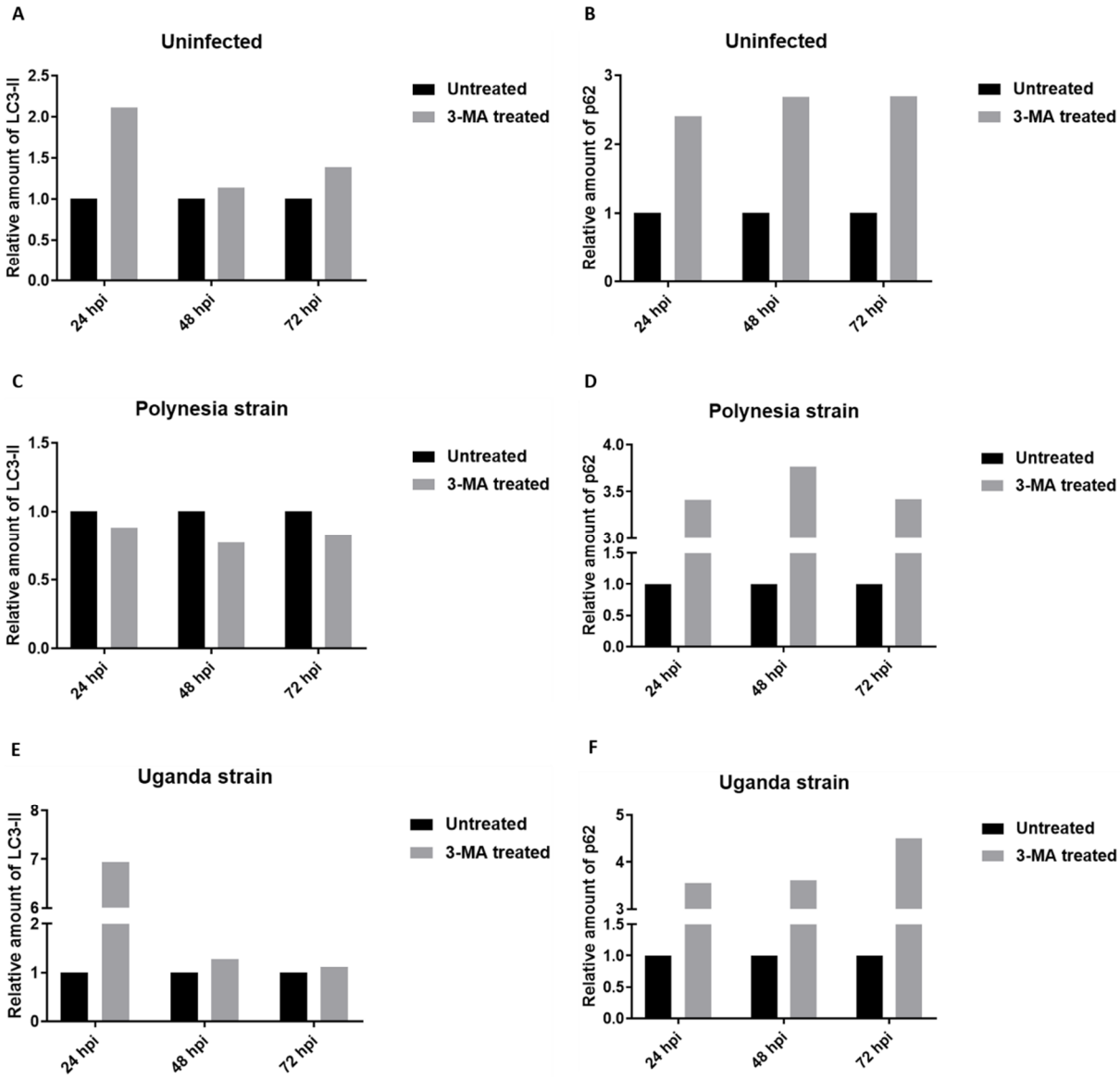

Figure 8.5 – Densitometric quantification of p62 and LC3-II of cell lysates from 3-MA-treated cells. Densitometric quantification of p62 and LC3-II after 24, 48, and 72 hpi was accomplished by Image Studio Lite software. Polynesia- **(C, D)** and Uganda-infected cells **(E, F)** were treated after (post-) infection with 3-MA. Furthermore, the effect of 3-MA on p62 and LC3-II levels was evaluated in uninfected cell lysates **(B, D)**. The values were first normalised to the loading control and then to untreated cell lysates. The relative amount of LC3-II corresponds to the ratio LC3-II/LC3-I.

8.6 Appendix VI – Densitometric quantification of cell lysates from Rapa-treated cells

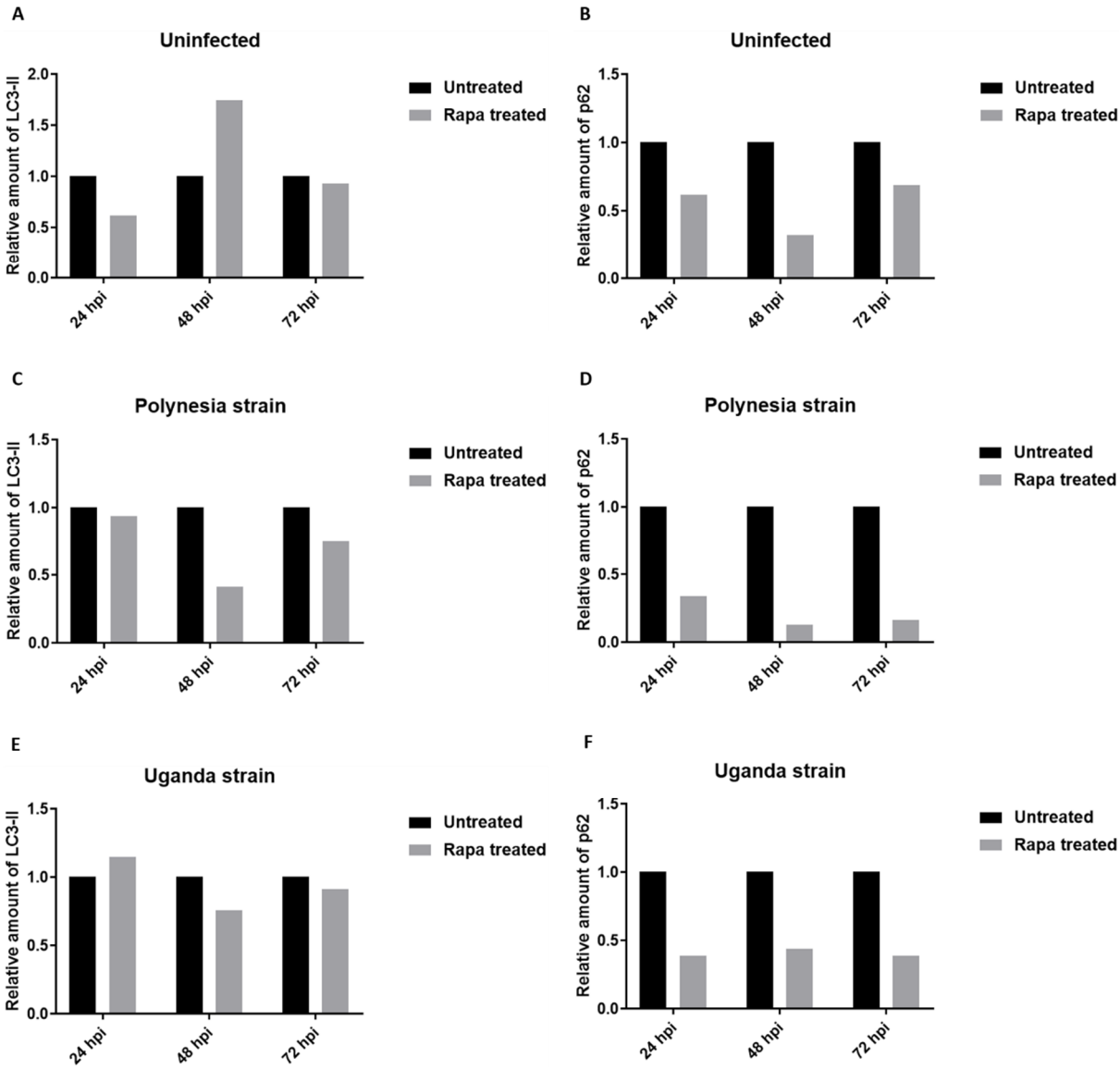

Figure 8.6 – Densitometric quantification of p62 and LC3-II of cell lysates from Rapa-treated cells. Densitometric quantification of p62 and LC3-II after 24, 48, and 72 hpi was accomplished by Image Studio Lite software. Polynesia- **(C, D)** and Uganda-infected cells **(E, F)** were treated after (post-) infection with Rapa. Furthermore, the effect of Rapa on p62 and LC3-II levels was evaluated in uninfected cell lysates **(B, D)**. The values were first normalised to the loading control and then to untreated cell lysates. The relative amount of LC3-II corresponds to the ratio LC3-II/LC3-I.